The Dissertation Committee for Kwan-Woong Gwak certifies that this is the approved version of the following dissertation:

STRUCTURAL ANALYSIS, DESIGN AND OPTIMIZATION OF NONLINEAR CONTROL SYSTEMS USING THE LINEAR ALGEBRAIC EQUIVALENCE OF NONLINEAR CONTROLLERS

Committee:

Glenn Y. Masada, Supervisor

Benito Fernández

John R. Howell

David P. Morton

S. Joe Qin

STRUCTURAL ANALYSIS, DESIGN AND OPTIMIZATION OF NONLINEAR CONTROL SYSTEMS USING THE LINEAR ALGEBRAIC EQUIVALENCE OF NONLINEAR CONTROLLERS

by

KWAN-WOONG GWAK, B.S., M.S.

DISSERTATION

Presented to the Faculty of the Graduate School of

The University of Texas at Austin

in Partial Fulfillment

of the Requirements

for the Degree of

DOCTOR OF PHILOSOPHY

The University of Texas at Austin

August 2003

Dedication

This dissertation is dedicated to my wife, Won-Kyoung Yang, and to my son, Brian Joon-Young Gwak, for their love, sacrifice, and encouragement that made this achievement possible. To my father and mother, for their love and sacrifice. Most of this work belongs to them

Acknowledgements

First of all, I would like to give my special thanks to Dr. Glenn Y. Masada for being my mentor. He has always kept me motivated, and treated me with a confidence that had led me to freely pursue my goals. I am also grateful to my committee members Dr. Benito Fernández, Dr. John R. Howell, Dr. David P. Morton, and Dr. S. Joe Qin for serving as my committee members.

I wish to acknowledge the assistance of Dr. John R. Howell and Dr. Hakane Erturk in providing the parameter values and configuration of the thermal system used in this dissertation, and for their discussions on the ill-conditioned problems.

Thanks to all my colleagues in the Department of Mechanical Engineering, especially Dr. Ravishankar Shivarama, Dr. Horacio Orozco-Mendoza, and Dr. Marc Compere, for their discussions and encouragement. In addition, my thanks go to my friends of Mechanical Engineering Korean Student Association for great memories in beautiful Austin.

The financial support of the University of Texas Continuing Fellowship, the Department of Mechanical Engineering and the National Science Foundation, Project ECS-9412933, is greatly appreciated.

Finally, I would like to thank my parents and all my family for their unceasing love and encouragement.

STRUCTURAL ANALYSIS, DESIGN AND OPTIMIZATION OF NONLINEAR CONTROL SYSTEMS USING THE LINEAR ALGEGRAIC EQUIVALENCE OF NONLINEAR CONTROLLERS

Publication No._____

Kwan-Woong Gwak, Ph.D.

The University of Texas at Austin, 2003

Supervisor: Glenn Y. Masada

Designing a nonlinear control scheme addressing major design issues in a unified way is a difficult task. However, structural information of a system/controller allows one to diagnose and identify performance characteristics at the design stage, to select better solution methods, and identify and eliminate potential problems, thereby improving the design of the controllers. In this research, structural analysis, design and optimization of nonlinear control systems are presented using the linear algebraic equivalence of nonlinear controllers (LAENC) to address the design issues of nonlinear control systems in a systematic way.

It is shown that feedback linearization and sliding mode control possess the very useful structural feature, the linear algebraic equivalence, on which many well-developed linear algebraic solution techniques can be applied directly. Using this LAENC, input-constrained nonlinear optimal controllers are proposed. Investigation of the nonlinear control structure by applying the singular value decomposition to the LAENC shows that control inputs/outputs are composed of a linear combination of finite number of mode shapes and that the linear combination coefficients for the control input determine the final distribution of the control inputs. It is also shown that the contribution of each output mode towards the target vector is determined by colinearity, and colinearity can be used as a criterion for mode truncation optimization.

The proposed algorithms are applied to the temperature control of an enclosed and radiation-dominant thermal system. The pure nonlinear controllers generate input-constraint-violating and large-oscillating solutions due to the ill-conditionedness, hence regularization methods that reduce the effects of ill-conditionedness are embedded into the nonlinear controller designs based on the LAENC. Also, the proposed input-constrained nonlinear optimal controller is applied and successful results are obtained. Using structural analysis, control input modes that cause input-constraint-violation and that contribute little to the total performance but use large control energy are truncated. As a result, input-constraint-satisfying solutions with a reduction in control effort are obtained.

Table of Contents

List of Tables

List of Figures

Chapter 1

Introduction

1.1. MOTIVATION AND OBJECTIVES

Most physical systems are inherently nonlinear, and highly-nonlinear systems cannot be effectively controlled over a wide range of conditions using controllers designed on the basis of linearized system models. Thus the area of nonlinear control design has been one of the most active control research areas over the last two decades, resulting in the development of many nonlinear control system designs [12, 27, 31, 33 45, 60, 62, 63]. However, most of these nonlinear controllers still have major issues that must be addressed, such as their inability to accommodate explicit input constraints, optimality, efficiency, optimization (tradeoff), etc.

The ill-effects of input constraints manifest themselves in the form of sluggish response and even instability [44], hence input constraint is a critical issue for practical implementation. If a controller is not optimal with respect to a meaningful cost function, then it does not satisfy control objectives with the smallest possible control action [44]. This non-optimal control solution directly leads to inefficiency and may also lead to actuator saturation. Also, optimization—typically the tradeoff between control effort and tracking error—is a key to flexible design and may provide solutions to input-constraint and efficiency issues. As indicated, these issues are closely related and are critical for

practical implementation, therefore they should be considered altogether in a unified manner at the design stage.

Feedback linearization (FBL) [27, 31, 45] and sliding mode control (SMC) [12, 60, 62, 63] are two widely used control schemes for nonlinear systems. FBL is popular because well-developed design techniques for linear systems can be applied to synthesize the appropriate controller for the linearized systems. SMC is attractive because it provides high-speed response, good transient performance and is insensitive to certain parameter variations and external disturbances [62, 63]. Despite these desirable features, few studies have attempted to address the above mentioned issues regarding FBL/SMC—they are not optimal with respect to a meaningful cost; they may generate unnecessarily large control effort to cancel beneficial nonlinearities [19, 20, 33], and they are unable to accommodate explicit input constraints. There have been several attempts to include the input-constraints [1, 29, 30, 39, 47, 48, 58, 64, 65], but the solutions could not be generalized, as will be explained in the next section. In terms of optimization of FBL/SMC, few studies have been reported.

To achieve optimality, which FBL and SMC solutions do not, nonlinear optimal control was proposed, however the difficulty in solving the Hamilton-Jacobi-Bellman/Isaac (HJB/HJI) equation makes it impractical [6, 40, 41, 42]. So, an inverse optimal control approach, which circumvents the task of solving a Hamilton-Jacobi equation and results in a controller optimal with respect to a meaningful cost functional, was employed [19, 20, 32, 34, 44]. Inverse optimal control uses a control Lyapunov function (clf), and it is based on the fact that

every clf solves the HJB equation associated with a cost functional. The clf method is effective for optimality and efficiency since it does not cancel beneficial nonlinearities, thereby possibly saving control effort [33]. However, a clf for a given system may be hard to find. The integrator backstepping method was introduced to provide a systematic construction procedure for a clf [31, 33]. However, they still have a limitation in handling explicit input constraints. Although nonlinear optimal control with input bounds was proposed in [40, 41], feedback gain matrices were extremely difficult to find and were valid for specific cases. Therefore, it is difficult to design a nonlinear control scheme to address all the major design issues in a unified way.

Hence, the following question arises: "How does one design a multi-purpose nonlinear controller in a unified manner but still satisfy special needs and optimizing efficiency?"

This question can be answered by using structural analysis in the design of the control systems. Structural information of a system/controller allows one to diagnose performance characteristics at the design stage and to make better selection of solution methods. By understanding the structure of the controller, the designer can deduce, a priori, the effects and contributions of control inputs and the behavior of the outputs. It is also possible to deduce the root causes of the specific problems (such as input-constraint-violation), the cost of control inputs, optimizing cost, etc—it is possible to identify the major design issues for the nonlinear controller.

Singular value decomposition is a powerful tool used for structural analysis, however, it is applicable only to linear systems, and therefore not applicable to nonlinear controllers directly. However, FBL/SMC possess a very useful structural feature—linear algebraic equivalence which will be shown and explained in Chapter 3—on which SVD structural analysis tools can be applied directly. Therefore, in this research, all controller designs will be developed based on FBL/SMC.

In this research, we develop a structural analysis, design and optimization method for nonlinear controllers using the linear algebraic equivalence to address major design issues in a systematic way. This work is an attempt to analyze and synthesize control technology using well-developed structural analysis tools, and to provide improved designs for the controllers.

1.2. OVERVIEW

In this research, the structural analysis and optimal design of FBL/SMC nonlinear controllers are proposed using SVD based on the linear algebraic equivalence of the nonlinear controller (LAENC). First, the LAENC of FBL/SMC are shown, and SVD is applied to the LAENC to show that the control inputs/outputs of the nonlinear controllers are composed of linear combinations of orthonormal vectors—control input/output mode shapes—just as the natural vibration of a linear mechanical system is composed of a linear combination of mode shapes. With those mode shapes and their corresponding weights (relative contributions), the pattern of control input/output (I/O) distribution is estimated.

The optimization (tradeoff) between control effort (energy saving) and performance, and input-constraint-satisfying control is explained by truncating control input/output modes. Control efficiency is described using the directionality of the output mode shapes.

It is also shown that it is possible to pose many different problems for nonlinear control designs using LAENC—minimization, maximization, optimization with constraints, and as a result, constrained nonlinear optimal controllers are proposed. Quadratic programming and constrained linear least squares methods are used to solve the proposed controllers. The proposed, general input-constraint-satisfying optimal nonlinear controllers are simple to design, directly applicable to nonlinear systems and are computationally efficient since they solve a linear least squares problem. It is structurally very similar to Linear Quadratic (LQ) control, model predictive control (MPC) and other optimal control problems since control actions are obtained through an optimal control strategy that minimizes a performance function. But it has the distinct advantage over LQ, MPC and other optimal controls in that it preserves the characteristics of FBL/SMC—one can design the output/state behavior with FBL and constrain the states to remain on the desired manifold with SMC. This is not possible with MPC and other optimal controls.

The proposed algorithms are applied to the temperature control of a thermal system with features that make it difficult to design the control system such as, more inputs than outputs (redundancy), high nonlinearity due to radiation heat transfer, input-constraints, ill-conditioned behavior (strong coupling effects

between elements), and large control effort. The proposed algorithms are applied to treat these issues. This application illustrates how the designer can apply the constrained nonlinear optimal controller, interpret mode shapes under constraints, modify the controller (mode shapes) to satisfy the input constraints, optimize the controller, and predict the input/output from the input/output mode shapes.

As part of the temperature control of a thermal system, new regularization embedded nonlinear controllers are proposed for the ill-conditioned and input constrained thermal system. Based on the analogy of LAENC and regularization method for the linear algebraic equations, Tikhonov, truncated singular value decomposition (TSVD) and modified TSVD (MTSVD) methods are embedded in the design of FBL/SMC controllers. These regularization embedded nonlinear controllers provide good temperature tracking and generate physically reasonable and actuator-constraint-satisfying solutions for the ill-conditioned system, in spite of modeling errors inherent in applying regularization.

In summary, this research explores structural analysis to the design of nonlinear control systems. It presents a unique interpretation of control input/output mode shapes and formulate the nonlinear problem in general form, LAENC: Finally the proposed approach is applied to physical system models with excellent optimal input–constraint-satisfying control designs.

1.3. LITERATURE REVIEW

The general nonlinear optimal control approach described by the HJB equation, clf, and inverse optimal control, was already mentioned in the previous

section. In this section, research reported on input-constrained nonlinear control systems are provided.

A common approach to designing nonlinear FBL control with constraints uses changes in the reference commands. Pappas et al. [48] calculated the regions of attraction of FBL controllers and characterized the space of feasible trajectories that do not violate input constraints. Similarly, Aguilar et al. [1] detuned the FBL to avoid input constraints. But these approaches [1, 48] generated unnecessarily poor performance [37]. Yip and Hedrick [65] devised a dynamic reference governor which changes the reference command to the feedback linearized system using a filtered version of the reference command. However, it is difficult to extend this approach to multi-input multi-output (MIMO) systems.

Valluri and Soroush [64] derived two nonlinear control laws satisfying input constraints by minimizing the difference between the closed loop output response and the nominal linear output response that the same control law induces when there are no constraints.

Another approach to accommodate input constraints is anti-windup schemes that modify the controllers to minimize the adverse effects of windup. It is based on an observer-based structure in which the difference between the computed input and the actual input to the process is fed back to the controller dynamics in an attempt to minimize the difference. Kendi and Doyle [30] proposed an instantaneous optimization method to minimize the performance loss associated with enforcing the actuator constraints. Within this framework, the nonlinear controller was represented as an optimal linear controller with an

auxiliary feedback loop which cancels the effects of nonlinear dynamics and measured disturbances. However, since the nonlinear corrective action is implemented by feedback, the difficulty arises in implementing a nonlinear internal-model-based-antiwindup contoller. Kapoor and Daoutidis [29] devised a nonlinear observer-based anti-windup algorithm, in which the anti-windup gain is a nonlinear function of the states of the system and with which it is possible to attenuate the effect of windup arbitrarily fast. However, in these researches ([29, 30, 64]), input constraints are not considered explicitly as part of the controller design. Instead, the controller is combined with an anti-windup compensator designed to minimize performance degradation caused by constraints [37]. Moreover, it is not possible to restrict the output behavior to the desired dynamics.

For SMC, Shyu and Lin [58] handled input constraints by computing a bound for the existence of sliding motion and used a switching surface with an integrator; but it is applicable only to linear systems. Lu and Chen [39] obtained the range of allowable reference inputs by estimating the maximum and minimum values of the control action to ensure sliding behavior throughout the response—but the approach is only applicable to linear time-varying systems. Okabayashi and Furuta [47] showed the effectiveness of using a nonlinear hypersurface (switching surface) instead of a conventional hyperplane as the switching surface; but this approach is applicable only to linear systems.

Popular approaches for the control of nonlinear systems with input constraints uses nonlinear optimization of MPC. MPC is a class of control

algorithms that utilize an explicit process model to predict the effects of future control actions on the output of the process [52]. The control sequence is computed using an optimal control strategy that minimizes a performance function which includes the differences between the desired and predicted process variables, and a penalty on the control effort. MPC is usually divided into nonlinear model predictive control (NMPC) and linear model predictive control (LMPC).

NMPC uses the nonlinear process model to predict the effects of future manipulated inputs on future values of the controlled outputs. NMPC handles input constraints by solving a nonlinear programming problem on-line for each sampling period. This approach is computationally expensive and potentially unreliable as the nonlinear programming algorithm may converge to a local minimum or even diverge [35].

LMPC minimizes a quadratic performance function, and the optimal solution, when subjected to linear constraints, is found by using quadratic programming (QP) routines. Using the convex nature of the problem, QP produces numerically efficient results by relying on fast gradient descent methods [7]. Despite the nice features of LMPC for linear systems, LMPC can not be applied directly to nonlinear processes. To exploit LMPC for nonlinear processes, a hybrid scheme is used by several researchers [7, 8, 35, 36, 37]—a combination of FBL and MPC. Using the resulting linearized system by FBL, the NMPC control problem is transformed into an optimization problem that minimizes a quadratic function, whose solutions can be found using reliable and fast quadratic

programming routines. However, FBL maps the original input linear constraints into nonlinear and state dependent constraints on the controller output [7], which invalidates the direct use of QP routines. Also, it requires the knowledge of future values of the input and state variables, which is not possible to determine until the constraints are specified. Instead of the exact mapping of future input constraints, Botto et al. [7] used iterative approximate mapping techniques, Henson and Kurtz [23] extended the linear constraint relations of the first prediction over the entire control horizon and others also proposed approximate mapping methods [8, 35, 36]. Therefore, MPC requires an additional complex approximation computation to utilize LMPC, and it is only applicable to feedback linearizable or linear systems.

All the above-mentioned methods of dealing with input constraints have disadvantages, such as complex designs, limits to linear systems only, and the need to change reference signals. Moreover, there is no way to restrict the output behavior to the desired dynamics. Therefore, a general nonlinear optimal input-constraint-satisfying control design process, that is easy to design and is able to restrict the output behavior to the desired dynamics, needs to be developed and is proposed in this work.

Chapter 2

Background Concepts

This chapter reviews the basic concepts of nonlinear controller designs and singular value decomposition that will be used to develop the structural analysis and optimization of nonlinear controllers in Chapters 3, 4 and 5. Also, a review of ill-conditioning is presented along with the regularization methods that address the difficulties in solving an ill-conditioned system—it will be used for the development of regularization embedded nonlinear controllers in Chapter 6.

2.1. NONLINEAR CONTROLLER DESIGNS: A BRIEF REVIEW OF FBL AND SMC

Feedback Linearization [18, 27, 31, 45, 60]: The FBL method finds a state feedback control law, such that the resulting closed loop system has desired linear input-output/input-state behavior. The terminology input-state and input-output linearization implies complete and partial linearization, respectively.

For a MIMO affine nonlinear system modeled as

$$\dot{\mathbf{x}}(t) = \frac{d\mathbf{x}(t)}{dt} = \mathbf{f}\big(\mathbf{x}(t)\big) + \sum_{k=1}^{m} g_k\big(\mathbf{x}(t)\big)u_k(t) = \mathbf{f}(\mathbf{x}) + \mathbf{g}(\mathbf{x})\mathbf{u} \tag{2.1}$$

$$y_i(t) = h_i\big(\mathbf{x}(t)\big) \quad i = 1,2,\ldots,p$$

where, $\mathbf{x} \in \mathbf{R}^n$ defines the system's model states, $\mathbf{u} \in \mathbf{R}^m$ are the controllable inputs, and $\mathbf{y} \in \mathbf{R}^p$ are the measurements or desired outputs, the FBL design

starts by finding the relative degree of the outputs, which is defined by the number of times one has to differentiate the output in order to solve for the input explicitly. In other words, each output y_i of Eq. (2.1) is differentiated with respect to time r_i times repeatedly, which is the relative order of the i^{th} output, i.e.

$$y_i^k = \frac{d^k y_i}{dt^k} = \begin{cases} L_f^k h_i(\mathbf{x}) & for \quad k < r_i \\ L_f^k h_i(\mathbf{x}) + L_g L_f^{k-1} h_i(\mathbf{x})\mathbf{u} & for \quad k = r_i \end{cases} \tag{2.2}$$

where, h_i denotes the i^{th} component of $\mathbf{h}$, $L_f^k h_i(x) : R^n \to R$ and $L_{g_k} h_i(x) : R^n \to R$ denote the Lie derivatives of $h_i(x)$ with respect to $f(x)$ and $g_k(x)$, respectively and they are defined in Appendix **A**. Equation (2.2) can be rewritten in vector-matrix form as follows

$$\mathbf{y^r} = \mathbf{c(x)} + \mathbf{D(x)u} \tag{2.3}$$

where $\mathbf{y^r} = \left[y_1^{r_1}, y_2^{r_2}, \cdots, y_p^{r_p}\right]^T$ and $\mathbf{r} = \left[r_1, r_2, \cdots, r_p\right]^T$ is the vector of relative degrees of the system. The decoupling matrix, **D**, is

$$\mathbf{D(x)} = \begin{bmatrix} L_{g_1} L_f^{r_1-1} h_1(\mathbf{x}) & \cdots & L_{g_m} L_f^{r_1-1} h_1(\mathbf{x}) \\ \vdots & \ddots & \vdots \\ L_{g_1} L_f^{r_p-1} h_p(\mathbf{x}) & \cdots & L_{g_m} L_f^{r_p-1} h_p(\mathbf{x}) \end{bmatrix} = \mathbf{L_g L_f^{r-1} h(x)}$$

$$\mathbf{c(x)} = \left[L_f^{r_1} h_1(x), \cdots, L_f^{r_p} h_p(x)\right]^T = \mathbf{L_f^r h} \ \ \mathbf{(x)} \tag{2.4}$$

If $\mathbf{D(x)}$ is nonsingular and $p = m$, we may choose the input-output decoupling control law

$$\mathbf{u} = \mathbf{D^{-1}(x)}\left[\mathbf{v} - \mathbf{c(x)}\right] = \left(\mathbf{L_g L_f^{r-1} h(x)}\right)^{-1}\left[\mathbf{v} - \mathbf{L_f^r h(x)}\right] \tag{2.5}$$

then,

$$\mathbf{y}^{\mathbf{r}} = \mathbf{c(x)} + \mathbf{D(x)}\,\mathbf{u} \xrightarrow{\mathbf{u}=\mathbf{D}^{-1}(\mathbf{x})[-\mathbf{c}(\mathbf{x})+\mathbf{v}]} \mathbf{y}^{\mathbf{r}} = \mathbf{v} \tag{2.6}$$

Under this feedback law, a suitable diffeomorphism (nonlinear coordinate transformation) $\begin{bmatrix}\boldsymbol{\xi} & \boldsymbol{\eta}\end{bmatrix}^{\mathbf{T}} = \boldsymbol{\Phi}(\mathbf{x})$ yields a partially linear system called *normal* form:

$$\begin{aligned}\dot{\boldsymbol{\xi}} &= \mathbf{A}\boldsymbol{\xi} + \mathbf{B}\mathbf{v} \\ \dot{\boldsymbol{\eta}} &= \mathbf{q}(\boldsymbol{\xi}, \boldsymbol{\eta}) \\ \mathbf{y} &= \mathbf{C}\boldsymbol{\xi}\end{aligned} \tag{2.7}$$

where, $\boldsymbol{\xi}$ and $\boldsymbol{\eta}$ are $\sum_{k=1}^{p} r_k$ and $n - \sum_{k=1}^{p} r_k$ dimensional state vectors, respectively, $\mathbf{v} \in \mathbf{R}^p$ is the fictitious input vector, and matrices **A**, **B** and **C** are in Brunovsky block canonical form. $\mathbf{q}(\cdot)$ is a vector of nonlinear functions when $\boldsymbol{\xi} = \mathbf{0}$, i.e., $\dot{\boldsymbol{\eta}} = \mathbf{q}(\mathbf{0}, \boldsymbol{\eta})$ which characterize the zero dynamics.

However, if the matrix $\mathbf{D(x)}$ is not invertible with $p = m$, i.e., singular, then a more elaborate procedure such as (modified-) Silverman's structure algorithm can be used [18, 27]. If $\mathbf{D(x)}$ is not square, i.e., $p \neq m$, the Moore-Penrose pseudo-inverse of $\mathbf{D(x)}$ can be used instead of inverse in Eq. (2.5).

To stabilize the linearized system described by Eq. (2.7), several well-developed linear control design methods can be applied. For example, the fictitious input $\mathbf{v}$ can use pole-placement as follows

$$v_i = w_i - \alpha_{i1} y_i^{r_i - 1} - \cdots - \alpha_{ir_i - 1} \dot{y}_i - \alpha_{ir_i} y_i \tag{2.8}$$

then the closed-loop output behavior is governed by

$$y_i^{r_i} + \alpha_{i1} y_i^{r_i - 1} + \cdots + \alpha_{ir_i - 1} \dot{y}_i + \alpha_{ir_i} y_i = w_i, i = 1, 2, \cdots, p \tag{2.9}$$

where w_i's are reference inputs, α_{ij}'s ($j = 1, 2, \cdots, r_i$), are the parameters to be chosen so that $s^{n_i} + \alpha_{i1} s^{r_i - 1} + \cdots + \alpha_{ir_i}$ are Hurwitz polynomials.

Sliding Mode Control [12, 60, 62, 63]: SMC was first proposed in the early 1950's, and it now enjoys a wide range of applications. In SMC, a candidate Lyapunov function is chosen such that it satisfies the reaching condition that the states move toward, reach and remain at the desired manifold S—the goal is to find a control that restricts the motion to the desired manifold S;

$$S = \left\{ x(t) \,\middle|\, s(x,t) = 0 \right\} \tag{2.10}$$

where $s = \left(s_1, s_2, \cdots, s_p\right)^T$ and $s_i(x)$, (i=1,2,…,p), are sliding surfaces which are continuous functions and can be defined by

$$s_i = \sum_{k=0}^{r_i - 1} \beta_k \frac{d^k e_i}{dt^k} \tag{2.11}$$

$$e_i = y_{d,i} - y_i \tag{2.12}$$

where $\left[r_1, r_2, \cdots, r_p\right]^T$ are the relative degrees of the system, similarly defined as in the FBL, but which are found by differentiating the sliding surface instead of the outputs. If the $\beta' s$ are selected as Hurwitz polynomials of the tracking errors of the associated states, the tracking errors, e_i's, converge to zero when the states are on the sliding surface, i.e., $s_i = 0$. A global reaching condition is given by Lyapunov stability theorem as

$$\dot{V}(S) < 0 \quad \text{when} \quad s \neq 0 \tag{2.13}$$

By choosing the candidate pseudo[1] Lyapunov function as

$$V(x,t) = \frac{s^T \cdot s}{2} \tag{2.14}$$

a reaching condition becomes equivalently for Eq. (2.14)

$$s^T \cdot \dot{s} < 0 \tag{2.15}$$

The condition can now be satisfied by setting

$$\dot{s} = -\eta \cdot \tanh(s) \tag{2.16}$$

where η is a strictly positive constant and tanh(·) is the hyperbolic tangent function which is used instead of a signum function to reduce the effects of chattering.

If Eq. (2.11) is substituted into Eq. (2.16), then

$$\begin{aligned} \dot{s} &= -\eta \cdot \tanh(s) \\ &= \sum_{k=1}^{\mathbf{r}} \beta_k \frac{d^k \mathbf{e}}{dt^k} = \sum_{k=1}^{\mathbf{r}} \beta_k \frac{d^k (\mathbf{y_d} - \mathbf{y})}{dt^k} \end{aligned} \tag{2.17}$$

where, $$\frac{d^{\mathbf{r}} \mathbf{y}}{dt^{\mathbf{r}}} = \mathbf{y}^{\mathbf{r}}(t) = \mathbf{L}_{\mathbf{f}}^{\mathbf{r}} \mathbf{h}(\mathbf{x}) + \mathbf{L}_{\mathbf{g}} \mathbf{L}_{\mathbf{f}}^{\mathbf{r}-1} \mathbf{h}(\mathbf{x})\, \mathbf{u} \tag{2.18}$$

Since Eq. (2.18) has an explicit expression of the control input, the control law now can be derived using Eqs. (2.17) and (2.18) as

$$\begin{aligned} \mathbf{u} &= \mathbf{D}(\mathbf{x})^+ \left\{ \mathbf{y}_{\mathbf{d}}^{\mathbf{r}} - \mathbf{c}(\mathbf{x}) - \sum_{k=1}^{\mathbf{r}-1} \beta_k \frac{d^k \mathbf{e}}{dt^k} - \eta \cdot \tanh(s) \right\} \\ &= \left(\mathbf{L}_{\mathbf{g}} \mathbf{L}_{\mathbf{f}}^{\mathbf{r}-1} \mathbf{h}(\mathbf{x}) \right)^+ \left\{ \mathbf{y}_{\mathbf{d}}^{\mathbf{r}} - \mathbf{L}_{\mathbf{f}}^{\mathbf{r}} \mathbf{h}(\mathbf{x}) - \sum_{k=1}^{\mathbf{r}-1} \beta_k \frac{d^k \mathbf{e}}{dt^k} - \eta \cdot \tanh(s) \right\} \end{aligned} \tag{2.19}$$

[1] V in Eq. (2.14) is not a true Lyapunov function because $\dot{s}$ depends not only on s, but also t, i.e., it contains $y_d(t)$.

2.2. SINGULAR VALUE DECOMPOSITION (SVD)

Consider a linear algebraic equation $\mathbf{Ax} = \mathbf{b}$ where $\mathbf{A}$ is a $m \times n$ matrix and $\mathbf{b}$ is $m \times 1$ vector. SVD of $\mathbf{A}$ is given by:

$$\mathbf{A} = \mathbf{U}\boldsymbol{\Sigma}\mathbf{V}^T \tag{2.20}$$

where $\mathbf{U} = [\mathbf{u}_1, \mathbf{u}_2, \cdots, \mathbf{u}_m]$, $\mathbf{V} = [\mathbf{v}_1, \mathbf{v}_2, \cdots, \mathbf{v}_n]$, $\boldsymbol{\Sigma} = diag\left(\sigma_1, \sigma_2, \cdots, \sigma_p \,\middle|\, \mathbf{0}\right)$ and $p = \min\{m, n\}$. $\mathbf{U} \in \mathbf{R}^{m \times m}$ and $\mathbf{V} \in \mathbf{R}^{n \times n}$ are unitary matrices and $\mathbf{u}_i$ and $\mathbf{v}_i$ are unit vectors and $\boldsymbol{\Sigma}$ contains the diagonal elements of singular values, σ_i's, arranged in descending order as $\sigma_1 \geq \sigma_2 \geq \cdots \geq \sigma_p$. The singular values σ_i's are the positive square roots of the p non-zero eigenvalues of the Hermitian matrix $\mathbf{A}^H\mathbf{A}$ or $\mathbf{A}\mathbf{A}^H$:

$$\sigma_i(\mathbf{A}) = \sqrt{\lambda_i\left(\mathbf{A}^H\mathbf{A}\right)} = \sqrt{\lambda_i\left(\mathbf{A}\mathbf{A}^H\right)} \tag{2.21}$$

The column vectors $\mathbf{v}_i$ of $\mathbf{V}$ are unit eigenvectors of the $n \times n$ matrix $\mathbf{A}^H\mathbf{A}$, and the column vectors $\mathbf{u}_i$ of $\mathbf{U}$ are unit eigenvectors of the $m \times m$ matrix $\mathbf{A}\mathbf{A}^H$. They are known as the right (input) and left (output) singular vectors of the matrix **A,** respectively.

Since the singular vectors form orthonormal bases, i.e., $\mathbf{V}^\mathbf{T}\mathbf{V} = \mathbf{I},\ \mathbf{U}^\mathbf{T}\mathbf{U} = \mathbf{I}$, an input vector $\mathbf{x}$ parallel to $\mathbf{v}_i$ yields the important relation

$$\mathbf{A}\mathbf{v}_i = \sigma_i\mathbf{u}_i \tag{2.22}$$

This equation states that each right singular vector is mapped onto the corresponding left singular vector with the magnification factor being the corresponding singular value. This input-output mapping can be better understood by the geometric interpretation in Fig. 2.1 [53]—vectors $\mathbf{v}_1$, $\mathbf{v}_2$ and $\mathbf{v}_3$ in the

input space are mapped to vectors $\sigma_1\mathbf{u}_1$, $\sigma_2\mathbf{u}_2$ and $\mathbf{\Phi}$ (zero vector) in the output space, respectively. Notice that each output vector $\mathbf{u}_i$ is scaled by the corresponding singular value σ_i, so $\mathbf{v}_3$ is mapped into the zero vector in the output space since the third singular value, σ_3, is zero. Thus any change made in the direction corresponding to the vector $\mathbf{v}_3$ maps into the zero vector in the output space—any input in that direction is not reflected in the output space. Alternatively from Eq. (2.22), if σ_i=0, then $\mathbf{A}\mathbf{v}_i = \mathbf{0}$—i.e. $\mathbf{v}_3$ forms the null space of **A** so any nonzero vector in the output space can be composed of a linear combination only of effective vectors $\mathbf{v}_1$ and $\mathbf{v}_2$ in the input space. These effective vectors are often called mode shapes in multivariable designs, or called design mode shapes specifically in structure modification applications where **A** represents the Jacobian matrix of the system, **x** is the design variable vector and **b** is the performance index vector as in [53].

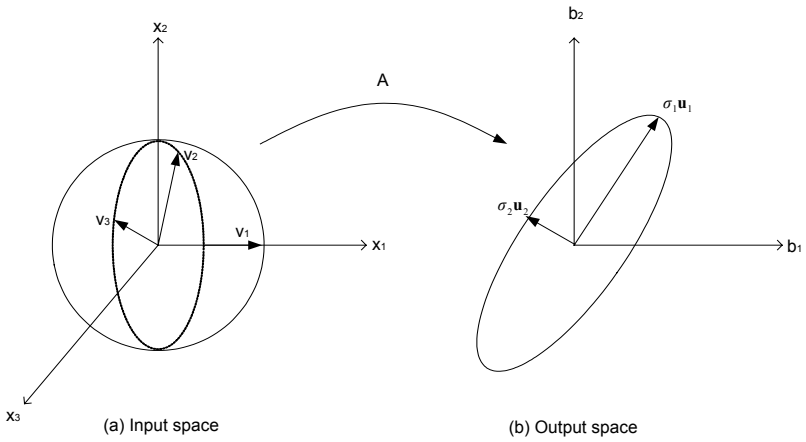

Figure 2.1 Geometric interpretation of SVD mapping (a) input mode shapes in the input space (b) scaled output mode shapes in the output space [53]

Using Eq. (2.20), the solution vector **x** to the linear algebraic equation $\mathbf{Ax} = \mathbf{b}$ is directly obtained as

$$\mathbf{x} = \sum_{i=1}^{rank(\mathbf{A})} \frac{\mathbf{u}_i^T \cdot \mathbf{b}}{\sigma_i} \mathbf{v}_i = \sum_{i=1}^{rank(\mathbf{A})} q_i \cdot \mathbf{v}_i \tag{2.23}$$

2.3. INVERSE PROBLEM, ILL-CONDITIONING AND REGULARIZATION

In many engineering problems that can be represented as Eq. (2.24) [21], the objective is to compute the output, given the input and the mathematical model of the system.

$$\int_{\Omega} system \times input \; d\Omega = output \tag{2.24}$$

However, one may be interested in determining the internal structure of a physical system from the system's measured behavior, or in determining the unknown input that gives rise to a measured output. This problem formulation is called the inverse problem [21]. This is in contrast to direct problems where the interest is in the system behavior given the input or internal structure. In general, the inverse problem is defined in terms of the Fredholm integral equation of the first kind:

$$f(x) = \int K(x, y) g(y) dy \tag{2.25}$$

where $f(x)$ is known or imposed, $g(y)$ is the unknown distribution and $K(x,y)$ is the kernel of the system. This formulation has received considerable attention because of its broad application in engineering, physics and other sciences.

However, the inverse problem, i.e. Fredholm integral equation of the first kind, is inherently ill-posed [21, 22, 24, 43]—the solution is extremely sensitive to arbitrarily small perturbations of the system, it does not depend continuously on the data, it is nearly indeterminate, and it may have multiple values. Therefore, infinitesimal perturbations in the input data may be amplified and the solution becomes unstable and is characterized by large oscillations.

Inverse problems in continuous domain are often divided into a certain number (m) of elements of uniform size, and Eqs. (2.24) and (2.25) are replaced by a set of algebraic descriptions;

$$\begin{aligned} &\sum_{j=1}^{m} \eta_{i,j} g_j = f_i \\ &or \qquad\qquad \Rightarrow \qquad \mathbf{Ax} = \mathbf{b} \\ &\sum_{j=1}^{m} \eta_{i,j} x_j = b_i \end{aligned} \tag{2.26}$$

Hansen [21] indicates that when an ill-posed problem (the set of integral equation, Eqs. (2.24) and (2.25)) is discretized into a set of linear algebraic equations for the input, the inherent difficulties also carry over to the discrete problem ($\mathbf{Ax} = \mathbf{b}$); the coefficient matrix $\mathbf{A}$ will have singular values that decay gradually toward zero and there is a large ratio of the largest to the smallest non-zero singular values (ratio called condition number). Such a discrete system is referred to as an ill-conditioned system [21, 24, 43].

The solution vector of $\mathbf{Ax} = \mathbf{b}$ can be directly obtained by singular value decomposition (SVD) as

$$\mathbf{x} = \sum_{i=1}^{rank(\mathbf{A})} \frac{\mathbf{u}_i^T \cdot \mathbf{b}}{\sigma_i} \mathbf{v}_i \tag{2.27}$$

where $\mathbf{u}_i$ and $\mathbf{v}_i$ are column vectors (the singular vectors of **A**) and σ_i are the singular values of **A**. Note in Eq. (2.27) that infinitesimal perturbations in **b** may be amplified by the corresponding small values of σ_i; if so, the resulting solution exhibits large fluctuations. In other words, the solution is potentially unstable to or extremely sensitive to perturbations in the data. Subsequently, standard matrix solvers such as Gaussian elimination, LU-decomposition and iterative solvers fail to generate physically reasonable solutions—the solution is practically underdetermined.

If an equation is ill-conditioned, meaningful solutions may still be found by introducing additional constraints on the possible solutions [21, 22, 24, 43]—this approach is called *regularization*. The dominating additional constraint is to require that the l_2-norm, or suitable norm of the solution, be small. This constraint tends to stabilize or regularize the solution, but introduces an error into the solution. Therefore the goal of the regularizing algorithm is to obtain a balance between minimizing the residual of the system of linear equations and minimizing the chosen regularizing norm of the solution.

In the early 1960's, Tikhonov developed the theory of regularization [43], and since then, several variants have been developed to compute the solution of ill-conditioned problems, such as truncated singular value decomposition (TSVD), modified TSVD (MTSVD), conjugate gradient method (CGM) and the

Tikhonov method. In this research, Tikhonov, TSVD and MTSVD methods will be used.

Tikhonov's Regularization [21, 22, 24, 43]: Tikhonov's regularization method minimizes a linear combination of the residual and weighted smoothing norms. That is,

$$\min_{\mathbf{x}} \mathbf{\Phi}_{\boldsymbol{\lambda}_{\mathbf{Tik}}}(\mathbf{x}) = \min_{\mathbf{x}} \left\{ \left\| \mathbf{A}\mathbf{x} - \mathbf{b} \right\|_2^2 + \boldsymbol{\lambda}_{\mathbf{Tik}}^2 \left\| \mathbf{L}_i \cdot (\mathbf{x} - \mathbf{x}_\mathbf{0}) \right\|_2^2 \right\} \tag{2.28}$$

where $\left\| \mathbf{L}_i \cdot (\mathbf{x} - \mathbf{x}_\mathbf{0}) \right\|_2$ is the smoothing norm, $\mathbf{L}_i$ is a diagonal weighting matrix or an approximation of the *i*-th derivative operator, $\boldsymbol{\lambda}_{\mathbf{Tik}}$ is the regularizing parameter, and $\mathbf{x}_0$ is an initial (biased) solution estimate. For $\mathbf{L}_i$, if *i*=0, the identity matrix will be used and

$$\mathbf{L}_1 = \begin{pmatrix} 1 & -1 & & \\ & \ddots & \ddots & \\ & & 1 & -1 \end{pmatrix} \in R^{(n-1)\times n}$$

$$\mathbf{L}_2 = \begin{pmatrix} 1 & -2 & -1 & \\ & \ddots & \ddots & \ddots \\ & & 1 & -2 & -1 \end{pmatrix} \in R^{(n-2)\times n} \tag{2.29}$$

Minimizing Eq. (2.28) with respect to **x** gives:

$$\frac{\partial \mathbf{\Phi}_{\boldsymbol{\lambda}_{\mathbf{Tik}}}(\mathbf{x})}{\partial \mathbf{x}} = 2\mathbf{A}^T(\mathbf{A}\mathbf{x} - \mathbf{b}) + 2\boldsymbol{\lambda}_{\mathbf{Tik}}^2 \mathbf{L}_i^T \{\mathbf{L}_i(\mathbf{x} - \mathbf{x}_0)\} = \mathbf{0}$$

$$\left(\mathbf{A}^T\mathbf{A} + \boldsymbol{\lambda}_{\mathbf{Tik}}^2 \mathbf{L}_i^T \mathbf{L}_i\right)\mathbf{x} = \mathbf{A}^T\mathbf{b} + \boldsymbol{\lambda}_{\mathbf{Tik}}{}^2 \mathbf{L}_i^T \mathbf{L}_i \mathbf{x}_0 \tag{2.30}$$

and this is simply equivalent to

$$\mathbf{A}_{\boldsymbol{\lambda}_i} \cdot \mathbf{x} = \mathbf{b}_{\boldsymbol{\lambda}_i} \tag{2.31}$$

where, $\mathbf{A}_{\lambda_i} = \mathbf{A}^T\mathbf{A} + \boldsymbol{\lambda}_{\mathbf{Tik}}^2\mathbf{L}_i^T\mathbf{L}_i$ and $\mathbf{b}_{\lambda_i} = \mathbf{A}^T\mathbf{b} + \boldsymbol{\lambda}_{\mathbf{Tik}}^2\mathbf{L}_i^T\mathbf{L}_i\mathbf{x}_0$.

Note, **x** is a function of $\boldsymbol{\lambda}_{\mathbf{Tik}}$, the relative weight of the regularization and residual norm terms. Larger $\boldsymbol{\lambda}_{\mathbf{Tik}}$ values provide a more smoothing effect. After regularization, any conventional matrix solver can be used to generate a solution that is accurate and stable.

The Tikhonov regularization parameter $\boldsymbol{\lambda}_{\mathbf{Tik}}$ is a design parameter that balances the residual and smoothing—its value should be selected carefully. A common approach is to use the L-curve [21, 22]—a convenient graphical tool to select an optimal parameter. It is a plot of the semi-norm of the smoothing constraint, $\left\|\mathbf{L}_i \cdot (\mathbf{x} - \mathbf{x_0})\right\|_2$, versus the corresponding residual norm, $\left\|\mathbf{Ax} - \mathbf{b}\right\|_2$, for different values of $\boldsymbol{\lambda}_{\mathbf{Tik}}$. When plotted on a log-log scale, the curve has an L-shaped corner for many problems. Since it balances the smoothing constraint and a small residual norm, this corner corresponds to the near optimal regularization parameter value [22, 43]. To generate the L-curve, Eq. (2.30) must be solved for several values of $\boldsymbol{\lambda}_{\mathbf{Tik}}$.

TSVD Regularization [21, 22, 24, 43]: For a rank-deficient matrix **A**, i.e. singular, some of the singular values of **A** will be exactly zero. For such a case, the least squares solutions to $\mathbf{Ax} = \mathbf{b}$ and $\min\left\|\mathbf{Ax} - \mathbf{b}\right\|_2$ are treated by eliminating the SVD components associated with the zero singular values and the solution is computed by Eq. (2.27).

For rank-deficient and ill-conditioned systems, the singular values may not be exactly zero but are very small numbers. These small singular values

inevitably cause the ill-conditioned nature. TSVD considers the given matrix as a noisy representation of a rank-deficient matrix, and replaces **A** by a matrix $\mathbf{A}_p$ that is close to **A** and also rank-deficient. A rank-*p* matrix is defined as

$$\mathbf{A}_p \equiv \sum_{i=1}^{p} \mathbf{u}_i \sigma_i \mathbf{v}^T{}_i \tag{2.32}$$

where small nonzero singular values $\sigma_{p+1},\cdots,\sigma_n$ are replaced by zeros. In other words, the TSVD solution is achieved by projecting the ill-conditioned matrix **A** onto the rank-p matrix—only the terms related to the largest *p* singular values are kept. Since **A** is replaced by $\mathbf{A}_p$, the TSVD solution is the least squares solution of the problem of $\min\left\|\mathbf{A}_p\mathbf{x}-\mathbf{b}\right\|_2$ and is given by

$$\mathbf{x_p} = \mathbf{A}_p^{+}\mathbf{b} = \sum_{i=1}^{p} \frac{\mathbf{u}_i^T \cdot \mathbf{b}}{\sigma_i} \mathbf{v}_i \tag{2.33}$$

where singular values $\sigma_{p+1},\cdots,\sigma_n$ are zero. In short, the solution of the TSVD is the minimum-norm least squares solution to

$$\min_{\mathbf{x}}\left\|\mathbf{x}\right\|_2 \text{ subject to } \min_{\mathbf{x}}\left\|\mathbf{A}_p\mathbf{x}-\mathbf{b}\right\|_2 \tag{2.34}$$

The number of singular values kept in the solution, *p*, is the regularization parameter of the TSVD method. For small *p* the solution is more stable but the residual $r=\left\|\mathbf{A}_p\mathbf{x}-\mathbf{b}\right\|_2$ is larger. Therefore, the TSVD solution requires an optimum balance between *p* and *r*.

MTSVD Regularization [21, 22, 24, 43]: The modified TSVD (MTSVD) regularization method is based on the problem of

$$\min_{\mathbf{x}}\left\|\mathbf{L}\mathbf{x}\right\|_2 \text{ subject to } \min_{\mathbf{x}}\left\|\mathbf{A_p}\mathbf{x}-\mathbf{b}\right\|_2 \tag{2.35}$$

where, **L** represents the smoothing operator being applied on the solution, and is chosen the same way as in the Tikhonov case [21, 43]. This is a more general method than the TSVD since other constraints can be imposed on the solution vector **x** rather than only imposing a minimum 2-norm as in Eq. (2.34). The solution to Eq. (2.35) is first obtained by getting the TSVD solution, $\mathbf{x_p}$, as given in Eq. (2.33) using the regularization parameter *p*. Next, a correction term to $\mathbf{x_p}$ is computed from the terms that were discarded from the linear combination of Eq. (2.33), i.e., from the numerical null space of matrix **A**. In this step, additional constraints or smoothing factors are introduced. The constraints are thus applied only to the terms that cause the solution's erratic or unstable behavior. Therefore, the MTSVD solution, $\mathbf{x_{L,p}}$, has the form

$$\mathbf{x_{L,p}} = \mathbf{x_p} - \mathbf{V_p^o}\left(\mathbf{LV_p^o}\right)^{+}\mathbf{Lx_p} \tag{2.36}$$

where $\mathbf{V_p^o}$ is formed by the remaining n-p singular vectors as

$$\mathbf{V_p^o} = \left[\mathbf{v_{p+1}}, \cdots, \mathbf{v_n}\right] \tag{2.37}$$

Notice that $\mathbf{z} = \left(\mathbf{LV_p^o}\right)^{+}\mathbf{Lx_p}$ is the solution to the least squares problem

$$\min_{\mathbf{x_p}} \left\| \left(\mathbf{LV_p^o}\right)\mathbf{z} - \mathbf{Lx_p} \right\|_2 \tag{2.38}$$

Also note that the TSVD solution $\mathbf{x_p}$ is the only regularized solution that has no component in the numerical null-space of **A**, spanned by the columns of $\mathbf{V_p^o}$. All other regularized solutions, such as the MTSVD solution, $\mathbf{x_{L,p}}$, have some component in the numerical null space of **A** in order to achieve the desired properties of the solution, as controlled by the matrix **L**.

As with the TSVD scheme, the regularization parameter of the MTSVD method is p. The choice of p is a compromise between the residual r and the level of smoothness imposed on the solution vector $\mathbf{x}$.

Chapter 3

Linear Algebraic Equivalence of Nonlinear Controllers (LAENC)

This chapter presents the linear algebraic equivalence of FBL/SMC controllers which will be used as a basis for the development of all the algorithms in the remaining chapters.

3.1. Linear Algebraic Equivalence of Nonlinear Controllers (LAENC)

From the design processes of FBL and SMC in Chapter 2, notice that both FBL and SMC controller designs (Eqs. (2.5) and (2.19)) are in the form

$$\mathbf{x_c} = \mathbf{A}^{+}\mathbf{b} \quad \Rightarrow \quad \mathbf{A}\mathbf{x_c} = \mathbf{b} \tag{3.1}$$

where,

$$\mathbf{u} = \mathbf{x_c} = \mathbf{A}^{+}\mathbf{b}$$

$$\mathbf{A} = \mathbf{L_g}\mathbf{L_f^{r-1}}\mathbf{h}(\mathbf{x})$$

$$\mathbf{b} = \begin{cases} \mathbf{v} - \mathbf{L_f^r}\mathbf{h}(\mathbf{x}) & for \quad FBL \\ \mathbf{y_d^r} - \mathbf{L_f^r}\mathbf{h}(\mathbf{x}) - \sum_{k=1}^{\mathbf{r}-1} \beta_k \frac{d^k \mathbf{e}}{dt^k} - \boldsymbol{\eta} \cdot \tanh(\mathbf{s}) & for \quad SMC \end{cases}$$

Equation (3.1) is a set of linear algebraic equations in which the solution $\mathbf{x_c}$ is the control input vector and is obtained by matrix inversion. This is a significant representation of the nonlinear control design since well-developed

linear algebraic equation solution techniques can be applied directly to satisfy the FBL and SMC nonlinear controller characteristics. Therefore, this useful linear algebraic equivalence of the nonlinear controllers (LAENC) will be used as a basis for the development of many different algorithms presented in the remaining chapters. Note that the LAENC is based upon the assumption that the system can be represented in the normal form, matrix **D(x)** is invertible, i.e., Silverman's structure algorithm is not required, and the system has stable zero dynamics.

3.2. SOLUTIONS TO THE LAENC

Note that the control input vector $\mathbf{x_c}$ in Eq. (3.1) is simply obtained by matrix inversion. However, the solution to Eq. (3.1) is neither unique nor does it always exist. Once the dimension of the solution vector (number of inputs, i.e. controllers) is less than the number of equations (outputs/sliding surfaces), and matrix $\mathbf{A} \in \mathbf{R}^{p \times m}$ has full column rank (m), the solution does not exist and the problem becomes a least squares problem. On the other hand, if the dimension of the solution vector is larger than the number of equations and matrix **A** has full row rank (p) for $\mathbf{A} \in \mathbf{R}^{p \times m}$, the problem is redundant and has an infinite number of solutions. In selecting an optimal solution, a unique solution can be found by considering certain constraints, such as minimizing the control input vector $\|\mathbf{x_c}\|_2^2$. Such an optimal solution can be found by using the pseudo-inverse of **A,** represented as $\mathbf{A}^+$. Even if there is no solution, the psedo-inverse provides the best approximation that minimizes the squared error;

$$\|\mathbf{A}\mathbf{x_c} - \mathbf{b}\|_2^2 \tag{3.2}$$

Chapter 4

Constrained Nonlinear Optimal Control

Physical systems are often subject to input constraints which makes control design more difficult. If a design does not take into account bounds on control inputs and if the control signals saturate during operation, the stability and performance of the closed loop system are diminished. Hence, control solutions for highly nonlinear systems with input constraints are important research areas.

Feedback linearization and sliding mode control are two widely used control schemes for nonlinear systems, however, their design processes do not accommodate explicit input constraints. Furthermore, they are not optimal and are inefficient since they may generate unnecessarily large control effort to cancel beneficial nonlinearities [19, 20, 33]. The issues of input constraint, optimality, and efficiency are important for practical implementation. Therefore, in this chapter, a general nonlinear optimal control design is developed which accommodates input constraints, optimality and efficiency using the linear algebraic equivalence of the nonlinear controller (LAENC).

4.1. Problem Formulation using LAENC: Quadratic Minimization (Minimum Effort Control)

As indicated in Chapter 3, the FBL/SMC nonlinear control designs are in the form of $\mathbf{Ax_c=b}$—a set of linear algebraic equations. Hence many different

problems can be formulated based on the LAENC—minimization, maximization, optimization (tradeoff) and constraints can be treated.

As an example, first consider the design of a nonlinear control (FBL/SMC) with minimum control energy. Assume the cost associated with the inputs is represented as follows:

$$J = m_1^2 x_1^2 + m_2^2 x_2^2 + \cdots + m_m^2 x_m^2 = \|\mathbf{Mx}\|_2^2 \tag{4.1}$$

where **M** is the weighting matrix and x_i's are control inputs for each controller. The subscript $_{\mathbf{c}}$ on control input vector $\mathbf{x}_{\mathbf{c}}$ was omitted in Eq. (4.1) and for the sake of simplicity, will be omitted hereafter for the remainder of this chapter. The vector **x** appearing in this chapter represents the control input vector, not a state vector.

The solution that minimizes the cost function and that satisfies the control performance of FBL/SMC can be obtained by solving the following problem:

$$\min_{\mathbf{x}} \|\mathbf{Mx}\|_2^2 \quad \text{such that} \quad \mathbf{Ax} = \mathbf{b} \tag{4.2}$$

The solution can be interpreted as finding an inverse (or pseudo-inverse) of **A,** i.e., $\mathbf{x} = \mathbf{A}^{+}\mathbf{b}$ when the weighting matrix **M** is identity. This problem is a special case of the general quadratic minimization problem defined by

$$\min_{\mathbf{x}} \left\{ \frac{1}{2}\mathbf{x}^{\mathrm{T}}\mathbf{Hx} + \mathbf{f}^{\mathrm{T}}\mathbf{x} \right\} \quad \text{such that} \quad \mathbf{Ax} = \mathbf{b} \tag{4.3}$$

where **H** is an $m \times m$ positive definite matrix and **f** is a coefficient vector. Fast and reliable quadratic programming routines can be used to find the solution to this problem.

4.2. CONSTRAINED NONLINEAR CONTROL

It is of interest to consider the case of controllers with constraints on their magnitudes. The problem now becomes a quadratic minimization problem with bounds on the solution:

$$\min_{\mathbf{x}} \frac{1}{2}\mathbf{x}^{\mathrm{T}}\mathbf{H}\mathbf{x} + \mathbf{f}^{\mathrm{T}}\mathbf{x} \quad \text{such that} \quad \mathbf{A}\mathbf{x} = \mathbf{b}\,, \quad \mathbf{x}_{\min} \le \mathbf{x} \le \mathbf{x}_{\max} \tag{4.4}$$

where $\mathbf{x}_{\min}$ and $\mathbf{x}_{\max}$ represent the lower and upper bounds for each controller, respectively.

The existence of a solution is not guaranteed with the bounds on the solution, therefore if the solution is not feasible, then the problem should be transformed into an optimization problem in which a residual arises to satisfy the input bounds, rather than a minimization problem in which $\mathbf{A}\mathbf{x} = \mathbf{b}$ is perfectly satisfied, i.e. no residual. Since the input constraints must be satisfied, one can think of the constrained linear least squares problem defined by

$$\min_{\mathbf{x}} \left\| \mathbf{A}\mathbf{x} - \mathbf{b} \right\|_2^2 \quad \text{such that} \quad \mathbf{x}_{\min} \le \mathbf{x} \le \mathbf{x}_{\max} \tag{4.5}$$

For this case, the solution is always guaranteed but a residual arises to satisfy the input bounds. This residual can be considered as a modeling error which diminishes performance.

4.3. CONSTRAINED NONLINEAR OPTIMAL CONTROL

The original problem was to minimize the control effort satisfying the constraint $\mathbf{A}\mathbf{x} = \mathbf{b}$, $\mathbf{x}_{\min} \le \mathbf{x} \le \mathbf{x}_{\max}$, but the constrained linear least squares problem, Eq. (4.5), does not deal with minimizing the control effort.

Therefore, a new cost function is defined as

$$J = \sum_{i=1}^{p} \left(A_i x - b_i\right)^2 + \gamma^2 \sum_{i=1}^{m} m_i^2 x_i^2 = \left\|\mathbf{Ax} - \mathbf{b}\right\|_2^2 + \boldsymbol{\gamma}^2 \left\|\mathbf{Mx}\right\|_2^2 \tag{4.6}$$

and a new optimization problem is posed as;

$$\min_{\mathbf{x}} J = \min_{\mathbf{x}} \left\{ \left\|\mathbf{Ax} - \mathbf{b}\right\|_2^2 + \boldsymbol{\gamma}^2 \left\|\mathbf{Mx}\right\|_2^2 \right\} \tag{4.7}$$

where, γ^2 is the weighting parameter that balances tradeoff between minimum control effort and control performance.

Equation (4.7) can also be represented in augmented form as

$$\begin{aligned} &\min_{\mathbf{x}} \left\| \begin{pmatrix} \mathbf{A} \\ \boldsymbol{\gamma}\mathbf{M} \end{pmatrix} \mathbf{x} - \begin{pmatrix} \mathbf{b} \\ \mathbf{0} \end{pmatrix} \right\|_2^2 = \min_{\mathbf{x}} \left\| \mathbf{A}_{aug}\mathbf{x} - \mathbf{b}_{aug} \right\|_2^2 \\ &\text{where,} \quad \mathbf{A}_{aug} = \begin{pmatrix} \mathbf{A} \\ \gamma\mathbf{M} \end{pmatrix} \in \mathbf{R}^{(p+m)\times m}, \ \mathbf{b}_{aug} = \begin{pmatrix} \mathbf{b} \\ \mathbf{0} \end{pmatrix} \in \mathbf{R}^{(p+m)\times 1} \end{aligned} \tag{4.8}$$

The analytical solution to this problem can be obtained by the following equation if there are no constraints on **x**. That is, minimizing Eq. (4.7) with respect to **x** gives:

$$\frac{\partial J}{\partial \mathbf{x}} = \mathbf{2A}^{\mathbf{T}}\left(\mathbf{Ax} - \mathbf{b}\right) + \mathbf{2}\boldsymbol{\gamma}^{\mathbf{2}}\mathbf{M}^{\mathbf{T}}\mathbf{Mx} = \mathbf{0} \tag{4.9}$$

$$\left(\mathbf{A}^{\mathbf{T}}\mathbf{A} + \boldsymbol{\gamma}^{\mathbf{2}}\mathbf{M}^{\mathbf{T}}\mathbf{M}\right)\mathbf{x} = \mathbf{A}^{\mathbf{T}}\mathbf{b}$$

$$\mathbf{x} = \left(\mathbf{A}^{\mathbf{T}}\mathbf{A} + \boldsymbol{\gamma}^{\mathbf{2}}\mathbf{M}^{\mathbf{T}}\mathbf{M}\right)^{-1}\mathbf{A}^{\mathbf{T}}\mathbf{b}$$

and similarly the minimizing Eq. (4.8) gives the solution as

$$\frac{\partial J}{\partial \mathbf{x}} = \mathbf{2}\mathbf{A}_{aug}{}^{\mathbf{T}}\left(\mathbf{A}_{aug}\mathbf{x} - \mathbf{b}_{aug}\right) = \mathbf{0}$$

$$
\begin{aligned}
\mathbf{x} &= (\mathbf{A}_{aug}^{T}\mathbf{A}_{aug})^{-1}\mathbf{A}_{aug}^{T}\mathbf{b}_{aug} \\
&= \left(\begin{bmatrix}\mathbf{A}^{T} & \gamma\mathbf{M}^{T}\end{bmatrix}\begin{bmatrix}\mathbf{A} \\ \gamma\mathbf{M}\end{bmatrix}\right)^{-1}\begin{bmatrix}\mathbf{A}^{T} & \gamma\mathbf{M}\end{bmatrix}\begin{bmatrix}\mathbf{b} \\ \mathbf{0}\end{bmatrix} \\
&= \left(\mathbf{A}^{\mathbf{T}}\mathbf{A} + \boldsymbol{\gamma}^{\mathbf{2}}\mathbf{M}^{\mathbf{T}}\mathbf{M}\right)^{-1}\mathbf{A}^{\mathbf{T}}\mathbf{b}
\end{aligned}
\tag{4.10}
$$

However, with the input constraints, an analytical solution for the optimal control vector can no longer be found.

Equation (4.7) is an optimization problem. The designer must make a tradeoff between minimizing the control effort and system performance by using weight γ. As γ increases, more weight is given to reduce the control effort thereby diminishing the system performance.

Notice that this approach is very similar to using linear optimal (LQ) control and MPC, where the basic idea is to find control inputs that minimize a cost function that balances error and control effort. However there is a distinct difference between this problem formulation and that using LQ and MPC—the control input obtained by this solution not only minimizes the cost function to balance error and control effort, which LQ and MPC can do as well, but it also preserves the characterstics of the nonlinear controller on which the process was based, i.e. FBL/SMC. In other words, satisfying $\mathbf{Ax} = \mathbf{b}$ guarantees the designer's desired output dynamics/sliding behavior. LQ and MPC minimizes the performance index but does not make the outputs follow the desired output dynamics/sliding behavior.

Due to the performance index tradeoffs, $\mathbf{Ax} = \mathbf{b}$ is not perfectly satisfied, but the solution can be close depending on the value of γ. This solution vector,

x, guarantees the output dynamics/sliding behavior to be as close as it was originally designed.

To summarize, the algorithm for the constrained nonlinear optimal control designs are:

1) if feasible solutions exist which satisfy

$$\mathbf{Ax} = \mathbf{b} \quad \text{such that} \quad \mathbf{x}_{\min} \le \mathbf{x} \le \mathbf{x}_{\max} \tag{4.11}$$

then the constrained quadratic minimization problem is

$$\min_{\mathbf{x}} \frac{1}{2}\mathbf{x}^{\mathrm{T}}\mathbf{Hx} + \mathbf{f}^{\mathrm{T}}\mathbf{x} \quad \text{such that} \quad \mathbf{Ax} = \mathbf{b} \text{ and } \mathbf{x}_{\min} \le \mathbf{x} \le \mathbf{x}_{\max} \tag{4.12}$$

2) if the solution is not feasible, then the constrained linear least squares problem is

$$\min_{\mathbf{x}} \left\{ \left\| \mathbf{Ax} - \mathbf{b} \right\|_2^2 + \gamma^2 \left\| \mathbf{Mx} \right\|_2^2 \right\} \text{ such that } \mathbf{x}_{\min} \le \mathbf{x} \le \mathbf{x}_{\max} \tag{4.13}$$

These two steps can be approximated with sufficiently small γ^2 in a unified manner as:

$$\min_{\mathbf{x}} \left\{ \left\| \mathbf{Ax} - \mathbf{b} \right\|_2^2 + \gamma^2 \left\| \mathbf{Mx} \right\|_2^2 \right\} \text{ such that } \mathbf{x}_{\min} \le \mathbf{x} \le \mathbf{x}_{\max} \tag{4.14}$$

since the solution to Eq. (4.14) when there exist feasible solutions—i.e., Eq. (4.9)—can be approximated as the solution to Eq. (4.12) with sufficiently small γ^2 and if **M** is chosen such that

$$\frac{1}{2}\mathbf{x}^{\mathrm{T}}\mathbf{Hx} + \mathbf{f}^{\mathrm{T}}\mathbf{x} = \left\| \mathbf{Mx} \right\|_2^2 \tag{4.15}$$

Equation (4.14) can be simplified, as shown in Eq. (4.8), to the constrained nonlinear optimal problem:

$$\min_{\mathbf{x}} \left\| \mathbf{A}_{aug}\mathbf{x} - \mathbf{b}_{aug} \right\|_2^2 \quad \text{such that} \quad \mathbf{x}_{\min} \le \mathbf{x} \le \mathbf{x}_{\max} \tag{4.16}$$

This formulation is in the same form as linear least squares; therefore the same solution techniques can be applied to solve the problem.

Notice here that this two criteria optimization problem (between residual and control effort) can be easily extended to multiple criteria optimization by adding additional linear criteria such as

$$\min_{\mathbf{x}} J = \min_{\mathbf{x}} \left\{ \left\| \mathbf{A}\mathbf{x} - \mathbf{b} \right\|_2^2 + \boldsymbol{\gamma}^2 \left\| \mathbf{M}\mathbf{x} \right\|_2^2 + \beta^2 \left\| \mathbf{L}\mathbf{x} \right\|_2^2 + \alpha^2 \left\| \mathbf{C}\mathbf{x} - \mathbf{d} \right\|_2^2 + \cdots \right\} \tag{4.17}$$

where **L**, **C**, **d** are arbitrary constraint matrices and β, α are optimization parameters. This means that the number of rows of matrix $\mathbf{A}_{aug}$ in Eq. (4.18) can be extended to any size depending on the size of the additional constraints added. Equation (4.17) is equivalent to

$$\begin{aligned} &\min_{\mathbf{x}} \left\| \begin{pmatrix} \mathbf{A} \\ \boldsymbol{\gamma}\mathbf{M} \\ \beta\mathbf{L} \\ \alpha\mathbf{C} \end{pmatrix} \mathbf{x} - \begin{pmatrix} \mathbf{b} \\ \mathbf{0} \\ \mathbf{0} \\ \alpha\mathbf{d} \end{pmatrix} \right\|_2^2 = \min_{\mathbf{x}} \left\| \mathbf{A}_{aug}\mathbf{x} - \mathbf{b}_{aug} \right\|_2^2 \\ &\text{where,} \quad \mathbf{A}_{aug} = \begin{pmatrix} \mathbf{A} \\ \gamma\mathbf{M} \\ \beta\mathbf{L} \\ \alpha\mathbf{C} \end{pmatrix}, \quad \mathbf{b}_{aug} = \begin{pmatrix} \mathbf{b} \\ \mathbf{0} \\ \mathbf{0} \\ \alpha\mathbf{d} \end{pmatrix} \end{aligned} \tag{4.18}$$

This problem is still in the same form as Eq. (4.8), hence it can be solved by the same solution methods used for Eq. (4.8).

If the constraints added are nonlinear instead of linear, the problem becomes a nonlinear optimization problem. Therefore in this work, the focus is

restricted to the linear constraints only such that the optimization problem can be solved without the use of nonlinear programming techniques which are computationally expensive and potentially unreliable.

4.4. SUMMARY

In this chapter, a general nonlinear optimal input-constraint-satisfying controller is developed which is simple to design, directly applicable to nonlinear systems and is computationally efficient since it solves a linear least squares problem. The fundamental approach is to use a linear algebraic equivalence of the nonlinear controllers. It is structurally very similar to LQ, MPC and other nonlinear optimal controllers that solve the HJB equation since control actions are obtained through an optimal control strategy that minimizes a performance function. However, it has the distinct advantage over LQ, MPC and HJB nonlinear optimal control in that it preserves the characteristics of FBL/SMC—one can design the output/state behavior with FBL and constrain the states to remain on the desired manifold with SMC. This is not possible with LQ, MPC and other nonlinear optimal control.

Chapter 5

Structural Analysis and Optimization of Nonlinear Control Systems using Singular Value Decomposition

The structure of a controlled system provides a designer with useful information to diagnose and enhance system performance in advance and to make a better choice of solution methods. Investigating the controllers/systems by structural analysis can provide key ideas about the nonlinear controller design issues such as input-constraints, optimization and efficiency.

Eigenstructure and singular value decomposition (SVD) methods are widely used structural analysis methods in linear system analysis. For example, the desired closed-loop performance characteristics of a MIMO system can be specified by eigenvalues and eigenvectors in an eigenstructure assignment [38]. SVD is often applied to multivariable decoupling systems to create structured inputs and outputs that are non-interacting [61]. SVD has been applied to many control problems such as the motion control of a rank deficient robot [55], state-order reduction [14], robust control system design [59, 66], measure of interactions between inputs and outputs in MIMO systems [5, 28], process directionality [56] and measure of the ill-conditionedness of a process [56].

Nonlinear controllers are used in many engineering applications, however, few have attempted to analyze the structure of nonlinear controllers since the typical structural methods are restricted to linear systems only. In this chapter, the structural analysis and optimization of nonlinear FBL and SMC controllers using

SVD are proposed based on the linear algebraic equivalence of the nonlinear controller (LAENC). By applying SVD to the LAENC, it is shown that the control inputs/outputs of the nonlinear controllers are composed of linear combinations of orthonormal vectors—control input/output mode shapes—just as free vibration of a linear mechanical system is composed of a linear combination of mode shapes. With those mode shapes and their corresponding weights (relative contributions), the pattern of control input/output (I/O) distribution is estimated. The optimization (tradeoff) between control effort (energy saving) and performance (residue) is achieved by truncating control input/output modes. Finally, controller efficiency is addressed using the directionality of the output mode shapes.

5.1. CONTROL INPUT/OUTPUT MODE SHAPES OF NONLINEAR CONTROLLERS

The LAENC form of the nonlinear controller design $\mathbf{A}\mathbf{x}_c = \mathbf{b}$ (Eq. (3.1)) is very similar to the multivariable design and optimization problem formulated in many cases as $\Delta\mathbf{P} = \mathbf{J}\Delta\mathbf{x}$ where **J** is the Jacobian matrix of the system, **x** is the design variable vector and **P** is the performance index vector as in [50, 51, 53, 54]. Hence many useful concepts and analysis tools used in multivariable design and optimization problems can be extended to the nonlinear controller designs using LAENC.

SVD is a very useful structural design method for multivariable systems, but it is only applicable to linear systems. However, using the LAENC one can take advantage of SVD for the structural design and analysis of nonlinear

controllers. Consider the nonlinear controller design defined as $\mathbf{A}\mathbf{x}_\mathbf{c} = \mathbf{b}$ where matrix $\mathbf{A} \in \mathbf{R}^{p \times m}$ is the characteristic of the controller (Lie derivatives of the output) as in Eq. (3.1), $\mathbf{b} \in \mathbf{R}^{p \times 1}$ is the target vector and $\mathbf{x}_\mathbf{c} \in \mathbf{R}^{m \times 1}$ is the control input. As mentioned in Chapter 3, if $m<p$, the solutions do not exist, therefore the discussions will focus on $m \geq p$ case only.

If Fig. 2.1 (Chapter 2) that describes the $\mathbf{A} \in \mathbf{R}^{2 \times 3}$ mapping is extended to the $\mathbf{A} \in \mathbf{R}^{p \times m}$ mapping, then any target vector **b** can be achieved by a linear combination of the scaled output vectors as

$$\mathbf{b} = q_1 \sigma_1 \mathbf{u}_1 + q_2 \sigma_2 \mathbf{u}_2 + \cdots + q_p \sigma_p \mathbf{u}_p \tag{5.1}$$

where $\mathbf{u}_i$'s and σ_i's are left singular vectors and singular values of the matrix **A**, respectively, but note that each scaled output in Eq. (5.1) is already obtained by a mapping from the corresponding input vectors $\mathbf{V} = [\mathbf{v}_1, \mathbf{v}_2, \cdots, \mathbf{v}_m]$. From this relation, it is inferred that any target vector **b** in the output space can be achieved by a linear combination of input vectors.

$$\begin{array}{ccccccc} \mathbf{b} = & q_1 \sigma_1 \mathbf{u}_1 & + q_2 \sigma_2 \mathbf{u}_2 & + \cdots + & q_p \sigma_p \mathbf{u}_p & & \\ & \updownarrow & \updownarrow & & \updownarrow & & \\ \mathbf{x}_\mathbf{c} = & q_1 \mathbf{v}_1 & + q_2 \mathbf{v}_2 & + \cdots + & q_p \mathbf{v}_p & + q_{p+1} \mathbf{v}_{p+1} + \cdots + & q_m \mathbf{v}_m \end{array} \tag{5.2}$$

However, if any singular values are zero or $m>p$, i.e. number of inputs exceed the number of outputs, then not all the input vectors are mapped to the output vectors. For example, if $m>p$, matrix **A** could have only p singular values (assuming rank(**A**)=p) hence input vectors $\mathbf{v}_{p+1}, \mathbf{v}_{p+2}, \cdots, \mathbf{v}_m$ do not have a mapping pair in the output space, since the corresponding singular values are zero. Therefore, only input vectors $\mathbf{v}_1, \mathbf{v}_2, \cdots, \mathbf{v}_p$ contribute to the output space.

The vectors $\mathbf{v}_{p+1}, \mathbf{v}_{p+2}, \cdots, \mathbf{v}_m$ spanned by the *m-p* independent vectors form the null space of **A** and are perpendicular to $\mathbf{v}_1, \mathbf{v}_2, \cdots, \mathbf{v}_p$—for a system with more inputs than outputs, i.e. $m > p$, matrix **A** always has a kernel. This indicates that control inputs that affect the target **b** in the output space should be in the subspace spanned by vectors $\mathbf{v}_1$ through $\mathbf{v}_p$, and this is expressed by

$$\mathbf{x}_\mathbf{c} = \sum_{i=1}^{rank(\mathbf{A})} q_i \cdot \mathbf{v}_i \tag{5.3}$$

These effective vectors, $\mathbf{v}_1, \mathbf{v}_2, \cdots, \mathbf{v}_p$ in the input space will be called control-input mode shapes. The term mode shape is used based on the analogy of mode shapes in vibration in that any natural response of a linear system is a linear combination of mode shapes [26] and on the analogy of design mode shapes in structural modification in that any performance of a system is a linear combination of design mode shapes as in [53, 54]. In the same manner, since all possible target vectors in the output space are linear combinations of vectors $\mathbf{u}_1, \mathbf{u}_2, \cdots, \mathbf{u}_p$ with weights corresponding to the singular values, $\mathbf{u}_1, \mathbf{u}_2, \cdots, \mathbf{u}_p$ will be called output mode shapes.

It should be noted that if any singular value is zero, then its corresponding control-input mode shape is also in the null space of **A**. The significance of the control-input null space is that any control inputs to the system that are in the same shape as the input modes belonging to the null space, will produce no changes in the output.

Since the control input is a linear combination of the control-input modes, the designer can examine all the modes to assess the control input distribution

pattern. For example, if an input mode has a high peak value, the designer could, in advance, predict that the control solution may violate input constraints. In this case, the designer could truncate that potentially dangerous input mode so that the total control solution does not violate constraints. However, this truncation will affect the system performance as will be discussed in the next section. It is also possible to estimate which controller requires a large control effort.

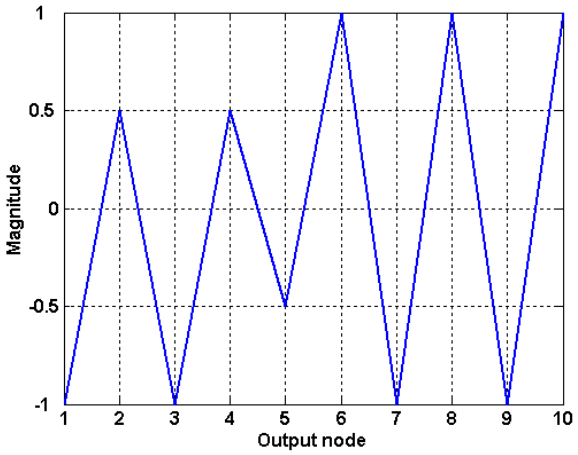

Figure 5.1 Arbitrary output mode shape

The designer can use the output mode shapes to assess tradeoffs in the outputs. For example, consider weight q_1 in Eq. (5.2) to be much larger than the other weights in the output combination. Since σ_1 is the largest singular value, $q_1\sigma_1$ is dominant among the coefficients of the linear combination—the actual output will be largely dependent on the first output mode shape. Assuming Fig. 5.1 is the first output mode shape, the designer can observe that even-numbered and odd-numbered output nodes have different signs, which means even and odd

output nodes can not be increased or decreased at the same time. In other words, to increase an even node, odd nodes must be decreased. Also, considering the size of each node, if the 6^{th} output node must be increased, then the 2^{nd} and 4^{th} output nodes must be increased half as much as the increase in the 6^{th} node.

5.2. COLINEARITY AND OPTIMIZATION

As indicated previously, input modes are mapped in pairs onto the output modes that are scaled by the corresponding singular values. Thus, truncating some input modes has the effect of truncating the paired output modes, and vice versa. Truncating the output modes that are part of the linear combination of the target vector would degrade performance. If, however, the truncated output mode contributes little to the target vector, then there would be little performance degradation and it would be possible to save control effort equal in size to the weighted input mode that is paired with the truncated output mode. Cutting off any input mode that consumes large control input—i.e. one with a large weight q_i in the input mode combination—but contributes little to the total performance, will save significant energy with little performance degradation.

Truncating input modes to save control effort results in performance degradation and creates an optimization problem. The mode truncation criteria should consider how much each output mode contributes to the output (target vector **b**) and how much each input mode contributes to the total control effort. This problem can be explained graphically by Fig. 5.2.

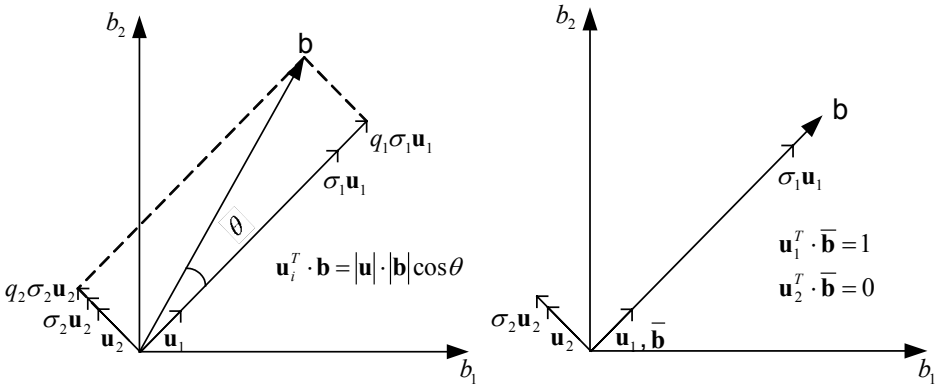

Figure 5.2 Graphical interpretation of colinearity (a) colinearity by inner product (b) normalized colinearity

Target vector **b** is made up of a linear combination of weighted (q_i) and scaled (σ_i) output modes $\mathbf{u}_i$'s. From Fig. 5.2(a), it is clear that the output mode shape $\mathbf{u}_i$ that leans more toward **b** contributes more to **b**—the degree of dependency of **b** on any output mode shape can be obtained by the inner product of those two vectors. The inner product can be used as a measure of the colinearity or parallelism of the two vectors—this performance dependency of the target vector **b** on each output mode will be called the colinearity, defined by $\mathbf{u}_i^T \cdot \mathbf{b}$. Using this indicator, the designer can identify which output modes are dominant in achieving the target vector and which modes contribute little. Instead of using an arbitrary-sized vector **b**, a normalized unit vector $\bar{\mathbf{b}}$ would make it simple to compare the colinearity of each output mode since colinearity spans from zero to one only as in Fig. 5.2(b). Note that the sum of the squares of the colinearities of the normalized vectors should equal one,

$$\sqrt{\sum_{i}^{p}\left(\mathbf{u}_i^T \cdot \bar{\mathbf{b}}\right)^2} = \mathbf{1} \quad or \quad \sqrt{\sum_{i}^{p}\left(\mathbf{u}_i^T \cdot \mathbf{b}\right)^2} = |\mathbf{b}|, \tag{5.4}$$

thus the normalized colinearity indicates relative contributions of each output mode to the target. This indicator can be used to establish a threshold below which an input mode shape can be truncated to save effort with little performance degradation.

If colinearity is divided by the corresponding singular value, the resulting value corresponds to the input mode weight and indicates how much each input mode contributes to the total control input vector, i.e. total control effort consumption.

$$\mathbf{x}_\mathbf{c} = \sum_{i=1}^{rank(\mathbf{A})} \frac{colinearity_i}{\sigma_i}\mathbf{v}_i = \sum_{i=1}^{rank(\mathbf{A})} \frac{\mathbf{u}_i^T \cdot \mathbf{b}}{\sigma_i}\mathbf{v}_i = \sum_{i=1}^{rank(\mathbf{A})} q_i \mathbf{v}_i \tag{5.5}$$

Consider an example case where the target vector **b** is almost colinear with the first output mode in the 2-D output space and assume the size of **b** is one, i.e. unit vector ($\mathbf{b} = \bar{\mathbf{b}}$). Assume that the colinearity is $\mathbf{u}_1^T \cdot \bar{\mathbf{b}} \approx 0.99$ ($\theta \approx 8.1^o$) in Fig. 5.2(a). Let the singular value σ_1 corresponding to $\mathbf{u}_1$ be the largest among all the singular values found by SVD and assume the singular values are normalized with respect to the size of σ_1. Then, $\bar{\sigma}_1$, normalized singular value of σ_1, would be one and input mode weight $\frac{\mathbf{u}_1^T \cdot \bar{\mathbf{b}}}{\bar{\sigma}_1}$ would almost be one. Since the target vector is almost colinear with the first output mode, colinearity of the 2nd mode would be very small $\mathbf{u}_2^T \cdot \bar{\mathbf{b}} \approx 0.1411$ ($\theta \approx 81.9^o$). This means $\mathbf{u}_1$ and $\mathbf{u}_2$ contribute 98.01% ($=0.99^2 \times 100\%$) and 1.9% ($=0.1411^2 \times 100\%$), respectively,

to the unit vector $\bar{\mathbf{b}}$. If $\bar{\sigma}_2 \le \frac{0.1411}{0.99}\bar{\sigma}_1 \approx 0.1425\bar{\sigma}_1$, where 0.1425 represents the decay ratio of the colinearity between *i*=1 and 2, then

$$\frac{\mathbf{u}_2^T \cdot \bar{\mathbf{b}}}{\bar{\sigma}_2} \ge 1 \approx \frac{\mathbf{u}_1^T \cdot \bar{\mathbf{b}}}{\bar{\sigma}_1} \qquad \Leftrightarrow \qquad q_2 \ge q_1$$

Since $q_2 \ge q_1$, the 2nd control input mode $\mathbf{v}_2$ paired with $\mathbf{u}_2$ that contributes only 1.9% of unit vector **b** consumes more control effort than the 1st control input mode $\mathbf{v}_1$ paired with $\mathbf{u}_1$ which contributes 98.01% to the output. Therefore truncating $\mathbf{u}_2$, i.e. removing $\mathbf{v}_2$, will save a large amount of control effort without serious performance degradation. This is a very critical observation since the example reveals that most of the control effort is spent to improve a very small portion of the total target performance. Conclusions from this 2-D example can be extended to the general *p*x*m* space—if $\mathbf{u}_i^T \cdot \mathbf{b}$ decays faster than σ_i does, then smaller contributing mode shapes consume more control effort. It should be noticed that even if $\mathbf{u}_i^T \cdot \mathbf{b}$ does not decay faster than σ_i does, it is still possible to save control effort but the savings would be smaller than in the previous case since $q_{i+1} < q_i$.

From these discussions, one can conclude that the contribution of each output mode towards the target vector **b** can be estimated by the colinearity, defined by $\mathbf{u}_i^T \cdot \mathbf{b}$, and the contribution of each input mode towards the total control effort is determined by the weight q_i. These conclusions reached by the above physical interpretation, can be represented by Eq.'s (5.6) and (5.7), respectively, and can be used as criteria for optimization.

$$\mathbf{b} = \sum_{i}^{p} q_i \sigma_i \mathbf{u}_i = \sum_{i}^{p} \frac{\mathbf{u}_i^T \cdot \mathbf{b}}{\sigma_i} \sigma_i \mathbf{u}_i = \sum_{i}^{p} (\mathbf{u}_i^T \cdot \mathbf{b}) \mathbf{u}_i \tag{5.6}$$

$$\mathbf{x_c} = \sum_{i=1}^{rank(\mathbf{A})} q_i \cdot \mathbf{v}_i = \sum_{i=1}^{rank(\mathbf{A})} \frac{\mathbf{u}_i^T \cdot \mathbf{b}}{\sigma_i} \mathbf{v}_i \tag{5.7}$$

5.3. CONTROL SYSTEM EFFICIENCY INDICATOR

In many linear control system designs, the input direction corresponding to the maximum singular value is called the high-gain direction since the input vector maps to an output vector amplified by the largest gain, i.e. large singular value [28, 56]. The low-gain direction is similarly defined by the input direction corresponding to the minimum singular value. This concept of high/low gain directions can be directly applied to the nonlinear controller designs using the LAENC. From these definitions, it can be inferred that the high gain direction is an efficient control input vector with respect to control effort since large changes in the output space can be achieved with the same amount of input control effort thanks to the large scaling factor σ. Similarly the low gain direction is an inefficient direction since the same unit input vector contributes small changes in the output space. This can be understood graphically as illustrated in Fig. 5.3.

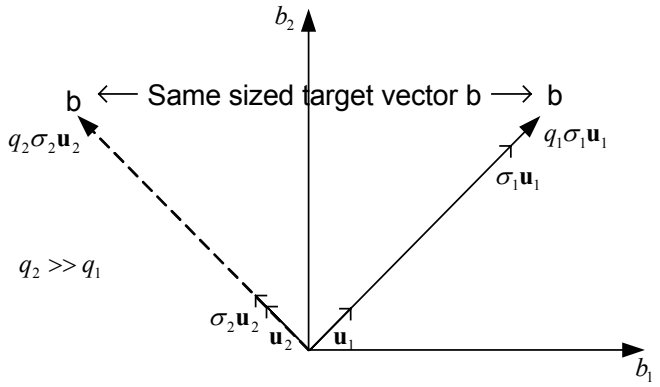

Figure 5.3 Graphical illustration of efficiency

All the output modes are unit vectors so their magnitudes are the same. Depending on the size of the target vector **b**, each output mode is amplified appropriately by q_i's. If target vector **b** is almost colinear with the first output mode, the unit input vector is mapped to the output mode vector with the largest gain (singular value). Even if vector **b** is large, only a small multiplication factor (weight q_1) to the first input mode vector will make the system output reach target vector **b**. If, on the other hand, **b** is colinear with the smallest direction as in Fig. 5.3, the multiplication factor (weight q_2) must be large enough to reach target vector **b**, thus resulting a large input control effort.

Based on the above interpretation, the designer knows a priori whether the designed controller is efficient just by comparing the mode directions to the target vector. Thus colinearity can be used as an efficiency indicator. The designer may

wish to gain a better efficiency by changing the direction of the target vector **b** towards the high gain directions.

5.4. SUMMARY

Structural analysis and optimization of nonlinear control systems using singular value decomposition of the LAENC are proposed. Based on the LAENC, SVD is applied to the nonlinear control designs, control input/output mode shapes are defined and the control input null space is identified. It is shown that colinearity of the output mode shapes with the target vector can be used as a sensitivity measure towards the target vector, and it can be used as a criterion for mode truncation optimization. The linear combination coefficient q_i for the control input is used to show the contribution of each input mode to the total control input distribution.

Chapter 6

Temperature Control of an Input-Constrained Enclosed Thermal System

In this chapter, the temperature control of a thermal system is presented. The system has features that make it difficult to design a control system, such as more inputs than outputs (redundancy), high nonlinearity due to radiation, input-constraints, ill-conditioned behavior, and large control effort consumption. The algorithms proposed in Chapters 4 and 5 are applied to treat these issues and regularization methods are embedded into the nonlinear controller designs to handle the ill-conditioned behavior.

6.1. INTRODUCTION

Estimating and controlling energy inputs from distributed energy sources to generate desired heating profiles (temperature or heat flux) for material processing is a classic optimal design problem. In many applications, such as the rapid thermal processing (RTP) of semiconductor wafers, infrared paint dryers, annealing furnaces, and directed energy manufacturing systems such as selective laser sintering, precise thermal control is necessary for quality assurance. This design problem has attracted much attention from control and thermal engineers, but they propose different solution strategies.

Thermal engineers approach the estimation/control problem in two ways—forward and inverse design methods. The forward method uses trial-and-

error; the designer estimates a solution and the governing equations are solved. If the design objective is not achieved, an iterative solution process continues until a satisfactory solution is found. The inverse design method assumes that both the required conditions at the design surface (design objective) and the governing equations are known, then the required input is computed. Many solution techniques for inverse analyses have been proposed [15-17, 24, 43]. In general, the inverse problem is defined in terms of the Fredholm equation of the first kind:

$$f(x) = \int K(x, y) g(y) dy$$

Here $f(x)$ is known or imposed (design objective), $g(y)$ is the unknown distribution and $K(x,y)$ is the kernel of the system. The equation solution is ill-posed—the solution is potentially unstable to small perturbations in the design objective. For a solution to be stable, accurate, and physically reasonable, the governing equation must be regularized; that is, additional constraints, such as minimizing a suitable norm, are imposed [24, 43]. Moreover, the kernel equations contain modeling errors, regularization introduces truncation errors, and the real system encounters disturbances, so the resulting open-loop/off-line solution results in offset-errors in the design objective. Thus, a robust feedback control algorithm is needed.

Control approaches to the energy input estimation/control problem use mathematical modeling and feedback control, and good examples are found in the RTP temperature control of semiconductor wafers [4, 9, 10, 11, 13, 25, 46].

Typical models of RTP systems are described by PDEs. Solving these equations is computationally expensive and it is practically difficult to implement

PDEs into the controller design. Instead, Galerkin's method [3] and empirical reduction methods [49] were applied to the infinite dimensional PDEs to derive finite ODE systems that accurately describe the dynamics of the dominant modes of the PDE systems. However, the conversion process is very complex and time consuming since the selection of an appropriate basis upon which to expand the solution of the PDE is not an easy task [3]. Therfore, many control engineers used lumped parameter models [4, 9, 10, 25, 46] and empirical models [10, 13]. Several feedback control algorithms have been applied on those models (linear programming [46], linear-quadratic [13], linear-quadratic-Gaussian [10], internal model control [25], and neural network [11]) and promising results have been reported, however, most of the designs are based on low-order (dimensional) linear dynamic models which are valid only for small RTP chambers. Strong coupling between the elements in the system that cause ill-conditioned behavior do not appear in their work because of using the low order models. Low order models cannot guarantee high performance for large dimensional systems such as infrared paint dryers and annealing furnaces. Also, variations in DC gain of a linearized model by temperature changes [57] can be a significant problem for precision control. Hence, in this research, a generalized high-order, nonlinear and highly coupled ill-conditioned thermal system model is used.

With such strong coupling, it is difficult to obtain acceptable control of the temperature profile using single loop conventional controller commonly used in industrial applications and the multiloop control would be problematic due to the fair amount of interactions [2]. Hence for the controller to be successful, the

system should be diagonally dominant [5]. Therefore, FBL/SMC are good candidate controller for such systems since they decouple inputs and outputs intrinsically.

6.2. SYSTEM MODELING

The problem considered in this research is to design a controller to manipulate the heat from heater surfaces to achieve a desired temperature profile on a design surface. Consider an enclosure shown in Fig. 6.1 with one side comparatively longer. Due to this aspect ratio, the enclosure can be approximated as two-dimensional and it is made up of the design surface (bottom center), reflective surfaces (sides and bottom sides), and heater surfaces (top). The design surface, heated by the heater surfaces, is controlled to a prescribed profile and to be spatially uniform in temperature. The dimensions, assumptions, exchange factors, material properties, and desired thermal objectives are adopted from [16].

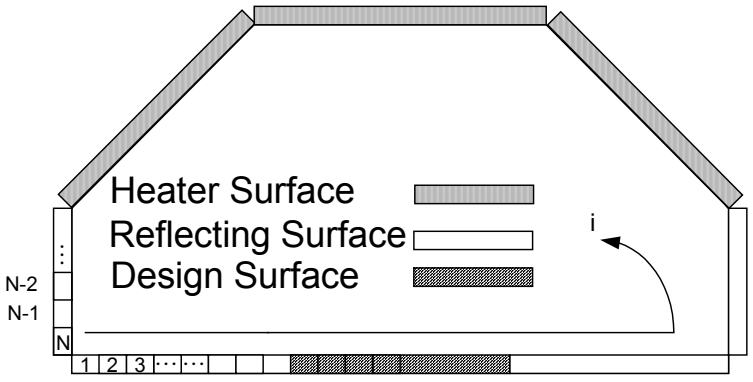

Figure 6.1 Geometry of the thermal system

The derivation of system model starts by applying the energy equation to the system as in Fig. 6.2(a).

$$\dot{E}_{in} + \dot{E}_g + \dot{E}_{out} = \frac{dE_{st}}{dt} \equiv \dot{E}_{st} \tag{6.1}$$

where,

E_{in} : Energy entering the control surface

E_g : Energy generation

E_{out} : Energy leaving the control surface

E_{st} : Stored Energy

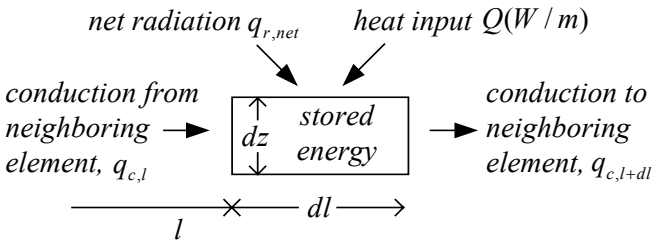

(a) Energy balance for an infinitesimal element

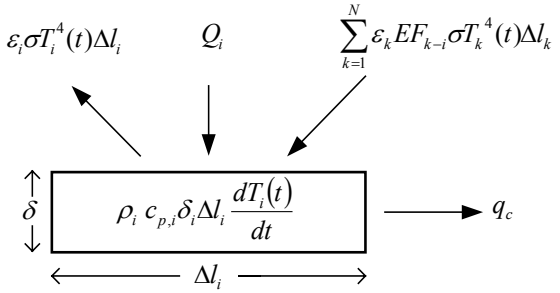

(b) Energy balance for a finite element *i*.

Figure 6.2 Energy balance

The differential form of the energy equation for an infinitesimal control volume (Fig. 6.2(a)) at point l (l: coordinate along the surface) in the system is

$$Q(l,t)+q_{r,net}(l,t)+q_{c,l}(l,t)-q_{c,l+dl}(l,t)=\rho c_p dldz\frac{\partial T(l,t)}{\partial t} \tag{6.2}$$

where,

$$\begin{aligned} q_{c,l}-q_{c,l+dl} &= q_{c,l}-\left(q_{c,l}+\frac{dq_{c,l}}{dl}dl\right) \\ &= -kdz\frac{\partial T(l,t)}{\partial l}-\left(-kdz\frac{\partial T(l,t)}{\partial l}+\frac{d}{dl}\left(-kdz\frac{\partial T(l,t)}{\partial l}\right)dl\right) \\ &= kdz\frac{\partial^2 T(l,t)}{\partial l^2}dl \end{aligned} \tag{6.3}$$

and

$$q_{r,net}(l,t)=\left\{\int \varepsilon(y)\sigma T^4(y,t)dEF_{y-l}-\varepsilon(l)\sigma T^4(l,t)\right\}dl \tag{6.4}$$

Therefore,

$$\begin{aligned} Q+\left[\int \varepsilon(y)\sigma T^4(y,t)dEF_{y-l}-\varepsilon(l)\sigma T^4(l,t)\right]dl \\ +kdz\frac{\partial^2 T(l,t)}{\partial l^2}dl=\rho c_p dldz\frac{\partial T(l,t)}{\partial t} \end{aligned} \tag{6.5}$$

where,

Q	=	power input for heater strips(W/m)
q	=	heat transfer rate(W/m)
l	=	coordinates along surfaces(m)
t	=	time(sec)
k	=	thermal conductivity(W/mK)
T	=	temperature(K)
c_p	=	specific heat(J/kg K)

ρ = density(Kg/m^3)

δ = plate thickness(m)

ε = emissivity of the surface

σ = Stefan-Boltzmann constant (σ=5.67 x 10^{-8} W/m^{2}K^4)

EF_{i-j} = exchange factor between element i and j

and subscripts $_r$ and $_c$ represent radiation and conduction, respectively.

The system is then divided into finite control elements with nodes as illustrated in Fig. 6.1. Using an explicit Euler scheme, the governing energy equation for an element *i* in Fig. 6.1, with heat input, radiation and conduction from neighboring elements, as described in Fig. 6.2(b) becomes

$$Q_i(t) - \varepsilon_i \sigma T_i\ (t)^4 \Delta l_i + \sum_{k=1}^{N} \varepsilon_k EF_{k-i} \sigma T_k(t)^4 \Delta l_k + k\delta \left(\frac{T_{i-1}(t) - T_i(t)}{\frac{\Delta l_{i-1}}{2} + \frac{\Delta l_i}{2}} + \frac{T_{i+1}(t) - T_i(t)}{\frac{\Delta l_{i+1}}{2} + \frac{\Delta l_i}{2}} \right) = \rho_i\ c_{p,i} \delta_i \Delta l_i \frac{dT_i(t)}{dt} \tag{6.6}$$

where Δl_i = length of i^{th} element(m)

N = total number of elements.

The exchange factor between elements *k* and *i*, EF_{k-i}, is the rate of energy emitted from element *k* that is absorbed by element i, and it includes all the effects of intermediate reflections. By definition, Eq. (6.7) is always satisfied:

$$\sum_{i=1}^{N} EF_{k-i} = 1 \tag{6.7}$$

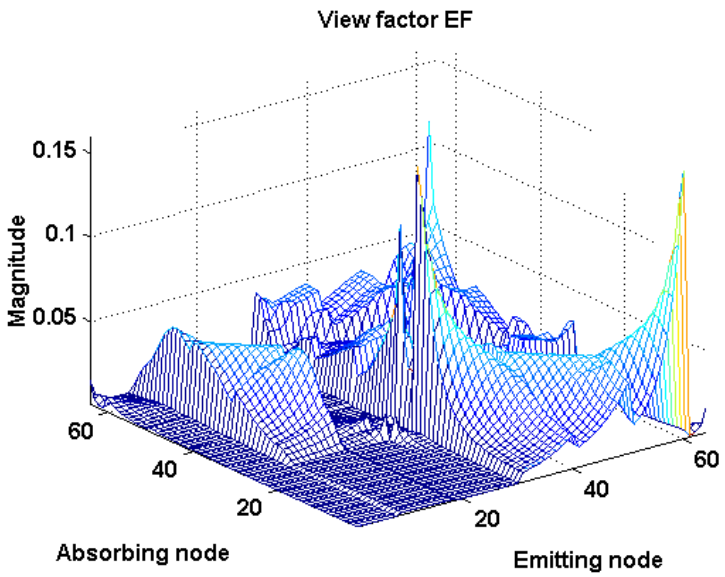

Figure 6.3 Exchange factors [16]

In this research, the exchange factors are obtained from [16] in which Monte Carlo methods (MCM) are used to sample photon bundles carrying transferred radiative energy. The method produces accurate solutions and is formulated to easily handle complexities like specular reflecting surfaces, effects of participating medium and scattering [16]. Figure 6.3 shows the exchange factors.

The system is divided into 64 elements (N=64 in Fig. 6.1) [16]; ten for the design surface (i=9-18), 30 for the heater surfaces (i=31-60) and 24 for the reflective surfaces (i=1-8, 19-30, 61-64). All elements have equal lengths, Δl_i=0.1m, and are assumed as gray. The heater surfaces are oxidized-cast iron and diffusely reflecting. The reflector surfaces are polished aluminum (k=227 W/mK) and specularly reflecting with small emissivity values. The design surface

is silicon carbide (k=454 W/mK) and diffusely reflecting. The heater surfaces are made up of 30 strip heaters—each at uniform temperature and slightly separated from each other. The backside of the design surface is insulated and does not touch the reflector surfaces at the edges, thus thermal radiation is the only means of exchanging heat from the design surface to its surroundings. Furthermore, it is assumed that the conduction across the plate thickness is negligible when compared with the thermal radiation and conduction along the plate so that the surfaces can be approximated as lumped across the plate thickness. All thermal properties are assumed to be constant and independent of the temperature variations and the system is considered to be at local thermodynamic equilibrium. The geometric and thermal parameters are listed in Table 6.1. The desired design surface temperature profile shown in Fig. 6.4 is described as

$$T_d(t) = T_{d,final} + (T_{d,initial} - T_{d,final}) \cdot \exp(-10 \cdot t/timetotal) \tag{6.8}$$

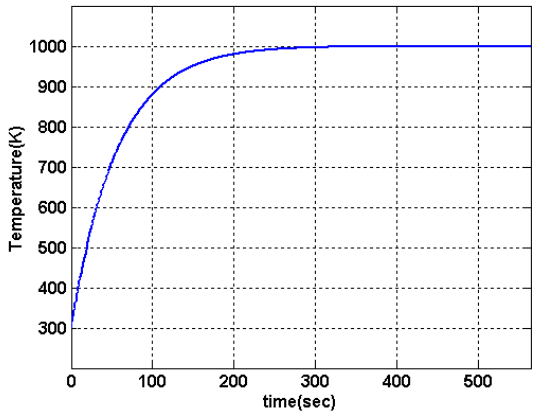

Figure 6.4 Desired temperature profile of the design surface [16]

Table 6.1. Geometric and thermal parameters of enclosure [16]

Surface	Material	δ (m)	ρ (kg/m^3)	C_p (J/KgK)	$\Delta l_i\ (m)$	k (W/mK)	ε
1-8	Polished aluminum	1E-3	2702	903	0.1	227	0.05
9-18	Silicon carbide	1E-3	3160	675	0.1	454	0.9
19-26	Polished aluminum	1E-3	2702	903	0.1	227	0.05
27-30		1E-3	2702	903	0.1	227	0.05
31-40	Oxidized-cast iron	1E-5	7870	447	0.1		0.95
41-50		1E-5	7870	447	0.1		0.95
51-60		1E-5	7870	447	0.1		0.95
61-64	Polished aluminum	1E-3	2702	903	0.1	227	0.05

6.3. NONLINEAR CONTROL DESIGN

Thermal systems with radiant heat are highly nonlinear coupled systems, so the use of nonlinear control appears to be a natural solution. Many nonlinear control laws have been developed [12, 27, 60, 62, 63] and feedback linearization (FBL) and sliding mode control (SMC) are two widely used schemes. For the system model previously discussed, the conduction terms are neglected since their magnitudes are very small compared to the radiation terms—this assumption can be considered to be a modeling error. Eq. (6.6) reduces to:

$$\begin{cases} \dot{T}_1 = f_1 \\ \quad \vdots \\ \dot{T}_{30} = f_{30} \\ \dot{T}_{31} = f_{31} + \dfrac{1}{\rho_{31} c_{p,31} \delta_{31} \Delta l_{31}} Q_{31} \\ \quad \vdots \\ \dot{T}_{60} = f_{60} + \dfrac{1}{\rho_{60} c_{p,60} \delta_{60} \Delta l_{60}} Q_{60} \\ \dot{T}_{61} = f_{61} \\ \quad \vdots \\ \dot{T}_{64} = f_{64} \end{cases} \tag{6.9}$$

where,

$$f_i(\mathbf{T}) = \frac{1}{\rho_i c_{p,i} \delta_i \Delta l_i} \left[-\varepsilon_i \sigma T_i^4 \Delta l_i + \sum_{k=1}^{N} \varepsilon_i E F_{k-i} \sigma T_k^4 \Delta l_k \right] \tag{6.10}$$

Generalizing: $$\dot{\mathbf{T}}(t) = \mathbf{f}(\mathbf{T}) + \mathbf{g}(\mathbf{T})\mathbf{Q} = \mathbf{f}(\mathbf{T}) + \mathbf{g} \cdot \mathbf{u} \tag{6.11}$$

where, **u** is the heat input from the heater surfaces and

$$\mathbf{f(T)} = [f_1, f_2, \cdots, f_{63}, f_{64}]^T \tag{6.12}$$

$$\mathbf{g} = \frac{1}{\rho_i c_{p,i} \delta_i \Delta l_i} \begin{bmatrix} \mathbf{0}_{30\times30} \\ --- \\ \mathbf{I}_{30\times30} \\ --- \\ \mathbf{0}_{4\times30} \end{bmatrix} \tag{6.13}$$

Setting the surface temperatures as states, the state equation for element *i* is:

$$\dot{x}_i = \frac{1}{\rho_i c_{p,i} \delta_i \Delta l_i}\left[-\varepsilon_i \sigma x_i^4 \Delta l_i + \sum_{k=1}^{N} \varepsilon_i EF_{k-i} \sigma x_k^4 \Delta l_k + Q_i \right] \tag{6.14}$$

Eq. (6.14) can be expressed in a more familiar and general form as:

$$\begin{aligned} \dot{\mathbf{x}} &= \mathbf{f}(\mathbf{x}) + \mathbf{g}(\mathbf{x})\mathbf{u} \\ \mathbf{y} &= \mathbf{h}(\mathbf{x}) \end{aligned} \tag{6.15}$$

where $\mathbf{x} \in \mathbf{R}^{64}, \mathbf{u} \in \mathbf{R}^{30}, \mathbf{y} \in \mathbf{R}^{10}, \mathbf{f} : \mathbf{R}^{64} \to \mathbf{R}^{64}, \mathbf{g} : \mathbf{R}^{64} \to \mathbf{R}^{64}, \mathbf{h} : \mathbf{R}^{64} \to \mathbf{R}^{10}$ and **f, g** and **h** are smooth functions of **x**. The output, **y**, is the temperature of the design surface, therefore

$$\mathbf{y}(t) = \mathbf{h}(\mathbf{x}) = \begin{bmatrix} x_9 \\ \vdots \\ x_{18} \end{bmatrix} = \begin{bmatrix} \mathbf{0}_{10\times 8} & \mathbf{I}_{10\times 10} & \mathbf{0}_{10\times 46} \end{bmatrix} \mathbf{x} = \mathbf{G}\mathbf{x} \tag{6.16}$$

The system equation is non-square; 30 inputs and 10 outputs. For non-autonomous, non-square, affine nonlinear systems described by Eq. (6.15), both FBL and SMC are appropriate control algorithms.

A closer look at the output equations reveals that a control law can not be achieved unless the output is differentiated twice, which gives the relative degree of the system as two. Differentiating the output with respect to time:

$$\begin{aligned} \dot{\mathbf{y}}(t) &= \mathbf{L}_\mathbf{f}\mathbf{h}(\mathbf{x}) + \mathbf{L}_\mathbf{g}\mathbf{h}(\mathbf{x})\mathbf{u} \\ &= \mathbf{G}\mathbf{f} + \mathbf{G}\mathbf{g}\mathbf{u} \end{aligned} \tag{6.17}$$

Since $\mathbf{L}_\mathbf{g}\mathbf{h}(\mathbf{x}) = \mathbf{0}$, the output is differentiated a second time:

$$\begin{aligned} \ddot{\mathbf{y}}(t) &= \mathbf{L}_\mathbf{f}^2\mathbf{h}(\mathbf{x}) + \mathbf{L}_\mathbf{g}\mathbf{L}_\mathbf{f}\mathbf{h}(\mathbf{x})\,\mathbf{u} \\ &= \mathbf{G}\frac{\partial \mathbf{f}}{\partial \mathbf{x}}\mathbf{f} + \mathbf{G}\frac{\partial \mathbf{f}}{\partial \mathbf{x}}\mathbf{g}\mathbf{u} \end{aligned} \tag{6.18}$$

$\mathbf{L_f h(x)}$ is the Lie derivative of **h(x)** with respect to **f(x),** i.e. the directional derivative, and defined as

$$\begin{aligned}\mathbf{L_f h(x)} &= \langle \mathbf{dh, f} \rangle \\ &= \frac{\partial \mathbf{h(x)}}{\partial x_1} f_1(\mathbf{x}) + \frac{\partial \mathbf{h(x)}}{\partial x_2} f_2(\mathbf{x}) + \cdots + \frac{\partial \mathbf{h(x)}}{\partial x_n} f_n(\mathbf{x}) = \frac{\partial \mathbf{h(x)}}{\partial \mathbf{x}} \mathbf{f(x)}\end{aligned} \tag{6.19}$$

$\mathbf{L_g h(x)}$ is defined in the same way as Eq. (6.19) and higher order Lie derivatives are also defined in [27].

FBL Nonlinear Control

Let the desired error dynamics for the FBL be defined as

$$\ddot{\mathbf{e}} + \boldsymbol{\lambda}_1 \dot{\mathbf{e}} + \boldsymbol{\lambda}_2 \mathbf{e} = \mathbf{0} \qquad \text{where,} \quad \mathbf{e} = \mathbf{y} - \mathbf{y_d} \tag{6.20}$$

Then

$$\ddot{\mathbf{y}} = \ddot{\mathbf{y}}_\mathbf{d} - \boldsymbol{\lambda}_1 \dot{\mathbf{e}} - \boldsymbol{\lambda}_2 \mathbf{e} \tag{6.21}$$

Substituting Eq. (6.21) into Eq.(6.18) yields

$$\left(\mathbf{L_g L_f h(x)}\right)\mathbf{u} = \left\{\ddot{\mathbf{y}}_\mathbf{d} - \boldsymbol{\lambda}_1 \dot{\mathbf{e}} - \boldsymbol{\lambda}_2 \mathbf{e} - \mathbf{L_f^2 h(x)}\right\} \tag{6.22}$$

Finally, the nonlinear controller is

$$\mathbf{u} = \left(\mathbf{L_g L_f h(x)}\right)^+ \left\{\ddot{\mathbf{y}}_\mathbf{d} - \boldsymbol{\lambda}_1 \dot{\mathbf{e}} - \boldsymbol{\lambda}_2 \mathbf{e} - \mathbf{L_f^2 h(x)}\right\} \tag{6.23}$$

where $^+$ represents the pseudo-inverse since $\mathbf{L_g L_f h(x)}$ is not square. The closed loop FBL behavior of the system is

$$\begin{aligned}\dot{\mathbf{x}} &= \mathbf{f} + \mathbf{g}\left(\mathbf{G}\frac{\partial \mathbf{f}}{\partial \mathbf{x}}\mathbf{g}\right)^+ \left\{\ddot{\mathbf{y}}_\mathbf{d} - \boldsymbol{\lambda}_1 \dot{\mathbf{e}} - \boldsymbol{\lambda}_2 \mathbf{e} - \mathbf{G}\frac{\partial \mathbf{f}}{\partial \mathbf{x}}\mathbf{f}\right\} \\ &= \mathbf{f} + \mathbf{g}\left(\mathbf{L_g L_f h(x)}\right)^+ \left\{\ddot{\mathbf{y}}_\mathbf{d} - \boldsymbol{\lambda}_1 \dot{\mathbf{e}} - \boldsymbol{\lambda}_2 \mathbf{e} - \mathbf{L_f^2 h(x)}\right\}\end{aligned} \tag{6.24}$$

λ_1=0.1, λ_2=0.1 are selected as the gains for FBL such that the poles of the error dynamics are 3~4 times larger than the poles (time constant) of the desired temperature profile (see Appendix B). Figure 6.5 shows the desired temperature trajectory and desired error behavior based on Eq. (6.21).

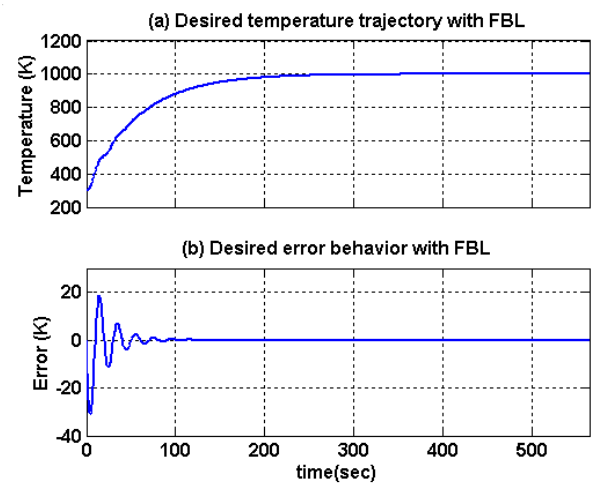

Figure6.5 Desired trajectories for FBL with λ_1=0.1, λ_2=0.1 (a) desired temperature trajectory and (b) desired error behavior

SMC Nonlinear Control

For SMC, instead of setting the design surface temperature as the output, the sliding surfaces $\mathbf{S} = \dot{\mathbf{e}} + \boldsymbol{\lambda}_{\mathbf{SMC}}\mathbf{e}$ are selected as the outputs. With only one differentiation, the explicit control input term appears.

$$\begin{aligned}\dot{\mathbf{S}} &= \ddot{\mathbf{e}} + \boldsymbol{\lambda}_{\mathbf{SMC}}\dot{\mathbf{e}} = \ddot{\mathbf{y}} - \ddot{\mathbf{y}}_{\mathbf{d}} + \boldsymbol{\lambda}_{\mathbf{SMC}}\dot{\mathbf{e}} = -\mathbf{D}\cdot\tanh(\mathbf{S}) \\ &= \mathbf{L}_{\mathbf{f}}^{2}\mathbf{h}(\mathbf{x}) + \mathbf{L}_{\mathbf{g}}\mathbf{L}_{\mathbf{f}}\mathbf{h}(\mathbf{x})\mathbf{u} - \ddot{\mathbf{y}}_{\mathbf{d}} + \boldsymbol{\lambda}_{\mathbf{SMC}}\dot{\mathbf{e}} = -\mathbf{D}\cdot\tanh(\mathbf{S})\end{aligned} \tag{6.25}$$

Rearranging:

$$\left(\mathbf{L_g L_f h(x)}\right)\mathbf{u} = \left\{\ddot{\mathbf{y}}_\mathbf{d} - \boldsymbol{\lambda}_\mathbf{SMC}\dot{\mathbf{e}} - \mathbf{L_f^2 h(x)} - \mathbf{D}\cdot\tanh(\mathbf{S})\right\} \tag{6.26}$$

where **D** is a positive definite diagonal gain matrix and tanh(**S**) is the hyperbolic tangent function.

The nonlinear control and the closed loop behavior of the system with SMC are

$$\mathbf{u} = \left(\mathbf{L_g L_f h(x)}\right)^{+}\left\{\ddot{\mathbf{y}}_\mathbf{d} - \boldsymbol{\lambda}_\mathbf{SMC}\dot{\mathbf{e}} - \mathbf{L_f^2 h(x)} - \mathbf{D}\cdot\tanh(\mathbf{S})\right\} \tag{6.27}$$

$$\begin{aligned}\dot{\mathbf{x}} &= \mathbf{f} + \mathbf{g}\left(\mathbf{L_g L_f h(x)}\right)^{+}\left\{\ddot{\mathbf{y}}_\mathbf{d} - \boldsymbol{\lambda}_\mathbf{SMC}\dot{\mathbf{e}} - \mathbf{L_f^2 h(x)} - \mathbf{D}\cdot\tanh(\mathbf{S})\right\} \\ &= \mathbf{f} + \mathbf{g}\left(\mathbf{G}\frac{\partial \mathbf{f}}{\partial \mathbf{x}}\mathbf{g}\right)^{+}\left\{\ddot{\mathbf{y}}_\mathbf{d} - \boldsymbol{\lambda}_\mathbf{SMC}\dot{\mathbf{e}} - \mathbf{G}\frac{\partial \mathbf{f}}{\partial \mathbf{x}}\mathbf{f} - \mathbf{D}\cdot\tanh(\mathbf{S})\right\}\end{aligned} \tag{6.28}$$

λ_{SMC} = 0.2 is selected such that the error dynamics (sliding behavior) has a pole at –0.2 which is four times larger than the poles of desired temperature profile. Figure 6.6 shows the desired temperature trajectory, desired error behavior and desired sliding behavior based on Eq. (6.25).

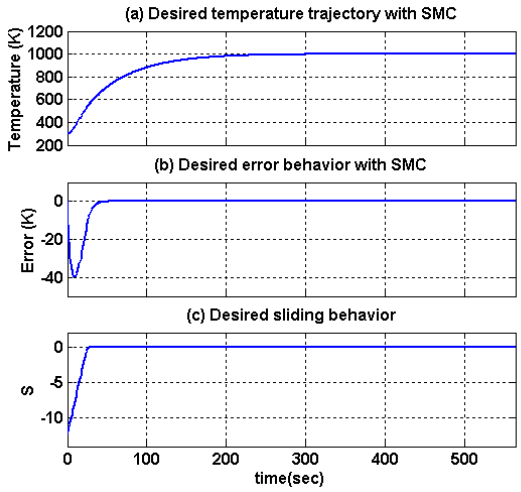

Figure 6.6 Desired trajectories for SMC with D= 0.5, λ_{SMC}= 0.2 (a) desired temperature trajectory (b) desired error behavior (c) desired sliding behavior

6.4. RESULTS OF NONLINEAR CONTROLLERS

Figure 6.7 shows the system response using a classic nonlinear FBL controller with λ_1=0.1, λ_2=0.1 selected as the gains for FBL—Fig. 6.7(a) shows excellent tracking of the design surface temperatures (nodes 9-18) to the desired temperature trajectory. Fig. 6.7(b), the cross sectional plot of the Fig. 6.7(a) at t=350 sec, i.e., temperature distribution at t=350, shows clearly that the all design surfaces (i=9~18) follow the desired temperature trajectory uniformly. Figs. 6.7(a), (b), (e) and (f) show good temperature uniformity in the design surfaces temperature (maximum difference of 2.8E-4 K for t > 100 sec). However, the heater surface control input distribution (Fig. 6.7(c)) and cross sectional plot of Fig. 6.7(c) at t=350 sec (Fig. 6.7(d)) shows that 17 out of 30 heaters have negative heat inputs—the heaters act as heat sinks rather than heat sources. The control input solutions (heating surface Q's) are not practical solutions. In other words, the solution violates input constraints that all control inputs must be positive since the actuators are heaters. Moreover, the heaters that are positive must generate large Q's (up to 7531W/m).

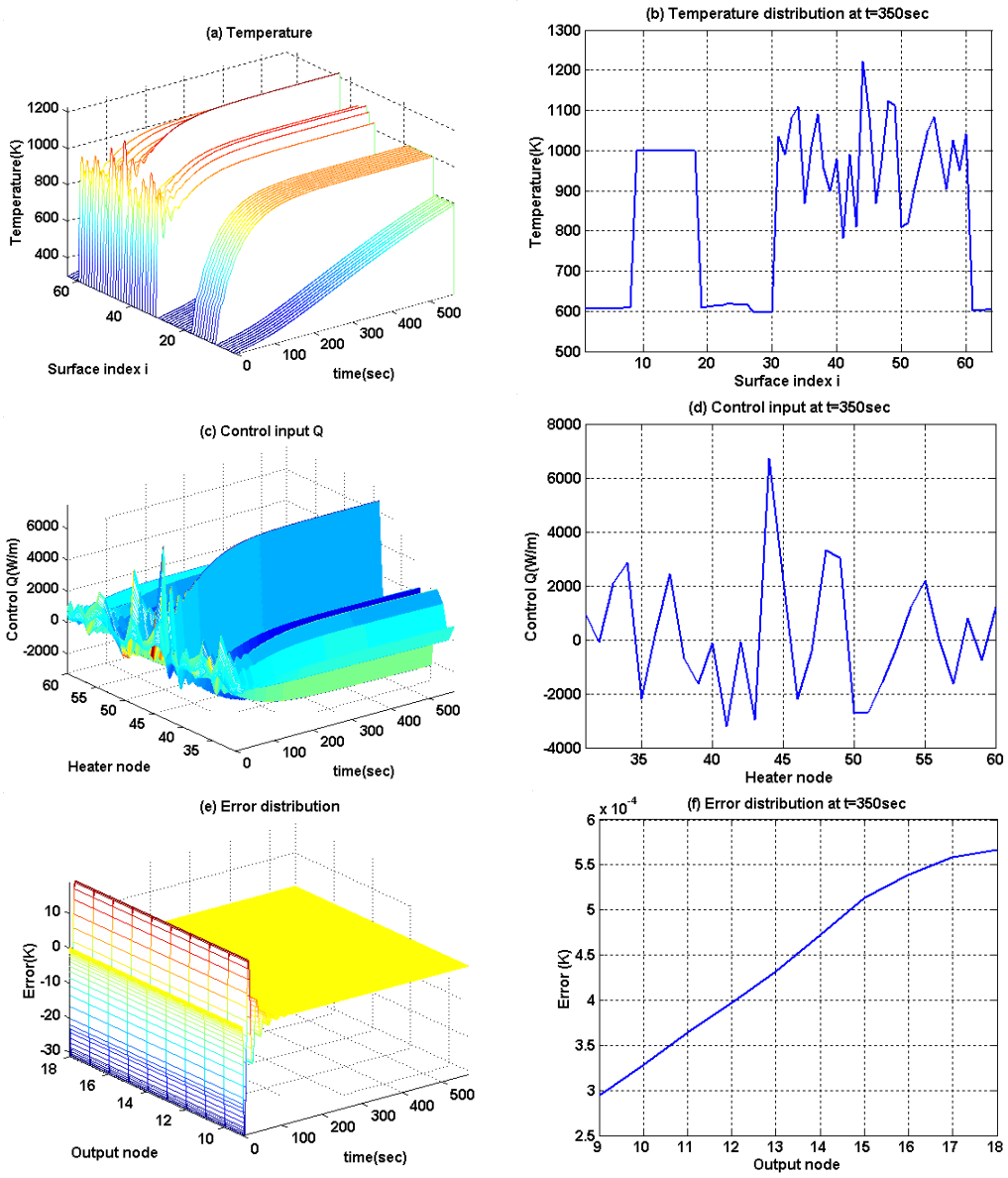

Figure 6.7 Responses for FBL with λ_1 =0.1, λ_2 =0.1 (a) temperature distribution along the surfaces over the entire process time and (b) at t=350 sec, (c) control input Q distribution over the entire process time and (d) at t=350 sec, (e) output (design surfaces) error distribution over the entire process time and (f) at t=350 sec

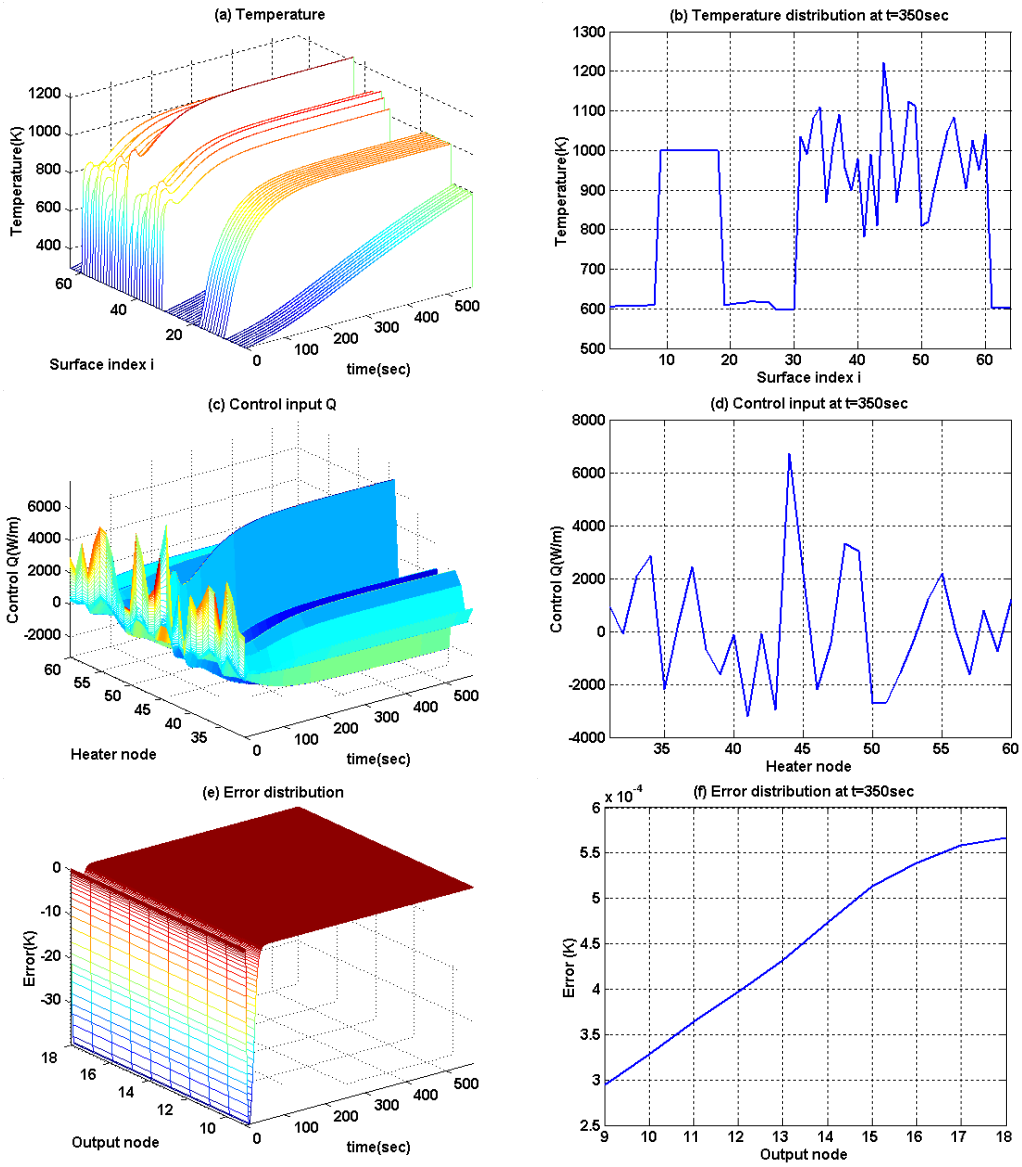

Figure 6.8 Responses for SMC with D = 0.5, λ_{SMC} = 0.2 (a) temperature distribution along the surfaces over the entire process time and (b) at t=350sec, (c) control input Q over the entire process time and (d) at t=350sec, (e) output (design surfaces) error distribution over the entire process time and (f) at t=350sec

Figure 6.8 shows the system response for a classic nonlinear SMC controller with D = 0.5, λ_{SMC} = 0.2. As expected, it shows similar behavior—excellent tracking of the outputs but violates input-constraints—since the closed-loop dynamics (Eq. (6.24) and (6.28)) are almost similar to FBL.

6.5. REGULARIZATION EMBEDDED NONLINEAR CONTROLLERS

6.5.1. Ill-conditioned linear-algebraic-equivalent nonlinear controllers

In the previous section, it was shown that both FBL and SMC nonlinear control solutions violated the input-constraints, therefore it is important to understand what caused the constraint-violations.

Notice that both controller designs (Eqs. (6.22) and (6.26)) are in the form of the LAENC, i.e.,

$$\mathbf{A}_c \mathbf{x}_c = \mathbf{b}_c, \tag{6.29}$$

where,

$$\mathbf{A}_c = \mathbf{L}_g \mathbf{L}_f \mathbf{h}(\mathbf{x})$$

$$\mathbf{b}_c = \begin{cases} \ddot{\mathbf{y}}_d - \boldsymbol{\lambda}_1 \dot{\mathbf{e}} - \boldsymbol{\lambda}_2 \mathbf{e} - \mathbf{L}_f^2 \mathbf{h}(\mathbf{x}) & \textit{for} \quad \textit{FBL} \\ \ddot{\mathbf{y}}_d - \boldsymbol{\lambda}_{SMC} \dot{\mathbf{e}} - \mathbf{L}_f^2 \mathbf{h}(\mathbf{x}) - \mathbf{D} \cdot \tanh(\mathbf{S}) & \textit{for} \quad \textit{SMC} \end{cases}$$

$$\mathbf{u} = \mathbf{x}_c = \mathbf{A}_c^{+} \mathbf{b}_c$$

thus, SVD will be directly applied on this LAENC.

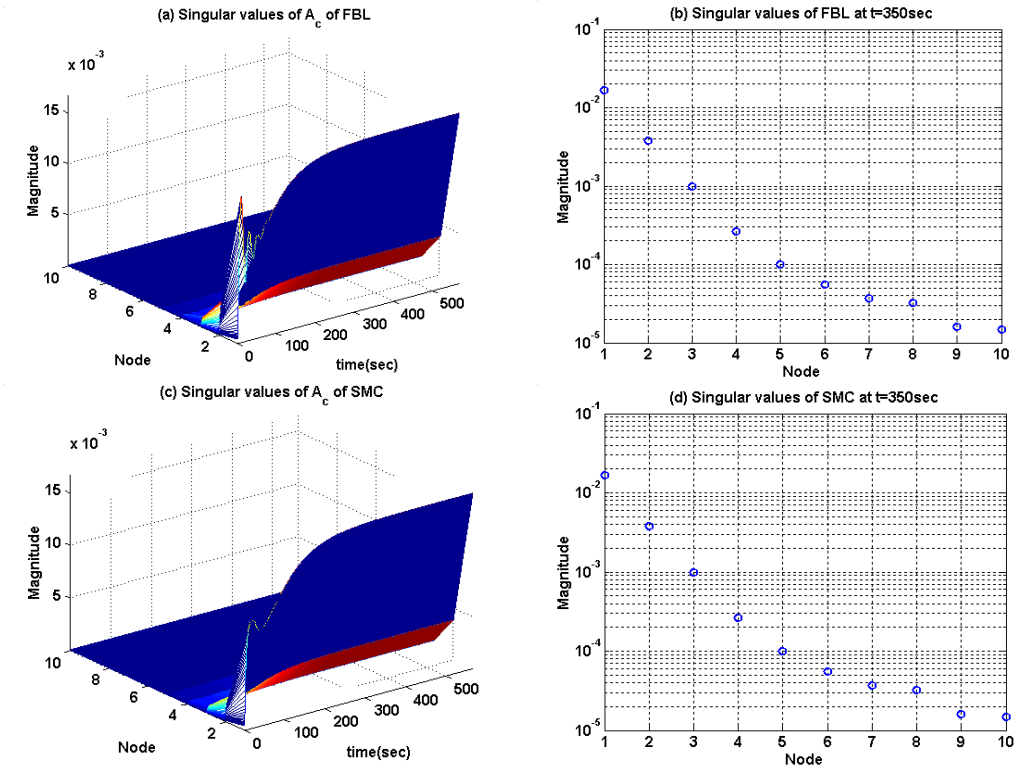

Figure 6.9 Singular values of $\mathbf{A_c}$ of FBL (a) over entire process time (b) at t =350 sec, and singular values of $\mathbf{A_c}$ of SMC (c) over entire process time (d) at t =350 sec.

Figures 6.9(a) and (c) show the singular values of $\mathbf{A_c}$ over the entire process time obtained by applying SVD on $\mathbf{A_c}$ of the FBL of Fig. 6.7 (Eq. (6.23)) and SMC of Fig. 6.8 (Eq. (6.27)), respectively. Figs. 6.9(b) and (d) show the singular values at t=350sec of FBL and SMC, respectively. The dimension of matrix $\mathbf{A_c}$ is 10×30, hence only ten non-zero singular values exist. Notice that the ratio of the smallest singular value to the largest value gives a large condition number. Notice the condition number along the entire process is very large as

shown in Fig. 6.10(a) and Fig. 6.11(a). The high condition number of $\mathbf{A_c}$ is suspected to be the cause of the large fluctuations in the control inputs as mentioned in Chapter 2—order of 1100 in both cases. Also, notice that despite the relatively flat distribution of $\mathbf{b_c}$ in Figs. 6.10(b) and 6.11(b), the control input solution (Figs. 6.7(c)), which is obtained by $\mathbf{u} = \mathbf{x_c} = \mathbf{A_c}^{+}\mathbf{b_c}$, is very oscillatory at the start. This means that small variations in $\mathbf{b_c}$ are amplified due to the small singular values in the solution obtained by SVD as in Eq. (6.30).

$$\mathbf{x_c} = \mathbf{A_c^{+}b_c} = \sum_{i=1}^{10} \frac{\mathbf{u}_{c,i}^{T} \cdot \mathbf{b_c}}{\sigma_{c,i}} \mathbf{v}_{c,i} \tag{6.30}$$

Therefore the oscillations in the control solution are assumed to originate from the large condition number.

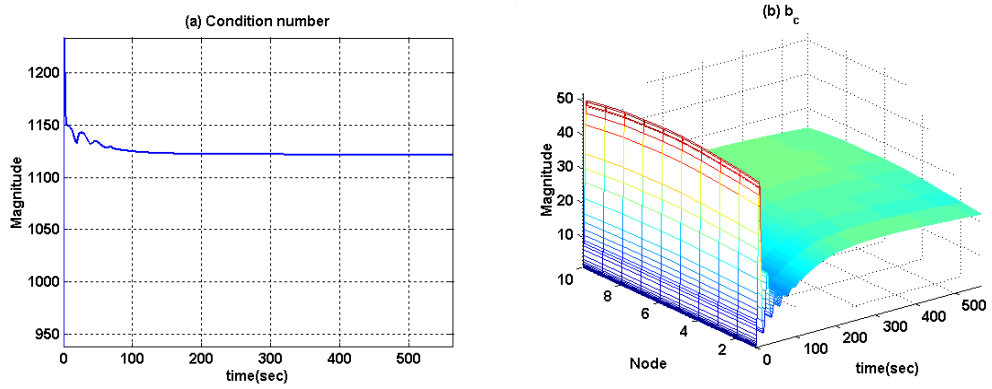

Figure 6.10 FBL with λ_1=0.1, λ_2=0.1 (a) condition number of $\mathbf{A_c}$ and (b) distribution of $\mathbf{b_c}$

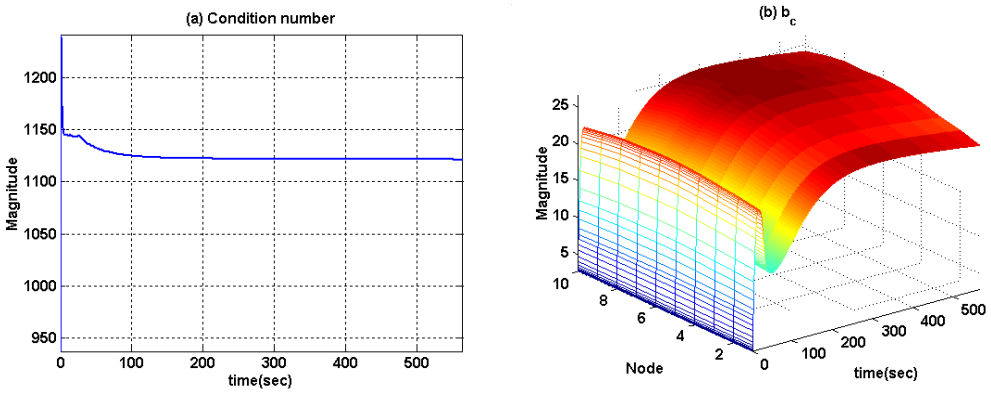

Figure 6.11 SMC with D= 0.5, λ_{SMC} = 0.2 (a) condition number of $\mathbf{A_c}$ and (b) distribution of $\mathbf{b_c}$

6.5.2. Design of regularization embedded nonlinear controllers

In Chapter 2, the regularization methods for the ill-conditioned behavior of the solutions were studied. Since the non-practical control solutions (Figs. 6.7(c) and 6.8(c)) are assumed to arise from the ill-conditioned nature of the controllers, the regularization methods can be embedded into the controller designs to handle the ill-conditionedness.

For any ill-conditioned linear system $\mathbf{Ax} = \mathbf{b}$, regularized solution with Tikhonov method is obtained by Eq. (2.30) as mentioned in Chapter 2.

Rewriting,

$$\left(\mathbf{A}^{\mathrm{T}}\mathbf{A} + \lambda_{\mathrm{Tik}}^{2}\mathbf{L}_{\mathrm{i}}^{\mathrm{T}}\mathbf{L}_{\mathrm{i}}\right)\mathbf{x} = \mathbf{A}^{\mathrm{T}}\mathbf{b} + \lambda_{\mathrm{Tik}}^{2}\mathbf{L}_{\mathrm{i}}^{\mathrm{T}}\mathbf{L}_{\mathrm{i}}\mathbf{x}_{\mathbf{0}}$$

$$\mathbf{x} = \left(\mathbf{A}^{\mathrm{T}}\mathbf{A} + \lambda_{\mathrm{Tik}}^{2}\mathbf{L}_{i}^{\mathrm{T}}\mathbf{L}_{i}\right)^{-1}\left(\mathbf{A}^{\mathrm{T}}\mathbf{b} + \lambda_{\mathrm{Tik}}^{2}\mathbf{L}_{i}^{\mathrm{T}}\mathbf{L}_{i}\mathbf{x}_{\mathbf{0}}\right)$$

Equivalently, therefore, Tikhonov regularization can be embedded directly into the ill-conditioned FBL, $\mathbf{A_c x_c} = \mathbf{b_c}$, exactly the same way as Eq. (6.31), i.e., replace **A** and **b** in Eq. (2.30) with $\mathbf{A_c}$ and $\mathbf{b_c}$ in Eq. (6.29),

$$\left(\mathbf{A_c}^T\mathbf{A_c} + \boldsymbol{\lambda}_{\mathbf{Tik}}^2\mathbf{L}_i^T\mathbf{L}_i\right)\mathbf{x_c} = \mathbf{A_c}^T\mathbf{b_c} + \boldsymbol{\lambda}_{\mathbf{Tik}}^2\mathbf{L}_i^T\mathbf{L}_i\mathbf{x_0} \tag{6.31}$$

where $\mathbf{A_c}$ and $\mathbf{b_c}$ are defined in Eq. (6.29).

Hence, Tikhonv embedded FBL controller (Tik-FBL) becomes

$$\begin{aligned}\mathbf{u} = \mathbf{x_c} &= \left(\mathbf{A_c}^T\mathbf{A_c} + \boldsymbol{\lambda}_{\mathbf{Tik}}^2\mathbf{L}_i^T\mathbf{L}_i\right)^{-1}\left(\mathbf{A_c}^T\mathbf{b_c} + \boldsymbol{\lambda}_{\mathbf{Tik}}^2\mathbf{L}_i^T\mathbf{L}_i\mathbf{x_0}\right)\\ &= \left\{\left(\mathbf{L_g}\mathbf{L_f}\mathbf{h}(\mathbf{x})\right)^T\left(\mathbf{L_g}\mathbf{L_f}\mathbf{h}(\mathbf{x})\right) + \boldsymbol{\lambda}_{\mathbf{Tik}}^2\mathbf{L}_i^T\mathbf{L}_i\right\}^{-1} \times\\ &\qquad \left\{\left(\mathbf{L_g}\mathbf{L_f}\mathbf{h}(\mathbf{x})\right)^T\left(\ddot{\mathbf{y}}_\mathbf{d} - \boldsymbol{\lambda}_\mathbf{1}\dot{\mathbf{e}} - \boldsymbol{\lambda}_\mathbf{2}\mathbf{e} - \mathbf{L_f}^2\mathbf{h}(\mathbf{x})\right) + \boldsymbol{\lambda}_{\mathbf{Tik}}^2\mathbf{L}_i^T\mathbf{L}_i\mathbf{x_0}\right\}\end{aligned} \tag{6.32}$$

Also, as the TSVD solution, $\mathbf{x_p}$, for any ill-conditioned $\mathbf{Ax} = \mathbf{b}$ is defined in Eq. (2.33) in Chapter 2, rewriting,

$$\mathbf{x_p} = \mathbf{A}_p^+\mathbf{b} = \sum_{i=1}^{p}\frac{\mathbf{u}_i^T\cdot\mathbf{b}}{\sigma_i}\mathbf{v}_i$$

where $\mathbf{A}_p \equiv \sum_{i=1}^{p}\mathbf{u}_i\sigma_i\mathbf{v}_i^T$ is an approximated rank-p matrix.

The TSVD embedded FBL controller (TSVD-FBL) for the ill-conditioned FBL, $\mathbf{A_c x_c} = \mathbf{b_c}$, can be designed as Eq. (6.33)

$$\begin{aligned}\mathbf{u} = \mathbf{x}_{\mathbf{c},p} &= \mathbf{A}_{\mathbf{c},p}^+\mathbf{b_c}\\ &= \sum_{i=1}^{p}\frac{\mathbf{u}_{\mathbf{c},i}^T\cdot\mathbf{b_c}}{\sigma_{c,i}}\mathbf{v}_{\mathbf{c},i}\\ &= \sum_{i=1}^{p}\frac{\mathbf{u}_{\mathbf{c},i}^T\cdot\left(\ddot{\mathbf{y}}_\mathbf{d} - \boldsymbol{\lambda}_\mathbf{1}\dot{\mathbf{e}} - \boldsymbol{\lambda}_\mathbf{2}\mathbf{e} - \mathbf{L_f}^2\mathbf{h}(\mathbf{x})\right)}{\sigma_{c,i}}\mathbf{v}_{\mathbf{c},i}\end{aligned} \tag{6.33}$$

where $\mathbf{A}_{\mathbf{c},p} \equiv \sum_{i=1}^{p} \mathbf{u}_{\mathbf{c},i}\sigma_{c,i}\mathbf{v}_{\mathbf{c},i}^{T}$ and, $\mathbf{u}_{\mathbf{c},\mathrm{i}}$ and $\mathbf{v}_{\mathbf{c},\mathrm{i}}$ are the column vectors (the singular vectors) of $\mathbf{A_c}$ and $\sigma_{c,i}$ are the singular values of $\mathbf{A_c}$ in Eq. (6.29).

For regularization embedded SMC controllers, the only difference in Eqs. (6.32) and (6.33) is reflected in $\mathbf{b_c}$. Therefore, Tik-SMC and TSVD-SMC are designed as in Eq. (6.34) and (6.35), respectively.

$$\begin{aligned}\mathbf{u} = \mathbf{x}_{\mathbf{c}} &= \left(\mathbf{A}_{\mathbf{c}}^{T}\mathbf{A}_{\mathbf{c}} + \boldsymbol{\lambda}_{\mathbf{Tik}}^{2}\mathbf{L}_{i}^{T}\mathbf{L}_{i}\right)^{-1}\left(\mathbf{A}_{\mathbf{c}}^{T}\mathbf{b}_{\mathbf{c}} + \boldsymbol{\lambda}_{\mathbf{Tik}}^{2}\mathbf{L}_{i}^{T}\mathbf{L}_{i}\mathbf{x}_{\mathbf{0}}\right) \\ &= \left\{\left(\mathbf{L}_{\mathbf{g}}\mathbf{L}_{\mathbf{f}}\mathbf{h}(\mathbf{x})\right)^{T}\left(\mathbf{L}_{\mathbf{g}}\mathbf{L}_{\mathbf{f}}\mathbf{h}(\mathbf{x})\right) + \boldsymbol{\lambda}_{\mathbf{Tik}}^{2}\mathbf{L}_{i}^{T}\mathbf{L}_{i}\right\}^{-1} \times \\ &\qquad \left\{\left(\mathbf{L}_{\mathbf{g}}\mathbf{L}_{\mathbf{f}}\mathbf{h}(\mathbf{x})\right)^{T}\left(\ddot{\mathbf{y}}_{\mathbf{d}} - \boldsymbol{\lambda}_{\mathbf{SMC}}\dot{\mathbf{e}} - \mathbf{L}_{\mathbf{f}}^{2}\mathbf{h}(\mathbf{x}) - \mathbf{D}\cdot\tanh(\mathbf{S})\right) + \boldsymbol{\lambda}_{\mathbf{Tik}}^{2}\mathbf{L}_{i}^{T}\mathbf{L}_{i}\mathbf{x}_{\mathbf{0}}\right\}\end{aligned} \tag{6.34}$$

$$\begin{aligned}\mathbf{u} = \mathbf{x}_{\mathbf{c},p} &= \mathbf{A}_{\mathbf{c},p}^{+}\mathbf{b}_{\mathbf{c}} \\ &= \sum_{i=1}^{p}\frac{\mathbf{u}_{\mathbf{c},i}^{T}\cdot\mathbf{b}_{\mathbf{c}}}{\sigma_{c,i}}\mathbf{v}_{\mathbf{c},i} \\ &= \sum_{i=1}^{p}\frac{\mathbf{u}_{\mathbf{c},i}^{T}\cdot\left(\ddot{\mathbf{y}}_{\mathbf{d}} - \boldsymbol{\lambda}_{\mathbf{SMC}}\dot{\mathbf{e}} - \mathbf{L}_{\mathbf{f}}^{2}\mathbf{h}(\mathbf{x}) - \mathbf{D}\cdot\tanh(\mathbf{S})\right)}{\sigma_{c,i}}\mathbf{v}_{\mathbf{c},i}\end{aligned} \tag{6.35}$$

6.5.3. Results with regularization embedded control

In this section, the new regularization embedded nonlinear controllers, Eqs. (6.32)-(6.35), are applied to the same thermal problem to handle the input-constraint-violating control solution that is assumed to be caused by the ill-conditionedness of the controllers. First, the results of applying the TSVD-FBL controller are shown in Fig. 6.12. The temperature distribution along all surfaces for the entire process time is shown in Fig. 6.12(a) with λ_1=0.1, λ_2=0.1 selected as the gains for FBL and truncation order p=3 for TSVD. Fig. 6.12(b) shows the

cross sectional view of the Fig. 6.12(a) at t = 350sec, i.e. the temperature distribution at t = 350 sec. As shown in Figs. 6.12(a), (b) and (f), the design surface temperatures track the desired trajectory well and maintain temperature uniformity well. And Fig. 6.12(c) shows all control inputs Q are positive—heat sources—a significant improvement over the results using a conventional nonlinear feedback controller where some heater were heat sinks (Figs. 6.7(c) and 6.8(c)). When seven of the smallest singular values are truncated, the condition number, shown in Fig. 6.12(e) is small (15-20). The initial condition number is higher than its steady value and causes initial oscillations in the control input Q. Fig. 6.12(g) shows a relatively flat responding $\mathbf{b_c}$, but due to the small condition number, the control input Q is much smoother compared to Figs. 6.7(c) and 6.8(c). The total energy used in the TSVD-FBL case is 4,114 KJ/m, which is almost 6 times less than the 26,425KJ/m required by the conventional nonlinear controller case.

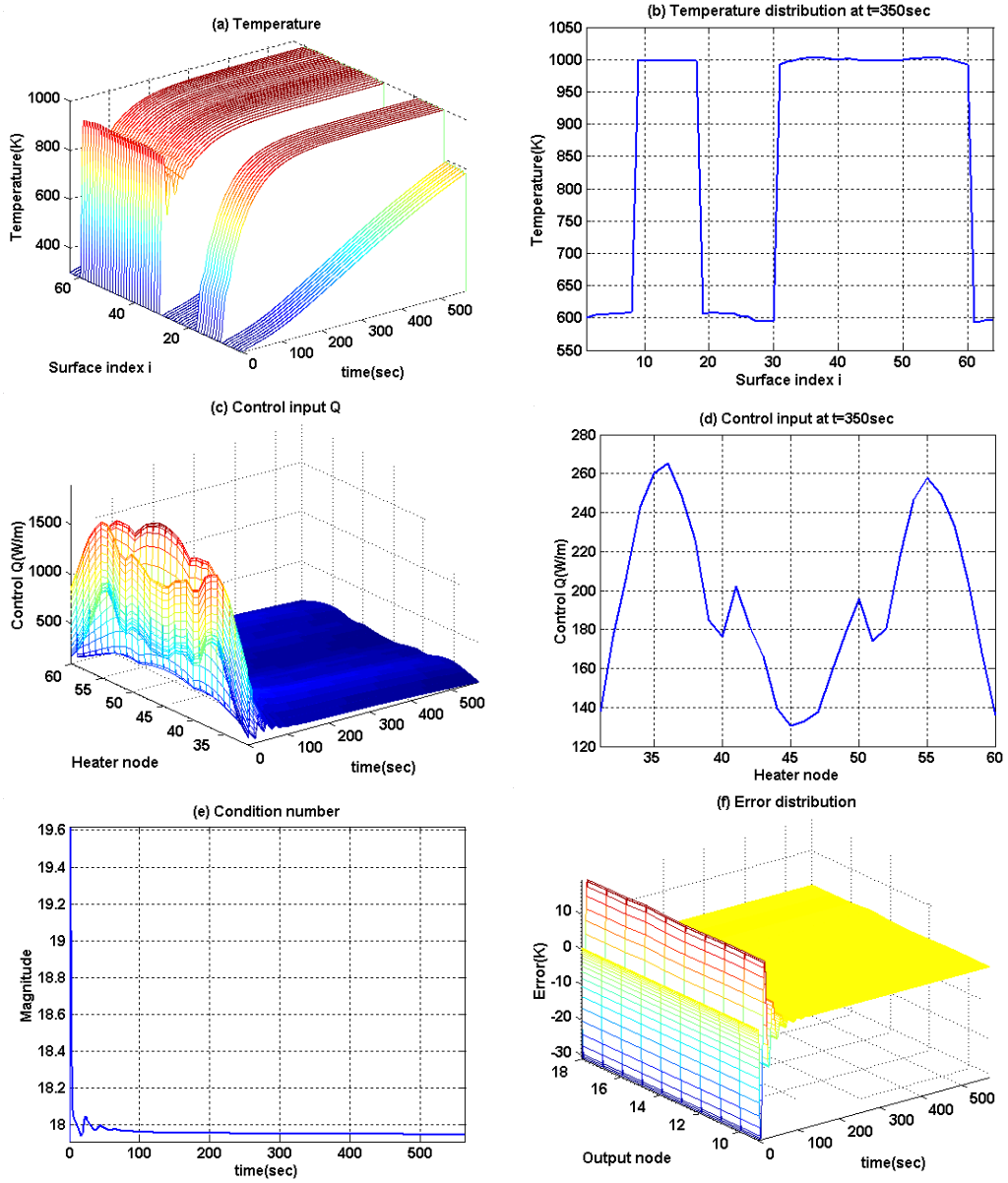
(a) Temperature
Temperature(K)
Surface index i
time(sec)
(b) Temperature distribution at t=350sec
Temperature(K)
Surface index i
(c) Control input Q
Control Q(W/m)
Heater node
time(sec)
(d) Control input at t=350sec
Control Q(W/m)
Heater node
(e) Condition number
Magnitude
time(sec)
(f) Error distribution
Error(K)
Output node
time(sec)

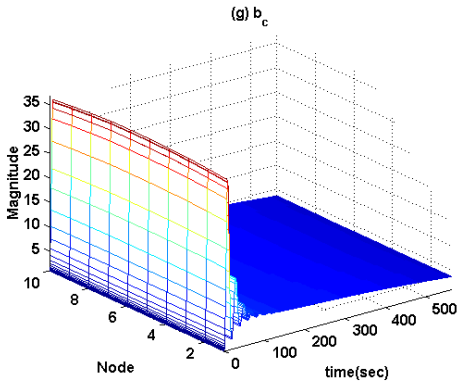

Figure 6.12 Responses of TSVD -FBL with p=3, λ_1=0.1, λ_2=0.1

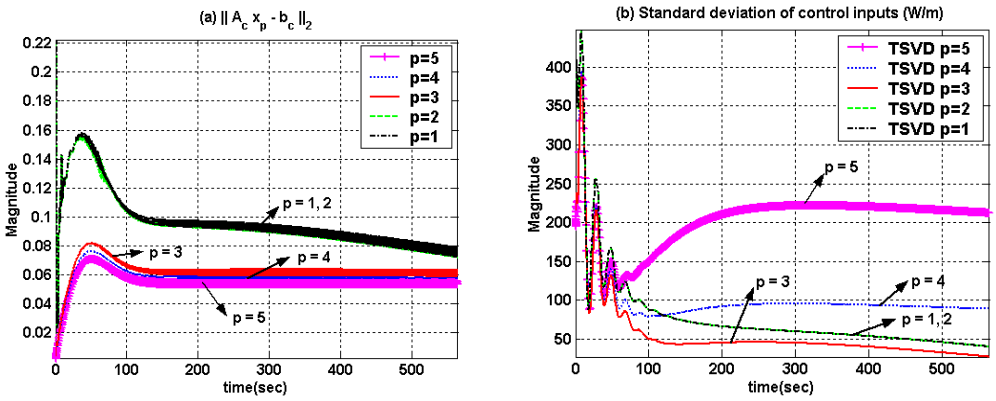

Figure 6.13 Optimal TSVD parameter (a) residual norm and (b) standard deviation of the control input for different TSVD parameters p

Figs. 6.13(a) and (b) show the 2-norm of the system residual with different TSVD parameters and the standard deviation of the heater input distribution—these figures are used to select the optimal TSVD parameter p. For large values of p, i.e. more singular values are kept, the residuals are small but the heater input

shows larger oscillations in its distribution, i.e. large standard deviation. In Fig. 6.13(a) p=3,4,5 responses have similar small residuals, but p=3 in Fig. 6.13(b) shows much smaller standard deviation in the heater input distribution than in the p=4,5 cases, and it is even smaller than in the p=1,2 cases. Therefore it appears that p=3 is the optimal value that achieves a balance between minimum residual and good smoothing effects. Table 6.2, that shows performance measures for different controllers and regularization parameters, shows that since p=3 has a more smooth distribution, energy for a certain time is also distributed more evenly for all the heaters, resulting in a smaller maximum (peak) control input than in the p=2 case (TSVD3 vs. TSVD2). Its smaller residual results in a smaller steady state error and smaller maximum error than in the p=2 case.

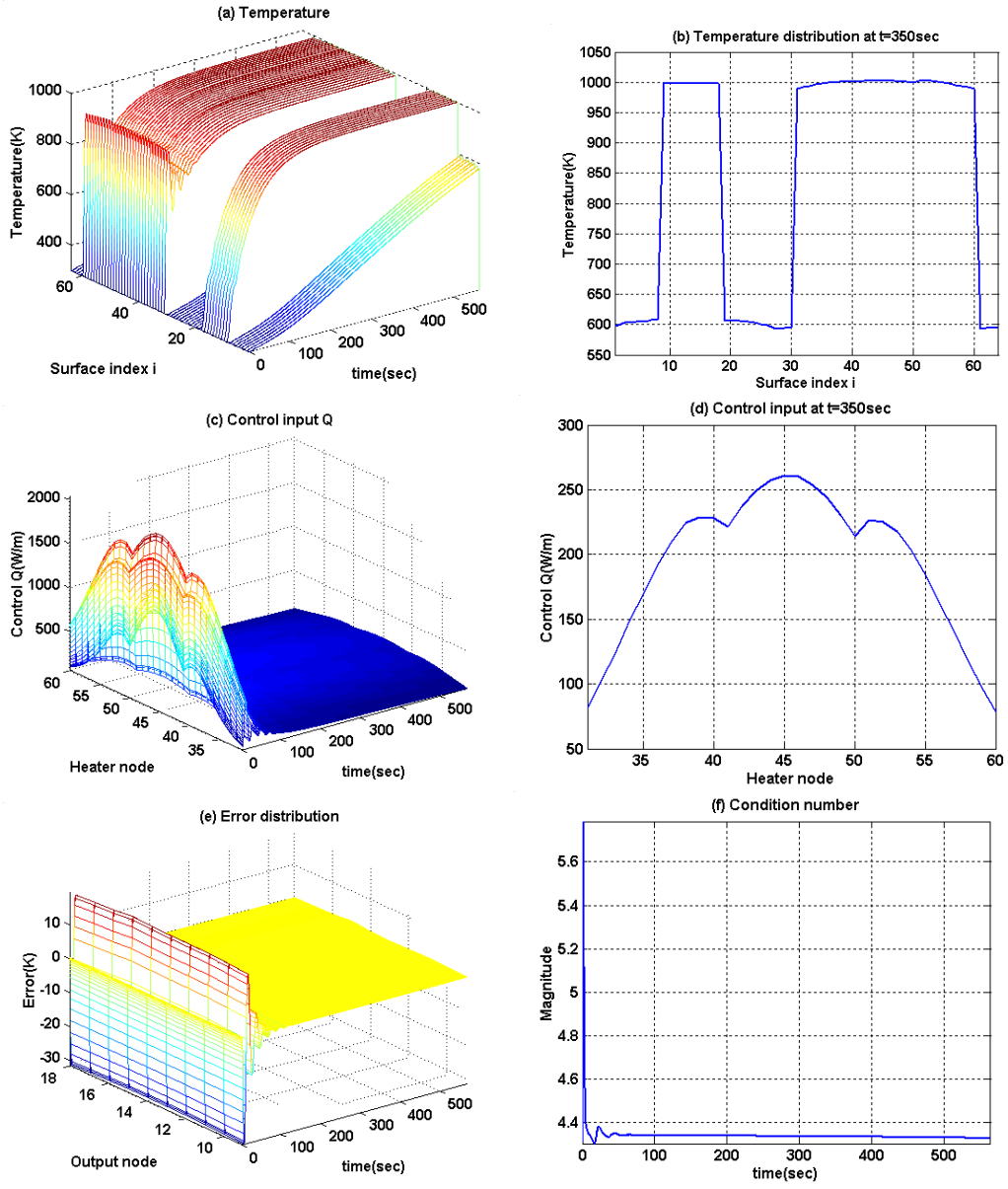

Figure 6.14 Responses of TSVD-FBL with p=2, λ_1=0.1, λ_2=0.1

If eight of the smallest singular values are truncated (p=2), the condition number is reduced by a factor of five than in the p=3 case (Fig. 6.12(e)), see Fig. 6.14(f), but the heater surface inputs still oscillate at the early stages. It appears that the condition number alone, does not cause the oscillations in the solution. The peak values of the control inputs also depend upon controller gain, regularization parameter, and type of controller.

The regularized nonlinear control designs inherently contain modeling errors since $\mathbf{A_c}$ is modified to $\mathbf{A}_{\mathbf{c},p}$ by regularization. Figs. 6.15(a) and (b) compare the temperature errors on the design surface for the nonlinear FBL and the TSVD3-FBL controlled systems, respectively. The errors are larger for the regularized system than the pure nonlinear FBL controlled system, but are still less than one degree K. More important, however, is the fact that the input solution with regularization is physically real—no heat sinks.

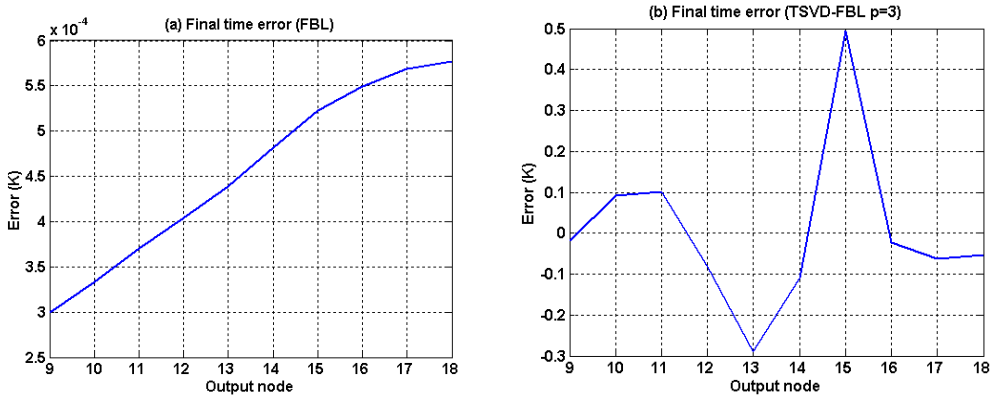

Figure 6.15 Final time errors in the design surface temperatures (a) FBL control (b) TSVD-FBL control with p=3, λ_1=0.1, λ_2=0.1

The optimal TSVD parameter has been previously found to be p=3—the TSVD solution for this case can now be applied to the MTSVD design using Eq. (2.36). The MTSVD solution with p=3 and $\mathbf{L}_1$ (Fig. 6.16) shows similar temperature and heater control input distribution to the TSVD solution with p=3 (Fig. 6.12). But the MTSVD solution provides a more uniform control input distribution than the TSVD solution (see standard deviation of inputs from Fig. 6.17). This is because the first-order derivatives of vector **x** were minimized through the operator $\mathbf{L}_1$ in the MTSVD regularization. Note that, since MTSVD minimizes $\|\mathbf{Lx}\|_2$, the total energy used is always larger than in the TSVD case since TSVD minimizes $\|\mathbf{x}\|_2$, which corresponds to the total size of control input vector (see Table 6.2, the MTSVD case requires 0.05% more energy than the TSVD case). Therefore the TSVD solution is always more energy efficient than the MTSVD solution, however, its control input distribution is less uniform.

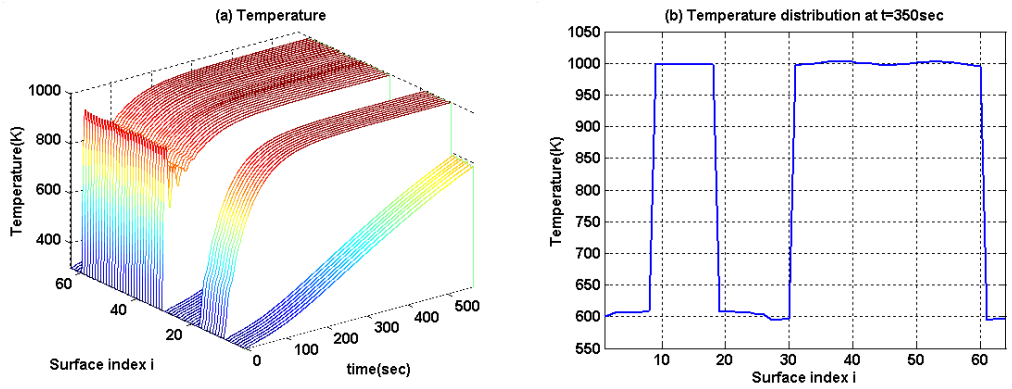

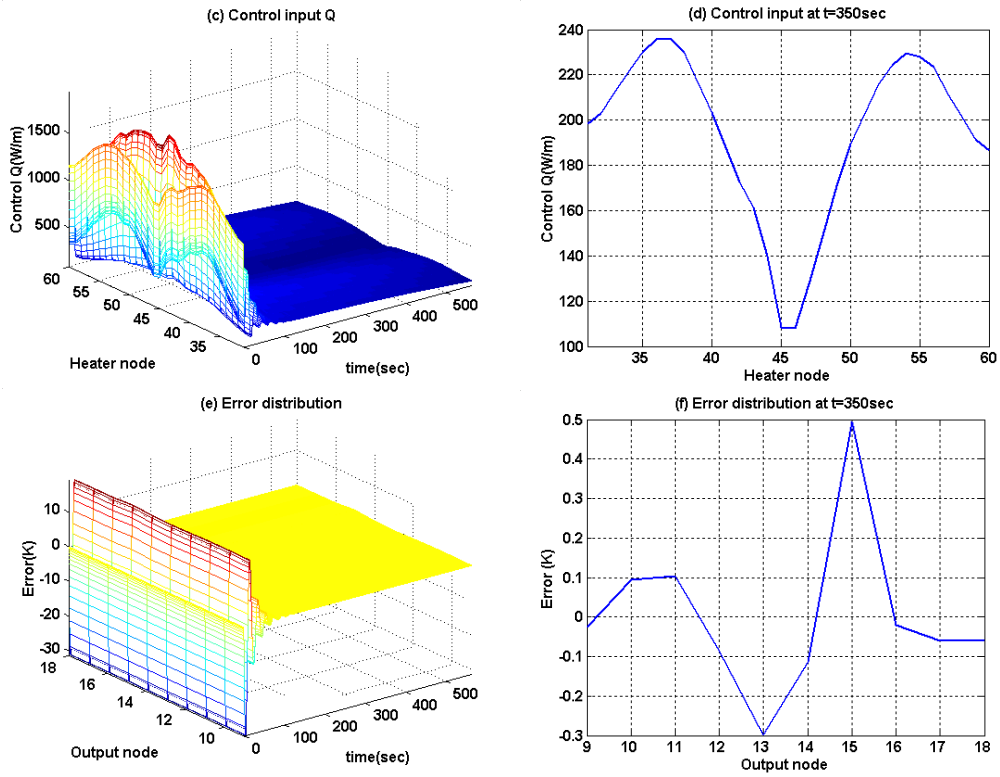

Figure 6.16 Temperature and heater input distribution with MTSVD p=3 for FBL with λ_1=0.1, λ_2=0.1

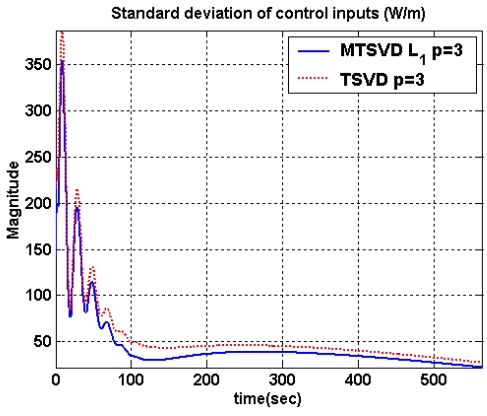

Figure 6.17 Standard deviation of control input for FBL with TSVD and MTSVD

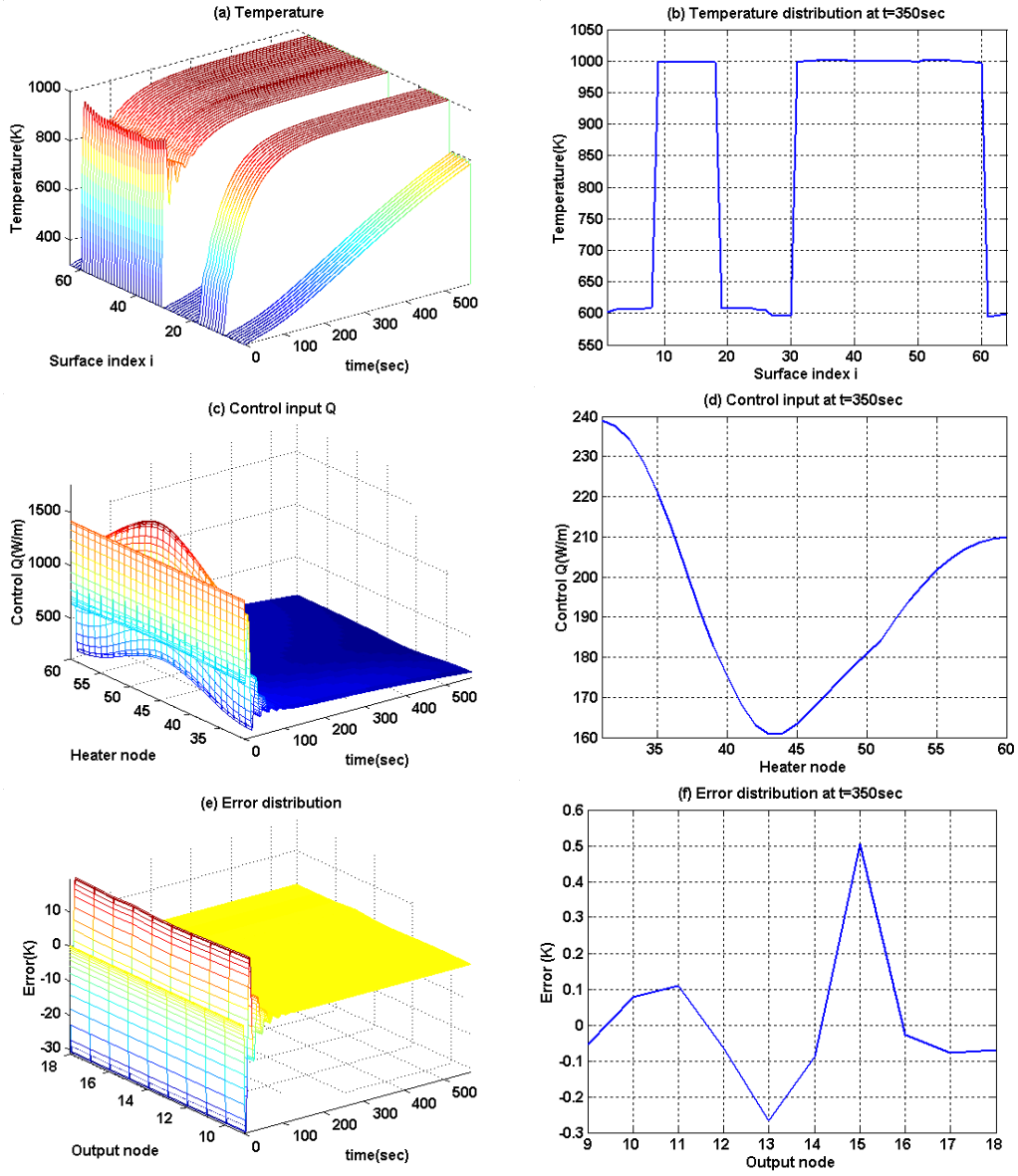

Figure 6.18 Responses for Tikhonov-FBL λ_{Tik}=0.001, λ_1=0.1, λ_2=0.1

Figure 6.18 shows the results of applying the Tikhonov-FBL using the same FBL gains as for the TSVD-FBL case. The first derivative operator $\mathbf{L}_1$ is used and the Tikhonov parameter was selected as 0.001 based on Figs. 6.19(a) and (b). In Fig. 6.18(a), the design surface temperature distribution matches the desired trajectory well but the heater surface input distribution in Fig. 6.18(c) is different compared to the TSVD3-FBL case (Fig. 6.12(c)). This observation shows that the solution is not unique.

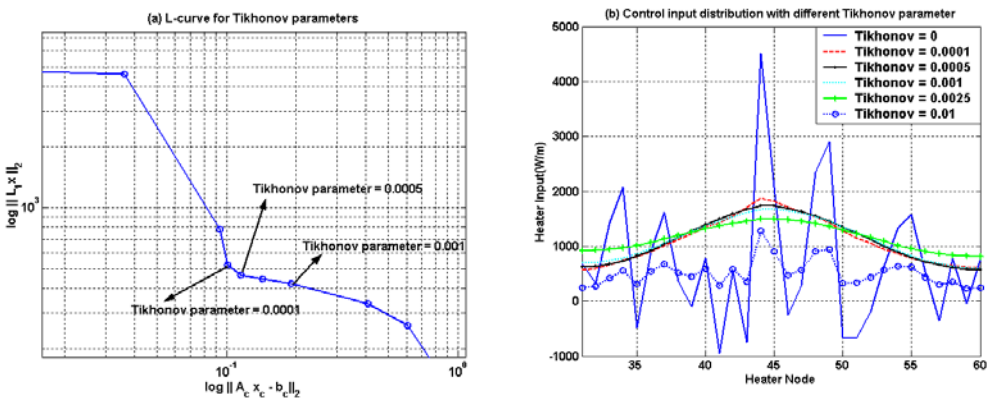

Figure 6.19. Optimal Tikhonov parameter (a) L-curve for the optimal parameter selection (b) control input distribution along the heaters for different Tikhonov parameters

Figure 6.19(a) is the L-curve for the Tikhonov parameter—the corner of the L-curve suggests the near optimal parameter value of around 0.0001~0.0005. Figure 6.19(b) shows the heater input distribution for the different Tikhonov parameters by solving Eq. (6.32). It is noticed that λ_{Tik} = 0.0001 shows all positive values, however it results in a high peak in the 15th heater, which could

violate (i.e. saturate) the upper bound of actuator constraint. While parameter $\lambda_{Tik} = 0.001$ shows a similar heater input distribution to the $\lambda_{Tik} = 0.0001$ case, it generates a smaller peak value—a more conservative solution with respect to the actuator constraint. Also note from Table 6.2 that when the smoothing effect is large, the total energy used decreases (4.52×10^6 J/m versus 4.42×10^6 J/m, 2.3% decrease). Since the residuals with three different Tikhonov parameters are similar in values at the final state error and although the L-curve suggests the use of smaller values, $\lambda_{Tik} = 0.001$ provides a more energy efficient and more stable solution. Therefore if the design criterion is to minimize total energy use, the smoothing effect should be emphasized at the cost of larger errors at the final state.

Regarding the condition number of the Tikhonov-FBL controller, the dimension of $\mathbf{A_c}$ is now 30x30, not 10x30 as in the TSVD-FBL controller case, so the number of singular values is 30 instead of 10. Therefore, it would not be meaningful to compare the singular values of the two cases. Figure 6.20(a) shows the condition number with the Tikhonov parameter set to zero—no regularization effect—and Fig. 6.20(b) shows the condition number for the case with λ_{Tik} =0.001 and $\mathbf{L}_1$ as the derivative operator. As expected, the condition number is orders of magnitude smaller with regularization.

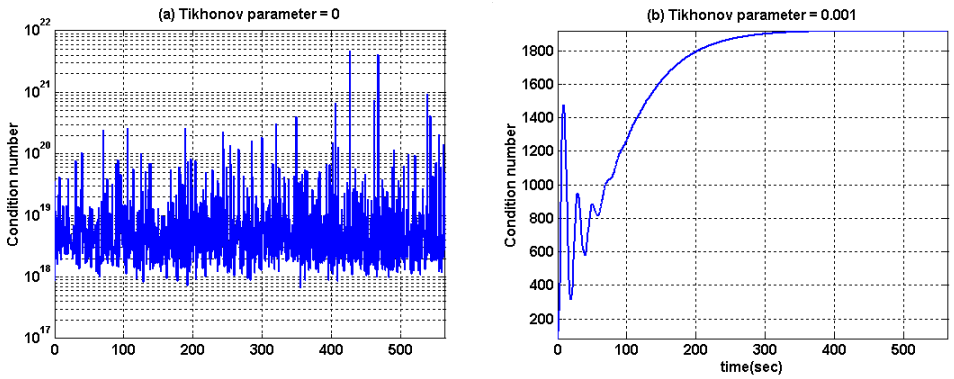

Figure 6.20 Condition numbers with (a) Tikhonov parameter zero and (b) with λ_{Tik} =0.001 and $\mathbf{L}_1$ as the derivative operator

Since regularization introduces modeling errors, sliding mode control is a promising candidate. However, since this system is inherently stable and modeling errors arise from the truncation of small singular values (in the case of TSVD) and/or the diminishing effects of small singular values, it is expected that modeling errors may not affect the system response much—a regularization-embedded SMC controller may not improve the system response over the Tikhonov-FBL cases.

Figure 6.21 shows the responses of the Tikhonov-SMC control with $\mathbf{D}$=0.5, λ_{SMC} = 0.2, λ_{Tik} = 0.001 and $\mathbf{L}_2$. As expected, the results are almost identical to the Tikhonov-FBL case (λ_{Tik} = 0.001 and $\mathbf{L}_1$) except for smaller initial oscillations in the heater temperatures and higher initial control inputs Q.

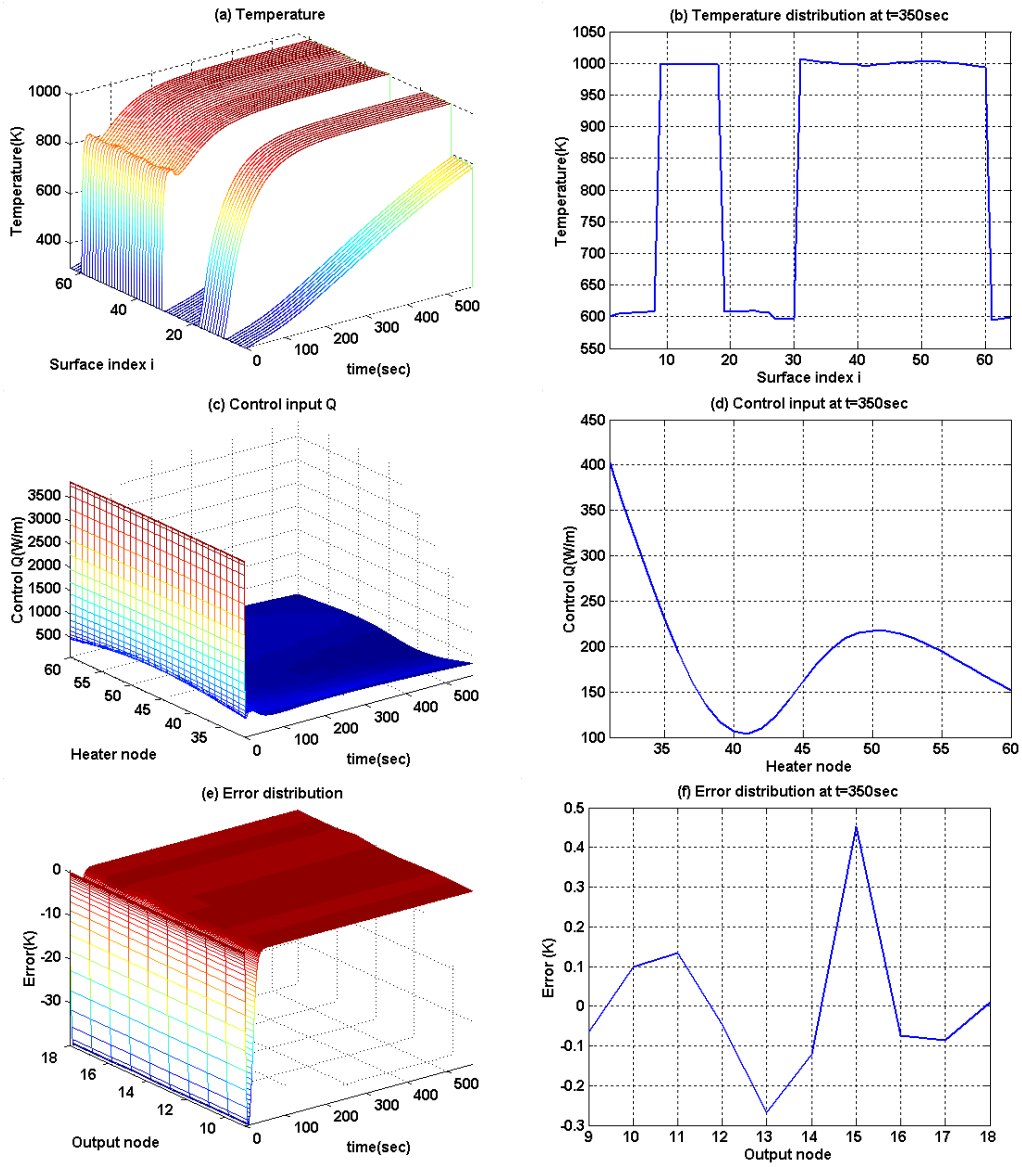

Figure 6.21 Responses for Tikhonov-SMC with D= 0.5, λ_{SMC} = 0.2 and λ_{Tik} = 0.001 and $\mathbf{L}_2$.

Figures 6.22(a) and (b) show the distributions of control input and temperature along the heater surfaces at final time, respectively; the smoothing effect is best for Tikhonov-FBL, smallest for the Tikhonov-SMC, and TSVD-FBL with p=2 shows a flatter distribution than the p=3 case. The temperature distribution along the heater surfaces is almost uniform due to regularization but they are not the same as the steady state temperature of the design surface. The heater surface distribution is such that the zero total heat flux condition is satisfied at the design surface. Since the reflector surfaces absorb and emit very little energy due to their high reflectivity, they do not reach the same steady state temperature as the design surface (see Fig. 6.23); their temperatures are lower than the heater and design surface temperatures which means that the heater and design surface are losing heat to the reflective surfaces. Therefore to maintain the design surface temperature at steady state, the heaters must continue to provide heat input to the system until the total system reaches equilibrium; this is verified in Fig. 6.22(a).

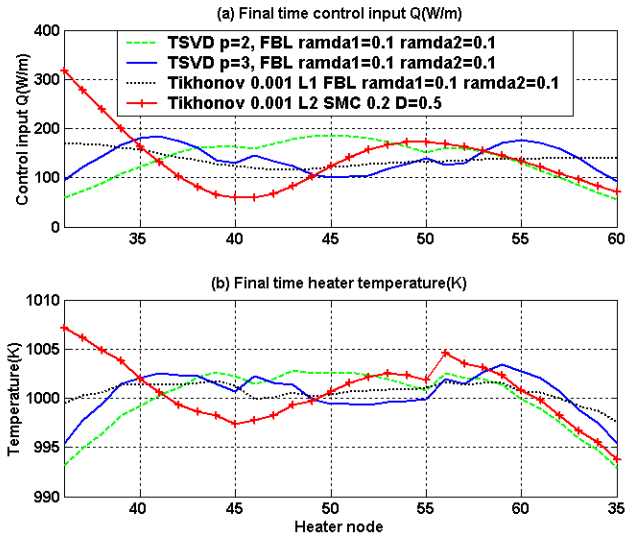

Figure 6.22 Final time distribution (a) final state heater input distribution (b) final state heater surface temperature distribution

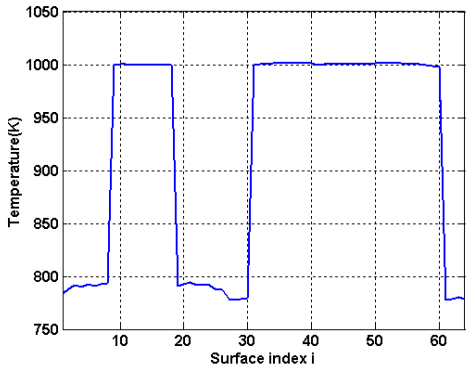

Figure 6.23 Final time temperature distribution for Tik-FBL with λ_{Tik}=0.001, λ_1=0.1, λ_2=0.1 and $\mathbf{L}_1$.

Thus far, it has been shown that all five regularization embedded nonlinear controllers (TSVD-FBL (p=2 and p=3), MTSVD-FBL(p=3), Tikhonov-FBL and Tikhonov-SMC) provide physically meaningful solutions and design surface temperatures that track the desired trajectories. However, performance measures, such as the maximum control input, maximum error, steady state error and total energy, depend on the gains, type of controllers and regularization methods as shown in Table 6.2.

The results can be used as a design tool: for example, the location and numbers of heaters could be redesigned and optimized since it has been shown that different heater surface input distributions can achieve the very similar design surface temperature distribution.

Table 6.2. Performance measures for regularization embedded nonlinear controllers

Controller	Max. control input (W/m)	Total energy (J/m)	Max. error in design surface (K)	Max. steady- state error(K)
MTSVD3-FBL $\mathbf{L}_1$	1937	4.4138E+6	-31.2	0.49
TSVD3-FBL	1890	4.4114E+6	-31.3	0.49
TSVD2-FBL	2034	4.4001E+6	-31.7	0.60
Tikhonov-FBL λ_{Tik} =0.001	1763	4.4171E+6	-31.2	0.49
Tikhonov-FBL λ_{Tik} =0.0005	1896	4.4179E+6	-31.3	0.47
Tikhonov-FBL λ_{Tik} =0.0001	2034	4.5212E+6	-31.1	0.42
Tikhon.-SMC	3846	4.4183E+6	-39.7	0.45
SMC	7687	2.6408E+7	-39.7	0.0005
FBL	7531	2.6425E+7	-31.2	0.0005

6.5.4. Summary

In this section, new regularization embedded nonlinear control designs were presented for the temperature control of an input-constrained and ill-conditioned thermal problem. The new controllers produced physically meaningful, actuator-constraint-satisfying solutions which were not obtained by the general nonlinear controller.

By applying SVD to the LAENC of the FBL/SMC, the reasons for input-constraint-violation, i.e. ill-conditionedness of the controller, was shown and accordingly regularization was embedded into the nonlinear controller to reduce/eliminate the effect of ill-conditionedness. This is the first attempt to overcome the input-constraint-violation of the nonlinear controller using regularization. Also, it is a unique attempt to diagnose the characteristics of the nonlinear controller using SVD on the LAENC.

Design guidelines were provided for the selection of regularization parameter values. While the embedded controllers worked well on the given thermal process model, the designs can be extended to any ill-conditioned process model which could generate input-constraint-violating control solutions. This regularization embedded controllers can be applied not only to ill-conditioned system, but also to any multi-input systems with constraints, because, by forcing all the controllers to be more uniform, it is possible to reduce the burden of any specific controller which may require large inputs, hence possibly violating the input-constraint. Also, instead of using derivative operators **L** in Tik-FBL/SMC, the designer may want to design a new operator for the optimization, i.e., larger weight on the expensive controller to save the cost.

6.6. CONSTRAINED NONLINEAR OPTIMAL CONTROL

In the previous section, it was shown that input-constraint-violating solutions were due to the ill-conditionedness of the system/controller, hence regularization embedded nonlinear controllers were proposed and successfully applied to the temperature control of the thermal system by eliminating/reducing the effects of ill-conditionedness. However, as the results in Table 6.2 show the choices of regularization method and parameters are critical to system performance. In this section, the regularization-parameter-free constrained nonlinear optimal controller proposed in Chapter 4, which is more robust in terms of the input-constraint, is analyzed. As mentioned in Chapter 3, the structure of FBL and SMC are similar except for the $\mathbf{b_c}$ term in Eq. (3.1), therefore in this section, the constrained nonlinear optimal controllers are analyzed only for FBL.

6.6.1. Linear least squares problem with nonnegative input constraints

As shown previously, both FBL/SMC controller designs (Eq. (6.29)) are in the form $\mathbf{A_c x_c} = \mathbf{b_c}$, and both control solutions violate the input constraints (see section 6.4). Here a linear least squares problem with nonnegative input constraints proposed in Eq. (4.5), is posed for the temperature control problem of the thermal system as follows.

$$\min_{\mathbf{x_c}} \left\| \mathbf{A x_c} - \mathbf{b} \right\|_2^2 \quad \text{such that} \quad \mathbf{x_c} \geq \mathbf{0} \tag{6.36}$$

The subscript $_c$ on matrix $\mathbf{A_c}$ and target vector $\mathbf{b_c}$ will be omitted hereafter for simplicity as in Eq. (6.36). Note that the vector $\mathbf{x_c}$ represent the control input vector, not a state vector.

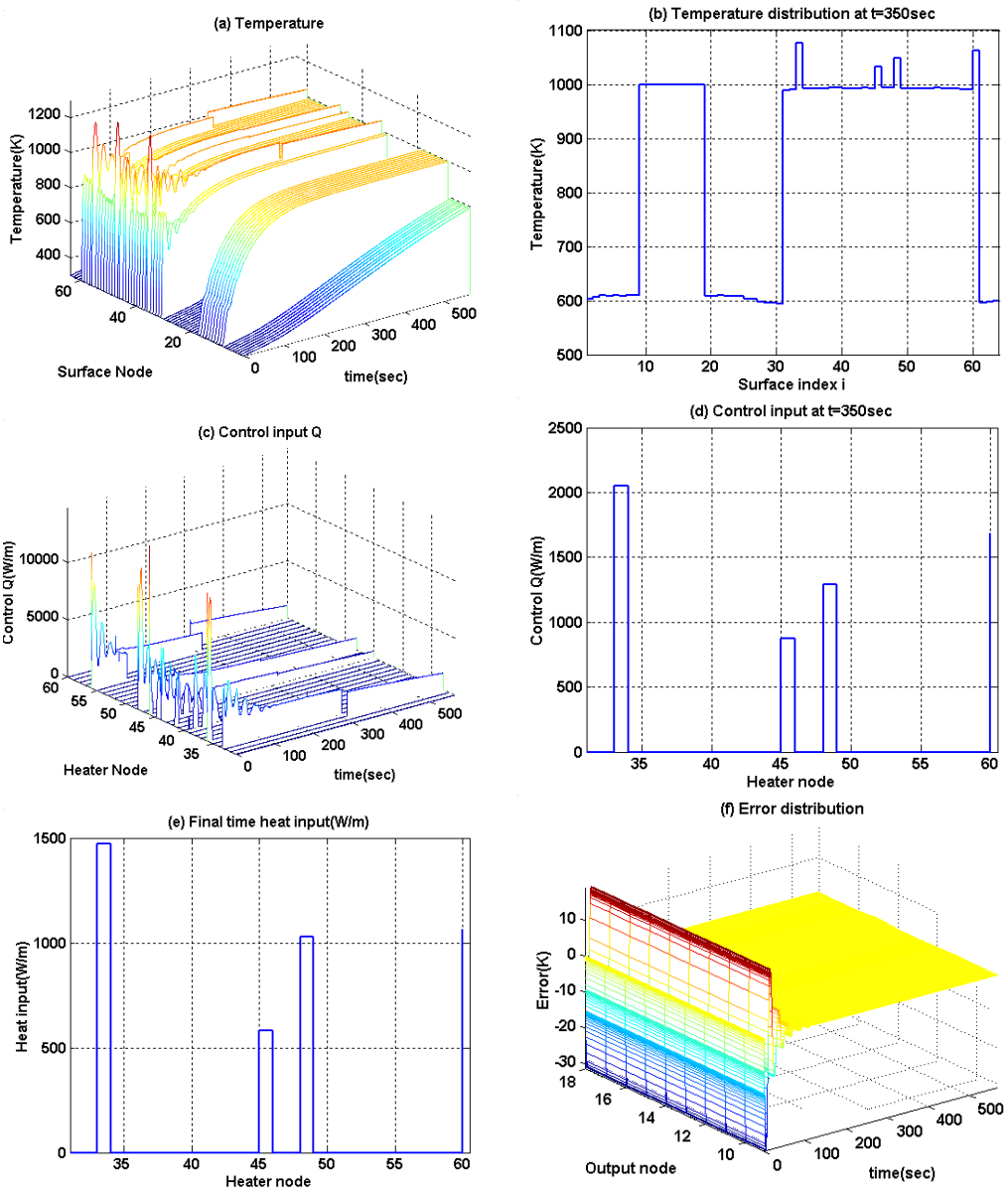

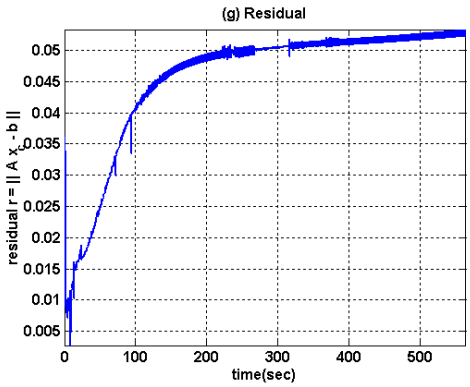

Figure 6.24 Responses for Eq. (6.36) (a) Temperature distribution along the surfaces over the entire process time and (b) at t=350sec, (c) control input Q over the entire process time and (d) at t=350sec, (e) final time heater input distribution (f) error distribution (g) residual

Figure 6.24(a) shows the temperature distribution of all the surfaces subject to the heater inputs computed by Eq. (6.36). The linear least squares algorithm with nonnegative constraints in MATLAB® is used to solve Eq. (6.36). Figure 6.24(a) shows that the proposed controller preserves the characteristics of FBL on which it was originally designed. In other words, the outputs (surfaces 9-18) follow the desired error dynamics shown in Fig. 6.5—design surface temperature distribution (Fig. 6.24(a)) and error behavior (Fig. 6.24(f)) show similar behaviors as Fig. 6.5. It is also verified in Fig. 6.24(b) that the output surfaces maintain temperature uniformity. Figure 6.24(c) shows that all heater inputs satisfy the input constraint, i.e. $Q \geq 0$. Figure 6.24(g) shows the Euclidean norm of the residuals, considered as a modeling error which is inevitably caused by the input constraints. The residuals are relatively small in magnitude; hence,

input-constraint-satisfying solutions are obtained with little degradation in performance which is verified in Fig. 6.24(a) and Fig. 6.24(f).

Positive net energy must be put into the system to control the design surface temperatures to follow the desired temperature profile. However due to the ill-conditioned nature of the FBL/SMC controllers, the control input distribution was uneven (Figs. 6.7 and 6.8), resulting in large positive inputs for some heaters and negative inputs for others. However to satisfy the constraint, i.e. $\mathbf{x}_c \geq \mathbf{0}$, in this case (Eq. (6.36)), it is expected that the linear least squares algorithm with nonnegative constraints will result in some inputs to be zero, i.e. some heaters are turned off, while the rest are strictly positive. This is verified in Fig. 6.24(c) where eighteen (surfaces 31, 32, 35, 37, 38, 39, 41, 43, 47, 49, 50, 51-55, 57, 59) out of 30 heaters are turned off throughout the process. The remaining heaters must provide all the energy needed to satisfy $\mathbf{A}\mathbf{x}_c=\mathbf{b}$, resulting in high peak values in certain heaters—in Fig. 6.24(c) the peak control input is 14788W/m, which may violate the heater capacity. Fig. 6.24(e) shows the heater inputs at the final time. Only four heaters (surfaces 33, 45, 48, 60) are active at the final time to maintain the final desired surface temperature at 1000K to compensate for the lower temperatures of the reflective surfaces which have not yet reached equilibrium temperature. Since only four heaters are active, their peak values are still high. Figures 6.24(c) and (d) show that the process is controlled by a few inputs, which implies that a smaller number of heater can satisfy the design goal—an economic and computation advantage. This observation can lead to a

system optimization problem in which different numbers and locations of heaters could be determined.

6.6.2. Constrained nonlinear optimal control

Next, a linear least squares problem with nonnegative input constraints for an augmented system, as mentioned in Eq. (4.8), is considered. The identity matrix $\mathbf{I}_{30\times30}$ is used for the weighting matrix M, i.e., the optimization problem is between performance (residual) and minimizing control effort. This is a combined nonlinear optimal control problem that solves a quadratic minimization if feasible solutions exist, or transforms it into a linear least squares optimization with nonnegative input constraint if the solutions are not feasible:

$$\min_{\mathbf{x_c}} \left\| \mathbf{A}_{aug}\mathbf{x_c} - \mathbf{b}_{aug} \right\|_2^2 \text{ such that } \mathbf{x_c} \geq \mathbf{0} \tag{6.37}$$

Figures 6.25 and 6.26 are the results of the linear least squares optimization with nonnegative input constraints (Eq. (6.37)) with γ^2=1E-6 and γ^2=1E-4, respectively. Larger γ^2 places more weight on reducing control effort, hence less total Q, resulting in larger maximum and total error values. However larger γ^2 does not always guarantee less total energy use since it tries to minimize control effort by sacrificing the residual—increased residual causes larger errors in the performance and performance degradation increases the control inputs. Therefore the value of γ^2 should be selected carefully.

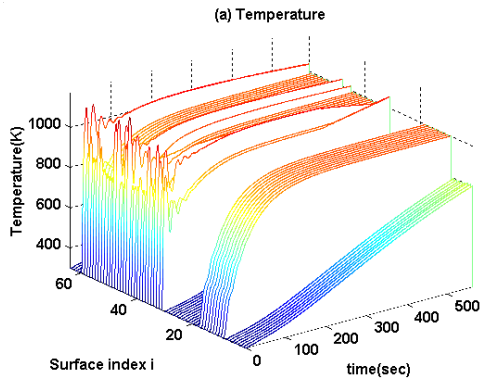
(a) Temperature
Temperature(K)
1000
800
600
400
60
40
20
Surface index i
0
100
200
300
400
500
time(sec)

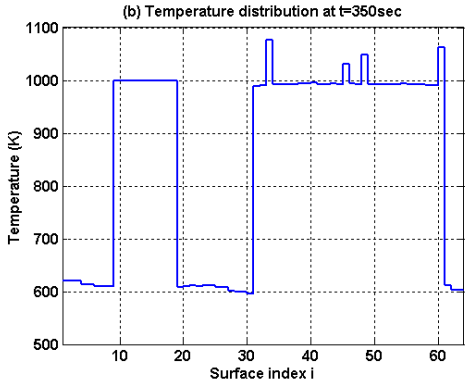
(b) Temperature distribution at t=350sec
Temperature (K)
1100
1000
900
800
700
600
500
10
20
30
40
50
60
Surface index i

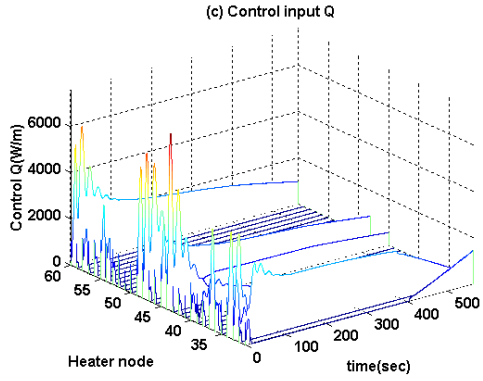
(c) Control input Q
Control Q(W/m)
6000
4000
2000
0
60
55
50
45
40
35
Heater node
0
100
200
300
400
500
time(sec)

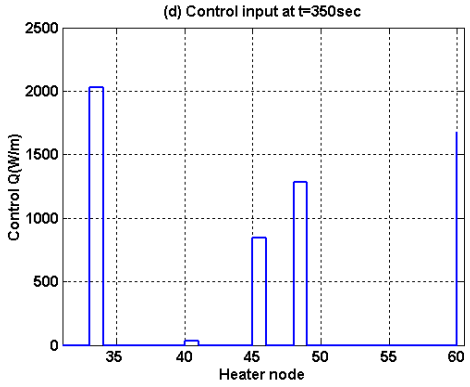
(d) Control input at t=350sec
Control Q(W/m)
2500
2000
1500
1000
500
0
35
40
45
50
55
60
Heater node

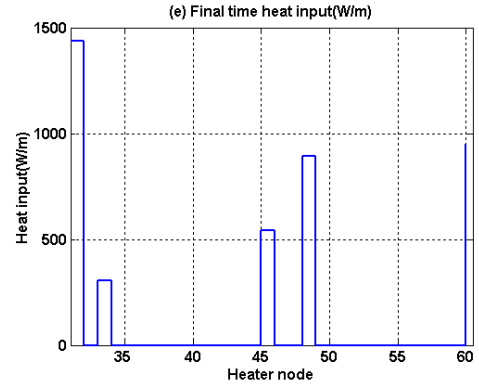
(e) Final time heat input(W/m)
Heat input(W/m)
1500
1000
500
0
35
40
45
50
55
60
Heater node

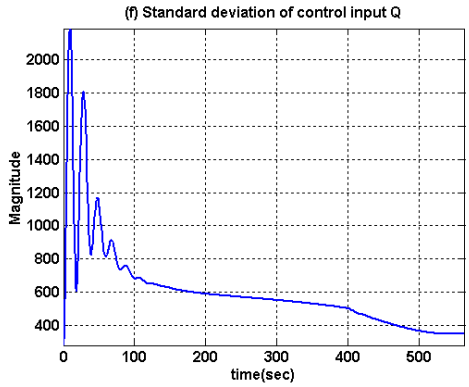
(f) Standard deviation of control input Q
Magnitude
2000
1800
1600
1400
1200
1000
800
600
400
0
100
200
300
400
500
time(sec)

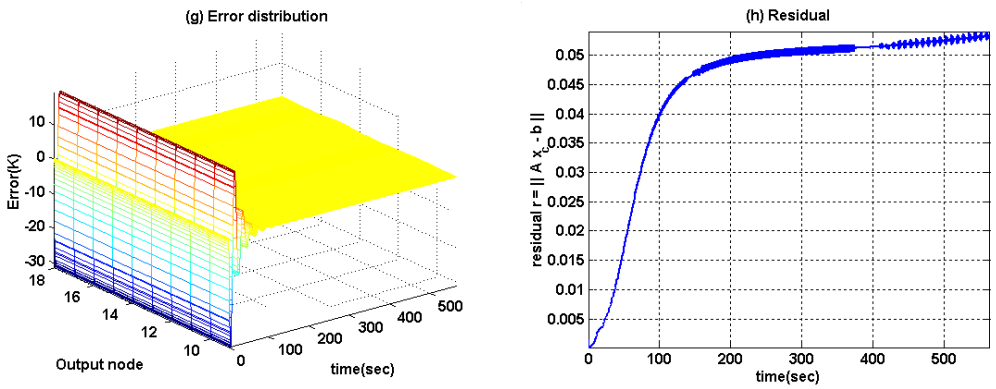

Figure 6.25 Responses for Eq. (6.37) with γ^2 =1E-6 (a) temperature distribution along the surface over the entire process time and (b) at t=350sec, (c) control input Q and (d) at t=350sec, (e) final time heater input distribution (f) standard deviation of heater inputs (g) error distribution (h) residual

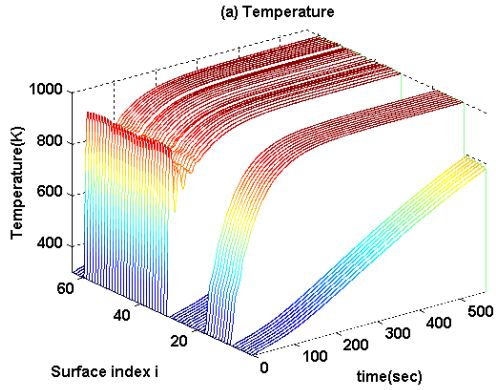
(a) Temperature
Temperature(K)
1000
800
600
400
60
40
20
Surface index i
0
100
200
300
400
500
time(sec)

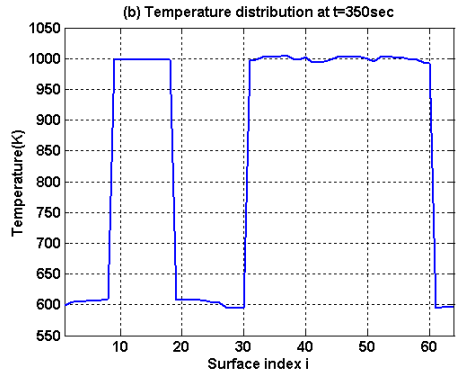
(b) Temperature distribution at t=350sec
Temperature(K)
1050
1000
950
900
850
800
750
700
650
600
550
10
20
30
40
50
60
Surface index i

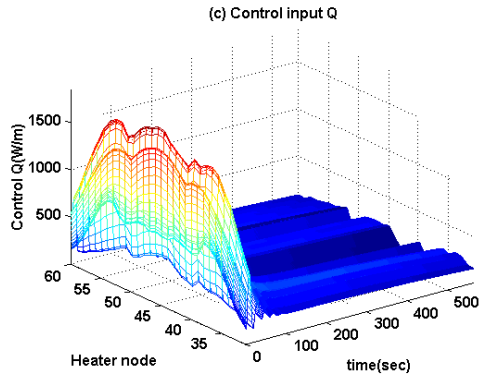
(c) Control input Q
Control Q(W/m)
1500
1000
500
60
55
50
45
40
35
Heater node
0
100
200
300
400
500
time(sec)

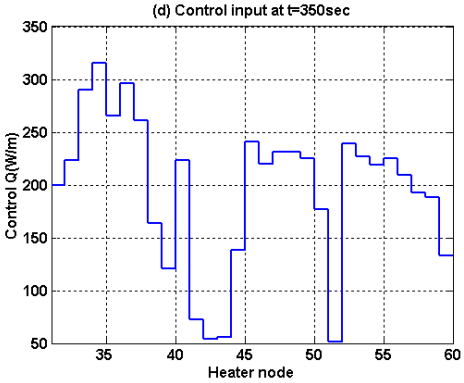
(d) Control input at t=350sec
Control Q(W/m)
350
300
250
200
150
100
50
35
40
45
50
55
60
Heater node

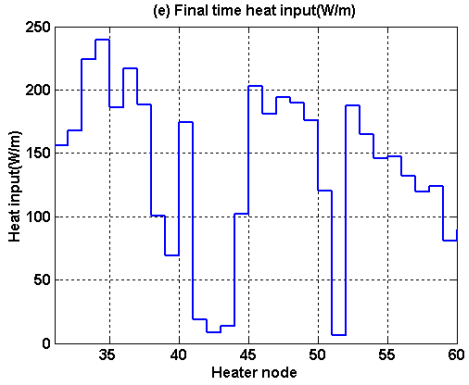
(e) Final time heat input(W/m)
Heat input(W/m)
250
200
150
100
50
0
35
40
45
50
55
60
Heater node

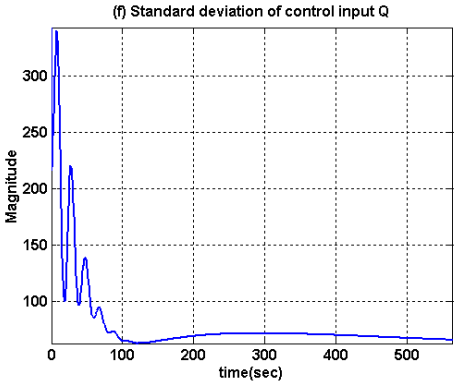
(f) Standard deviation of control input Q
Magnitude
300
250
200
150
100
0
100
200
300
400
500
time(sec)

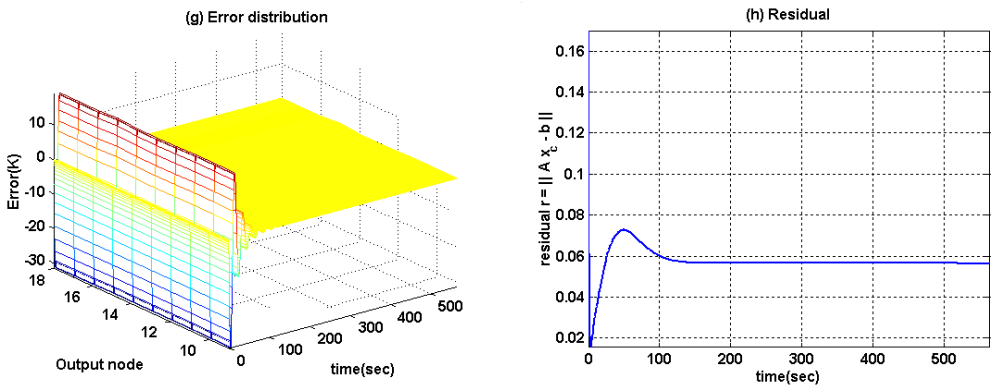

Figure 6.26 Responses for Eq. (6.37) with γ^2 =1E-4 (a) temperature distribution along the surface over the entire process time and (b) at t=350sec, (c) control input Q and (d) at t=350sec, (e) final time heater input distribution (f) standard deviation of heater inputs (g) error distribution (h) residual

Notice that Figs. 6.26(a) and (c) are similar to those of the Tikhonov-FBL results in Fig. 6.18—the control input distribution is more uniform than in the Fig. 6.25 case. Note that Eq. (6.37) is equivalent to

$$\min_{\mathbf{x_c}}\left\{\left\|\mathbf{A}\mathbf{x_c}-\mathbf{b}\right\|_2^2+\boldsymbol{\gamma}^2\left\|\mathbf{M}\mathbf{x_c}\right\|_2^2\right\} \text{ such that } \mathbf{x_c}\geq\mathbf{0},$$

where M = $\mathbf{I}_{30\times30}$. Hence larger γ^2 implies more weight on minimizing the Euclidean norm, $\left\|\mathbf{x_c}\right\|_2$—Euclidean distance of the vector $\mathbf{x_c}$ from the origin which can be written as $\left\|\mathbf{x_c}\right\|_2^2 = x_{c,1}^2 + x_{c,2}^2 + \cdots + x_{c,m}^2$. To minimize the Euclidean norm while keeping the total sum of all the elements the same (because the total amount of input energy at any moment must be kept as needed), the heater inputs should be more uniform. Hence, larger values of γ^2 result in more uniform heater input distributions, thereby γ^2=1E-4 is large enough to make the heater

inputs to be sufficiently uniform such that all the inputs are strictly positive and no inputs turned off. However, the smoothing effect for γ^2=1E-6 is not large enough, resulting in uneven heater input distribution, i.e. some are strictly positive and some are negative which are forced to be zero to satisfy the constraint as shown in Figs. 6.25(c), (d) and (e). Therefore a larger number of heaters are used in Figs. 6.26(d) and (e) compared to Figs. 6.25(d) and (e). The more smoothing effect of γ^2=1E-4 than γ^2=1E-6 is verified in Figs. 6.26(f) and (h).

Table 6.3 shows the values of the performance index of the proposed and Tikhonov-FBL (Fig. 6.18) controllers—the proposed controller with γ^2=1E-6 has 25% less cost while the controller with γ^2=1E-4 shows no significant difference, but the cost for having more uniform temperatures and more participating heaters (larger γ^2) increased by a factor of four (27.14 versus 117).

Table 6.3. Performance index $\int J dt = \int \left(\left\| \mathbf{A}\mathbf{x}_\mathbf{c} - \mathbf{b} \right\|_2^2 + \boldsymbol{\gamma}^2 \left\| \mathbf{M}\mathbf{x}_\mathbf{c} \right\|_2^2 \right) dt$

Controller	γ^2=1E-6	γ^2=1E-4
Tik-FBL 0.001 (Fig. 6.18)	36.64	117.1
Least Squares Problem for Augmented System: Eq. (6.37)	27.14	116.9

Although the nonlinear optimal controller with γ^2=1E-6 has less cost than the case with γ^2=1E-4, it generates relatively high peak control inputs in certain heaters as shown in Fig. 6.25(c) which may violate heater capacity. Hence, to include upper bound constraints on the control input, the problem described by

Eq. (6.37), a linear least squares problem with nonnegative input constraints, is now transformed to a linear least squares problem with upper and lower bounds on the inputs as in Eq. (4.16), resulting in the general constrained nonlinear optimal control problem. Figure 6.27 shows the results with the upper bound set to 5000W/m and γ^2=1E-6, i.e.

$$\min_{\mathbf{x_c}} \left\| \mathbf{A}_{aug}\mathbf{x_c} - \mathbf{b}_{aug} \right\|_2^2 \text{ such that } 0 \le \mathbf{x_c} \le 5000 \tag{6.38}$$

Figs. 6.27(c) and(d) shows all heater inputs satisfy the upper and lower bounds. The peak value is 4164W/m—almost half the peak value of the case with the lower bound only (7573W/m, Fig. 6.25). Placing the upper bound results in an input distribution that is uniform resulting more active heaters and all the inputs positive to meet a prescribed positive net energy level to follow the desired trajectory. Figure 6.27(e) shows that more heaters are active at the final state than is the case of Fig. 6.25(e), 30 versus 5. Also notice from Fig. 6.27(e) that the values of final state heat inputs are much less than in the Fig. 6.25(e) case, but still higher than the case with γ^2=1E-4 in which the values of inputs are lower due to more uniform distribution.

It is confirmed that the proposed controllers (Eq. (6.37) and (6.38)) preserve the characteristics of FBL—design surface temperature distribution (Figs. 6.25(a), 6.26(a) and 6.27(a)) and error behavior (Figs. 6.25(g), 6.26(g), and 6.27(g)) show almost identical behaviors of Fig. 6.5.

Performance measures for four different controllers are shown in Table 6.4. It is noticed from the Table 6.4 that the controller defined by Eq. (6.37) with

γ^2=1E-4 requires the smallest total energy consumption and maximum control input while generating similar size errors to other controllers in the Table 6.4.

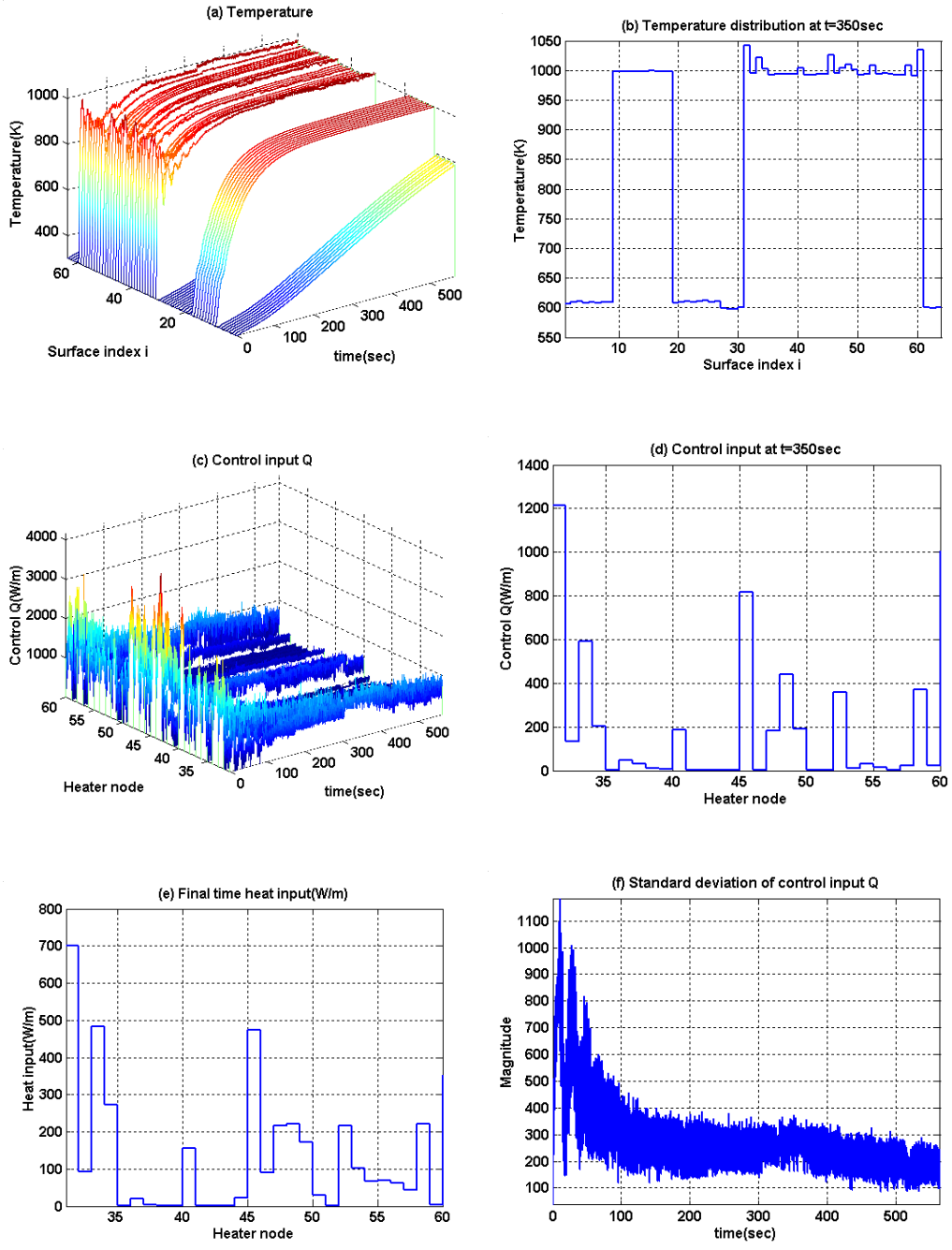

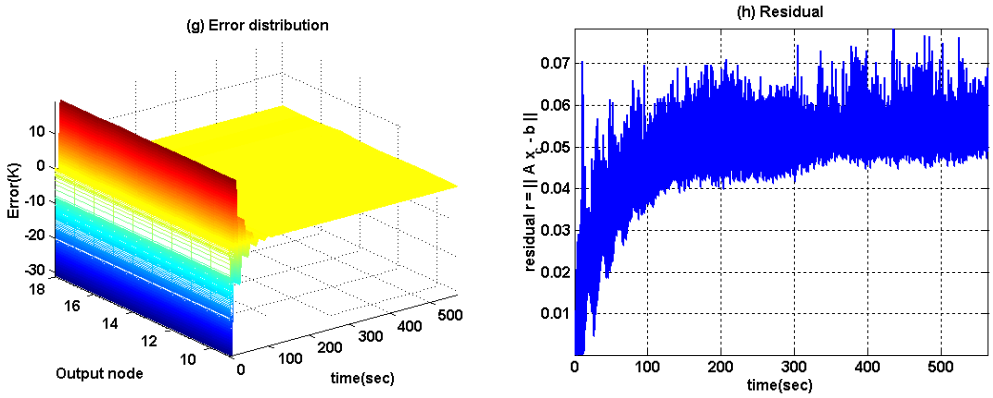

Figure 6.27 Responses for Eq. (6.38) (a) temperature distribution along the surface over the entire process time and (b) at t=350sec, (c) control input Q and (d) at t=350sec, (e) final time heater input distribution (f) standard deviation of heater inputs (g) error distribution (h) residual

Table 6.4. Performance Measures for Constrained Nonlinear Optimal Controllers

Controller	Max. control input (W/m)	Total energy (J/m)	Max. error in design surface (K)	Max. steady- state error (K)
Eq. (6.36)	14788	4.4305e+6	31.34	0.42
Eq. (6.37) with γ^2=1E-6	7572	4.4518e+6	31.27	0.42
Eq. (6.37) with γ^2=1E-4	1857	4.4132e+6	31.42	0.45
Eq. (6.38)	4164	4.4367e+6	31.29	0.44
FBL	7517	2.6425e+7	-31.1	0.0005

6.6.3. Summary

It has been shown that the design and tradeoffs of the proposed nonlinear optimal controllers with upper and lower bound constraints were successfully applied to the temperature control of an ill-conditioned thermal system. The designs are simple, easy to solve, free of regularization parameters, and simultaneously preserving the characteristics of FBL/SMC and satisfying the input constraints.

6.7. STRUCTURAL ANALYSIS AND OPTIMIZATION OF NONLINEAR CONTROL SYSTEMS

In the previous two sections, regularization embedded nonlinear controllers and constrained nonlinear optimal controllers were applied to handle input-constraints of nonlinear controllers. They provided very successful results on the temperature control of an input-constrained thermal system while addressing the cause of input-constraint-violation, i.e. ill-conditionedness of the controller, and optimization between the control effort and residual. However in this section, a more comprehensive analysis of the nonlinear controller will be presented to reveal the fundamental composition of the control input signals and output behavior, and to develop a more quantitative analysis between the tradeoffs for optimization using algorithms proposed in Chapter 5. The result is, a unified approach (structural analysis/design/optimization) to nonlinear controller design issues—input constraint, optimization, and efficiency. Specifically, SVD is used to identify control input/output mode shapes, and the control input/output distribution patterns are analyzed using the mode shapes. Optimizing control effort and performance is achieved by truncating some mode shapes in the linear mode shape combinations.

6.7.1. Structural analysis: control-input mode shape

Notice that both FBL/SMC control designs (Eq. (6.29)) are in the form $\mathbf{A}\mathbf{x}_c = \mathbf{b}$, thus SVD can be directly applied to the LAENC form of the nonlinear controller designs and the proposed methods in Chapter 5 are applicable. Both

controller design processes are almost identical, therefore discussion is given based on the FBL design only.

Applying SVD to $\mathbf{A}\mathbf{x}_c = \mathbf{b}$ gives the input vector $\mathbf{v}_i$'s, output vector $\mathbf{u}_i$'s and corresponding singular value σ_i's. These $\mathbf{v}_i$'s and $\mathbf{u}_i$'s will be referred to as the control input mode shapes and output mode shapes, respectively. The dimension of **A** is 10x30, so the controller has 30 input modes and 10 output modes. The controller designed for this thermal system has relative degree two, hence the matrix **A** is state-dependent, resulting in state-dependent control input/output modes shapes. However, it is well known that the singular values and singular vectors of a matrix are relatively insensitive to perturbations in the elements of the matrix [38] and the pattern of state changes are expected to be uniform in this problem, hence those mode shapes are not expected to change much and it is verified in Fig. 6.28. Figure 6.28 shows only the first three input/output modes of the FBL controller (Eq. (6.23)) due to space limitations and note that the mode shapes are almost uniform for the entire process. Thus the mode shapes at one time step can be used as a design tool as being representative of the entire process.

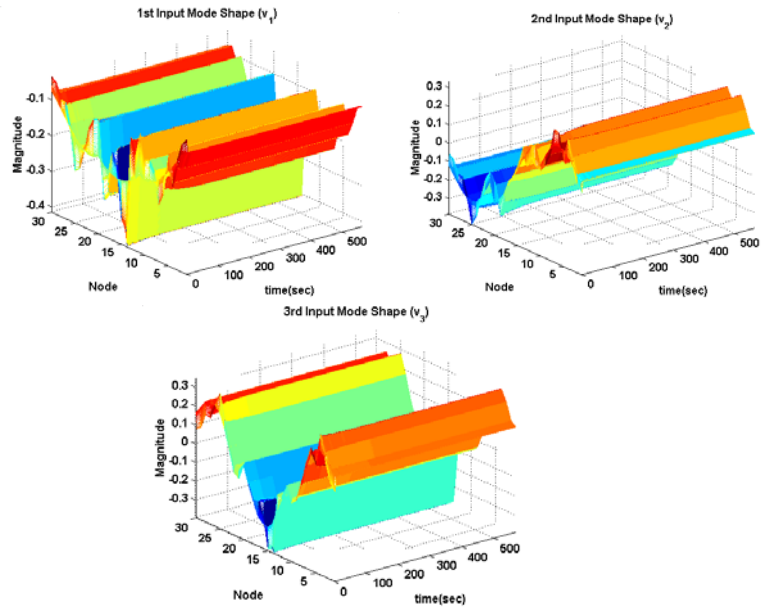

(a) First three control input mode shapes ($\mathbf{v}_1$, $\mathbf{v}_2$ and $\mathbf{v}_3$)

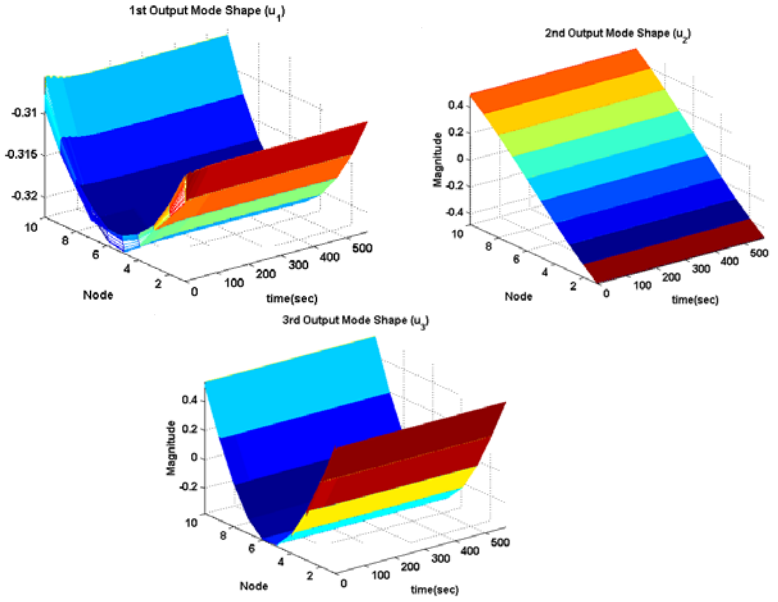

(b) First three output mode shapes ($\mathbf{u}_1$, $\mathbf{u}_2$ and $\mathbf{u}_3$)

Figure 6.28 First three input/output mode shapes of FBL with λ_1=0.1 and λ_2=0.1

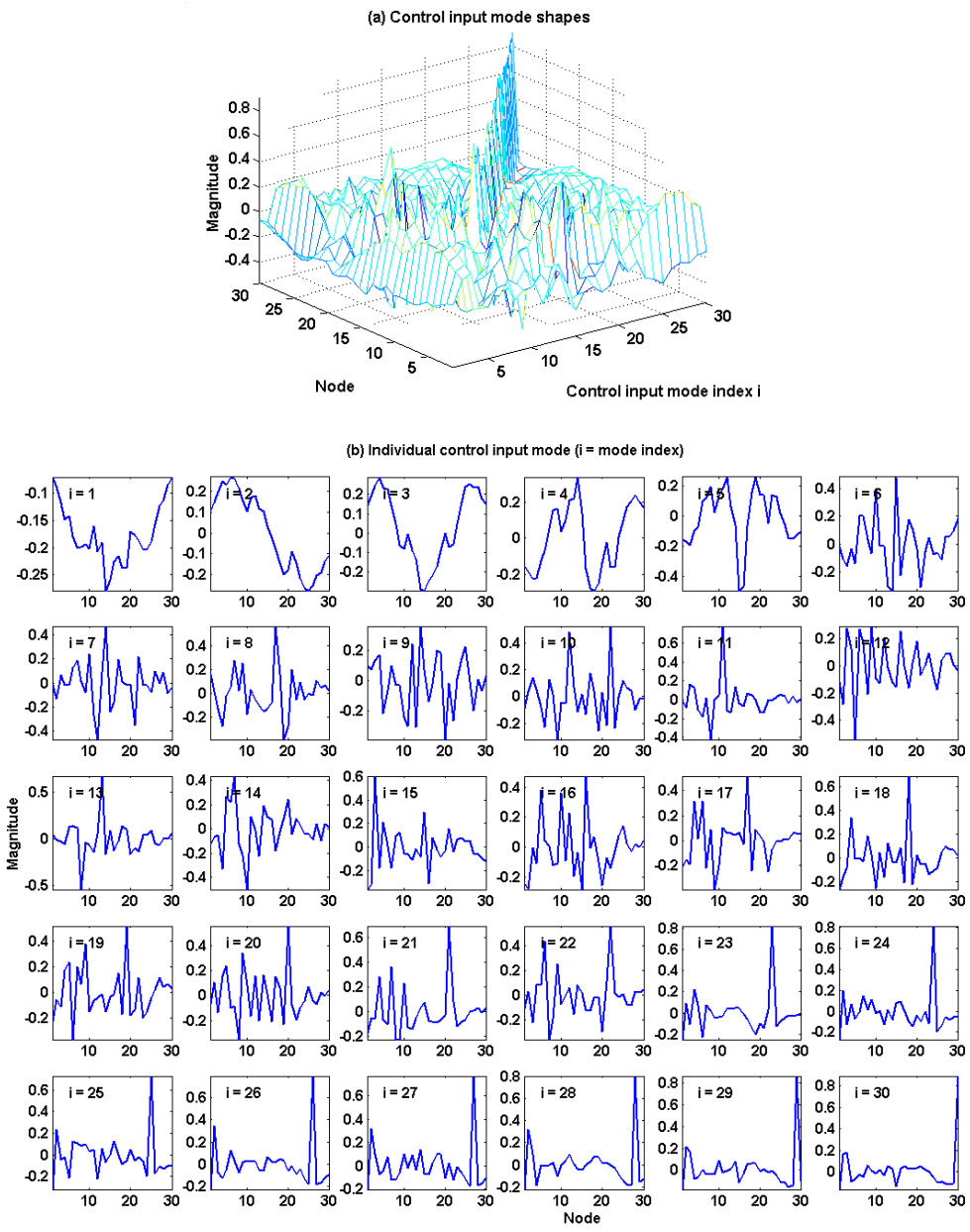

Figure 6.29 Control input mode shapes of FBL with λ_1=0.1 and λ_2=0.1 at 0.08 sec (a) in 3-D plot (b) 30 control input mode shapes

Figure 6.29 shows the 30 control-input mode shapes at the beginning of the process (@0.08sec). Figure 6.29 (a) shows the 3-D distribution to compare the relative size of each mode, and Fig. 6.29(b) shows the detailed shape of each control-input mode.

Notice the peak value of each mode increases as the mode index i increases. The last few modes with high peaks may create potential danger since the control input bounds may be exceeded even with small weights ($\mathbf{x}_\mathbf{c} = \sum_{i=1}^{rank(\mathbf{A})} q_i \cdot \mathbf{v}_i$). However, since the rank of matrix $\mathbf{A}$ is 10—has only 10 meaningful singular values to pair with—only the first 10 modes are active among the 30 input modes. Therefore the final control input distribution is a linear combination of the first ten modes only and the last 20 modes, which have large peak values, are no longer of concern.

Notice that all the input modes except for the first mode have sign changes in its distribution: positive inputs and negative inputs. But the controllers—heaters in the thermal system—can not have negative inputs otherwise the heaters must act as refrigerators—an input-constraint violation. However, since the final distribution of control input is a combination of all available input modes, choosing appropriate coefficients, q_i's, can make all solutions satisfy the constraint. Alternatively, using only the first mode which has all the same signs in its distribution would satisfy the input constraint also.

Now, weights of the linear combination of input modes should be compared to identify dominant modes and to assess the final control-input

distribution shape. Figure 6.30(a) is the plot of the weights of the 10 active input modes.

Weights $q_i = \dfrac{\mathbf{u}_i^T \cdot \mathbf{b}}{\sigma_i}$ for the linear combination of each input mode are scalars, therefore the size of each combination component $q_i \mathbf{v}_i$ is q_i times larger than $\mathbf{v}_i$ but the distribution pattern will be exactly the same shape as $\mathbf{v}_i$. Thus the final control input distribution will be similar to the shape of the dominant input mode with the largest corresponding weight q_i.

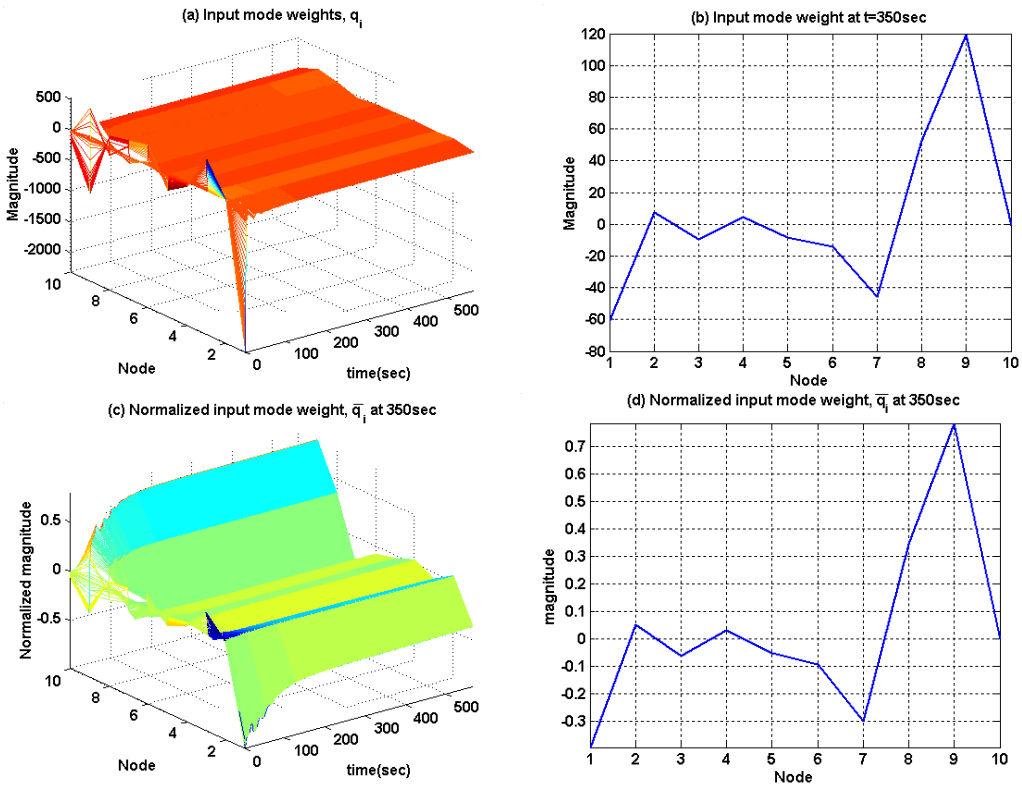

Figure 6.30 Input mode weight distribution of FBL with λ_1=0.1 and λ_2=0.1 (a) entire process and (b) at t=350sec, (c) normalized input mode weight distribution and (c) at t=350sec.

Figure 6.30(c) shows the normalized weights distribution. Except for very early times, the absolute value of the normalized weights on the 1st, 7th, 8th and 9th mode are relatively higher than weights of other modes throughout the process, and this infers that control input $\mathbf{x_c}$ largely depends on $\mathbf{v}_1$, $\mathbf{v}_7$, $\mathbf{v}_8$, and $\mathbf{v}_9$—the control input will be a linear combination mainly of $\mathbf{v}_1$, $\mathbf{v}_7$, $\mathbf{v}_8$, and $\mathbf{v}_9$. However, the control input mode shapes in Figs. 6.29 show that $\mathbf{v}_7$, $\mathbf{v}_8$, and $\mathbf{v}_9$ have large oscillations with some inputs positive and others negative. Since the total contribution $\mathbf{v}_7$, $\mathbf{v}_8$, and $\mathbf{v}_9$ are larger than for $\mathbf{v}_1$, that is

$$\left(\bar{q}_7^2 + \bar{q}_8^2 + \bar{q}_9^2\right) > \bar{q}_1^2$$

where $\bar{q}_i$ represents the normalized weight of q_i, the chances are high that the final control-input distribution will have oscillations in its distribution.

Figure 6.31(a) shows the system response using a classic nonlinear FBL controller (Eq. (6.23)), and Fig. 6.31(b) shows that the corresponding control input distribution has large oscillations as $\mathbf{v}_7$, $\mathbf{v}_8$, and $\mathbf{v}_9$ do. Note also that the control input becomes more similar to the shape of $\mathbf{v}_9$ as time elapses which is verified from Fig. 6.30 that q_9 becomes dominant with time. Although Fig. 6.31(a) shows excellent tracking of the design surface temperatures to the desired temperature trajectory, due to the oscillating dominant modes, 14 out of 30 heaters have negative heat inputs, thereby violating the input constraints.

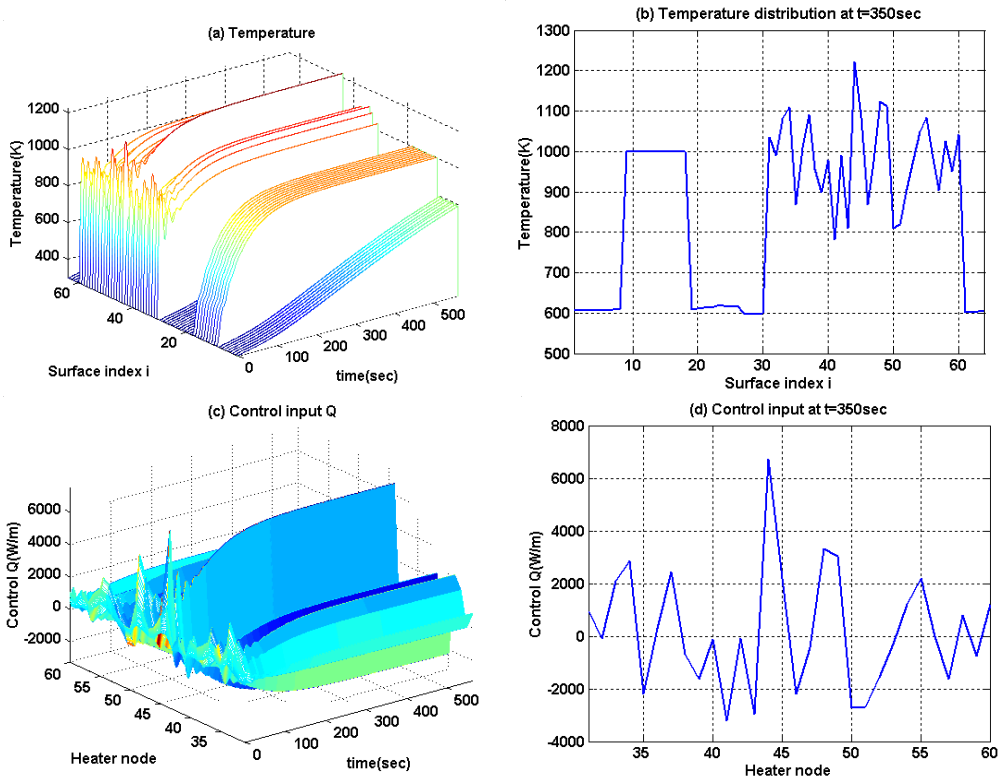

Figure 6.31 Responses for FBL with λ_1 =0.1, λ_2 =0.1 (a) temperature distribution along the surfaces and (b) at t=350sec, (c) control input Q over the entire process and (d) at t=350sec

6.7.2. Structural optimization: colinearity and mode truncation for satisfying input-constraints

So far, it has been proposed that input mode shapes can be used to estimate the control input distribution pattern and that input-constraint-violating solutions are caused by input modes with mixed signs and large oscillations. Can input-constraint-satisfying solutions be obtained by eliminating those mode shapes, with minimal performance degradation? Can the contribution of each

output mode corresponding to the input mode to be eliminated be checked to determine its effect on performance? The contribution of each output mode to the output vector **b** can be checked with its colinearity defined as $\mathbf{u}_i^T \cdot \mathbf{b}$. Using the normalized colinearity, it is easy to compare the relative contributions of the output modes to the output vector **b**.

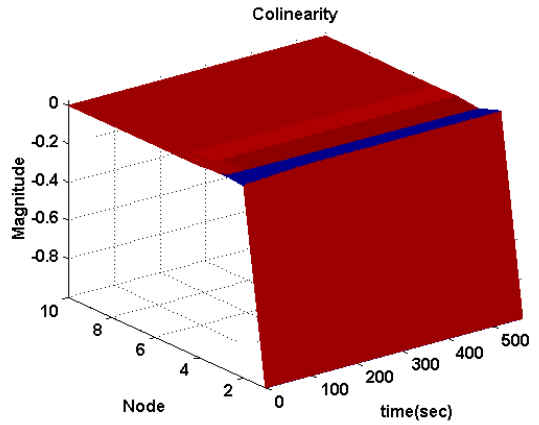

Figure 6.32 Normalized colinearity distribution of FBL with λ_1=0.1, λ_2=0.1

Figure 6.32 shows the normalized colinearity of all the ten input modes throughout the process time and note that colinearity does not change much over the time. Hence, the normalized colinearities at one time step (t=350sec) will be used as the representative of the entire process for the analysis and they are

-0.9995, 0.028, -0.0094, 0.0012, -0.0008, -0.0008, -0.0017, 0.0017, 0.0019, -1e-5

Since the sum of the squared normalized colinearities equals one, the percentile contribution of each output mode at 350sec are calculated by the square of the normalized colinearities as

99.91, 0.08, 0.01, 1e-6, 6e-7, 5e-7, 2e-6, 2e-6, 3e-6, 1e-10

These numbers indicate that the first mode shape contributes 99.91% of the target vector and the other nine remaining modes contribute only 0.09% of the total performance. This is a critical observation since $\mathbf{u}_2, \cdots, \mathbf{u}_{10}$ which contribute only 0.09% of the output, consumes more control effort than $\mathbf{u}_1$ which contributes 99.91% to the performance since

$$\sum_{2}^{10} \overline{q}_i^2 > \overline{q}_1^2$$

Moreover, these modes are suspected to be the cause of the input-constraint-violation. It can be inferred that eliminating these modes will not deteriorate the control performance and a large saving in effort can be achieved at the same time.

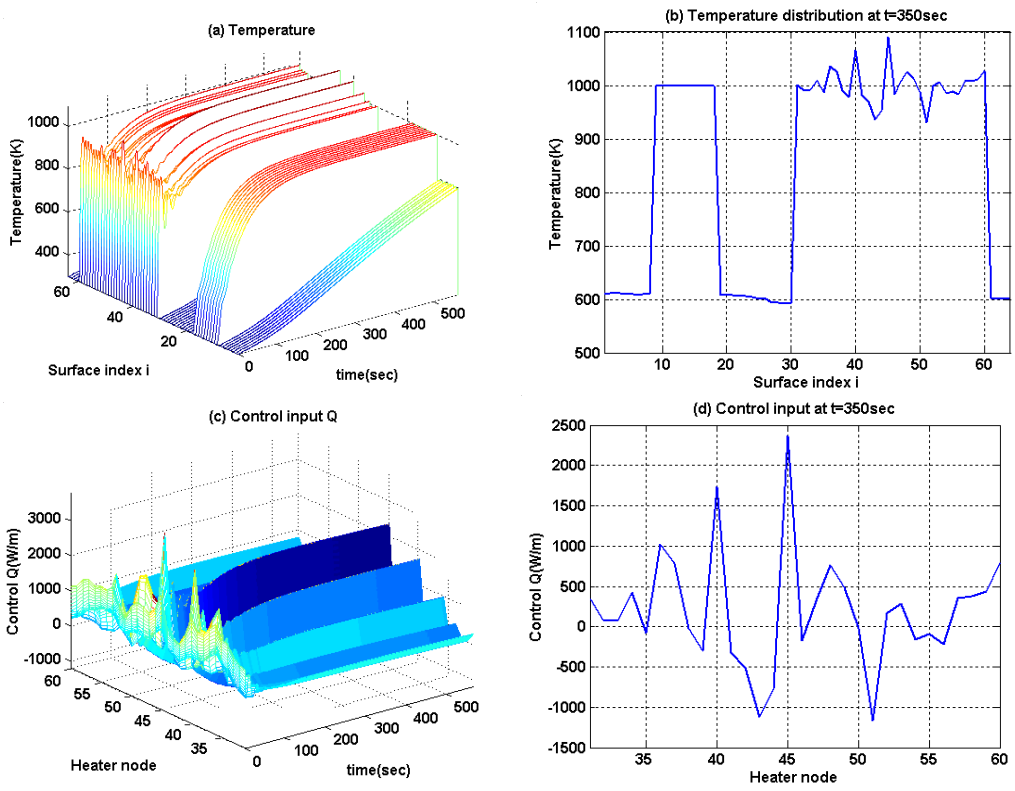

Figure 6.33 Responses when $\mathbf{v}_7$, $\mathbf{v}_8$, and $\mathbf{v}_9$ are truncated (a) temperature distribution along the surfaces over the entire process and (b) at t=350sec, (c) control input distribution over the entire process and (d) at t=350sec.

Figure 6.33 shows temperature responses and the input distribution when $\mathbf{v}_7$, $\mathbf{v}_8$, and $\mathbf{v}_9$ are truncated throughout the process. Unfortunately, the control input distribution still shows negative inputs. This can be explained using Fig. 6.34.

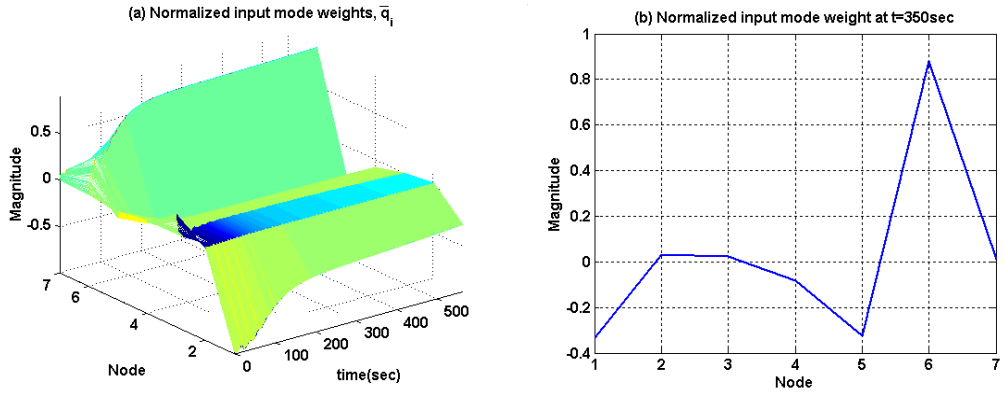

Figure 6.34 Input mode weight, q_i, distribution when $\mathbf{v}_7$, $\mathbf{v}_8$, and $\mathbf{v}_9$ are truncated (a) entire process and (b) at t=350sec.

Figure 6.34 shows the q_i distribution when $\mathbf{v}_7$, $\mathbf{v}_8$, and $\mathbf{v}_9$ are truncated. The last 7th mode in Fig. 6.34 corresponds to the original 10th mode since $\mathbf{v}_7$, $\mathbf{v}_8$, and $\mathbf{v}_9$, located between the 6th and 10th modes, are truncated. Truncating modes $\mathbf{v}_7$, $\mathbf{v}_8$, and $\mathbf{v}_9$, which corresponds to the truncation of output modes $\mathbf{u}_7$, $\mathbf{u}_8$ and $\mathbf{u}_9$, does not change the states much since their contribution to the output is small, thus resulting in similar singular values and mode shape distribution to the no-truncation case. Thus, the input weight distribution is also expected to be similar to the no-truncation case. However, the 5th and 6th weights that were larger than the others except for the 7th, 8th and 9th, now become dominant as shown in Fig. 6.34, after q_7, q_8, and q_9 are truncated which were relatively large in Fig. 6.30(b). These 5th and 6th modes have oscillations in their distribution and cause the constraint-violating-solution in Fig. 6.33(b). The mode shapes are still similar even after the truncation as expected and as confirmed in Fig. 6.35.

In this research, mode truncation is achieved by setting the singular value, σ_i's, which correspond to the control input modes to be truncated, zero because technically it is equivalent to truncating the input mode $\mathbf{v}_i$'s since $\mathbf{A} = \mathbf{U}\boldsymbol{\Sigma}\mathbf{V}^T$ where $\boldsymbol{\Sigma} = diag\left(\sigma_1, \sigma_2, \cdots, \sigma_p \middle| \mathbf{0}\right)$. Therefore, notice that, even though $\mathbf{v}_7$, $\mathbf{v}_8$, and $\mathbf{v}_9$ in Fig. 6.35(b) are not zero after the truncation, their effects on the control input/output are actually zero, i.e. they are actually zero.

As noticed from the above case, any input modes with relatively large weights can become dominant with mode truncation, so it would be safe to truncate as many of those modes that cause oscillations if they become dominant, as long as performance is not degraded much. One solution is to truncate input modes, $\mathbf{v}_2, \cdots, \mathbf{v}_{10}$, which have sign changes in their distributions.

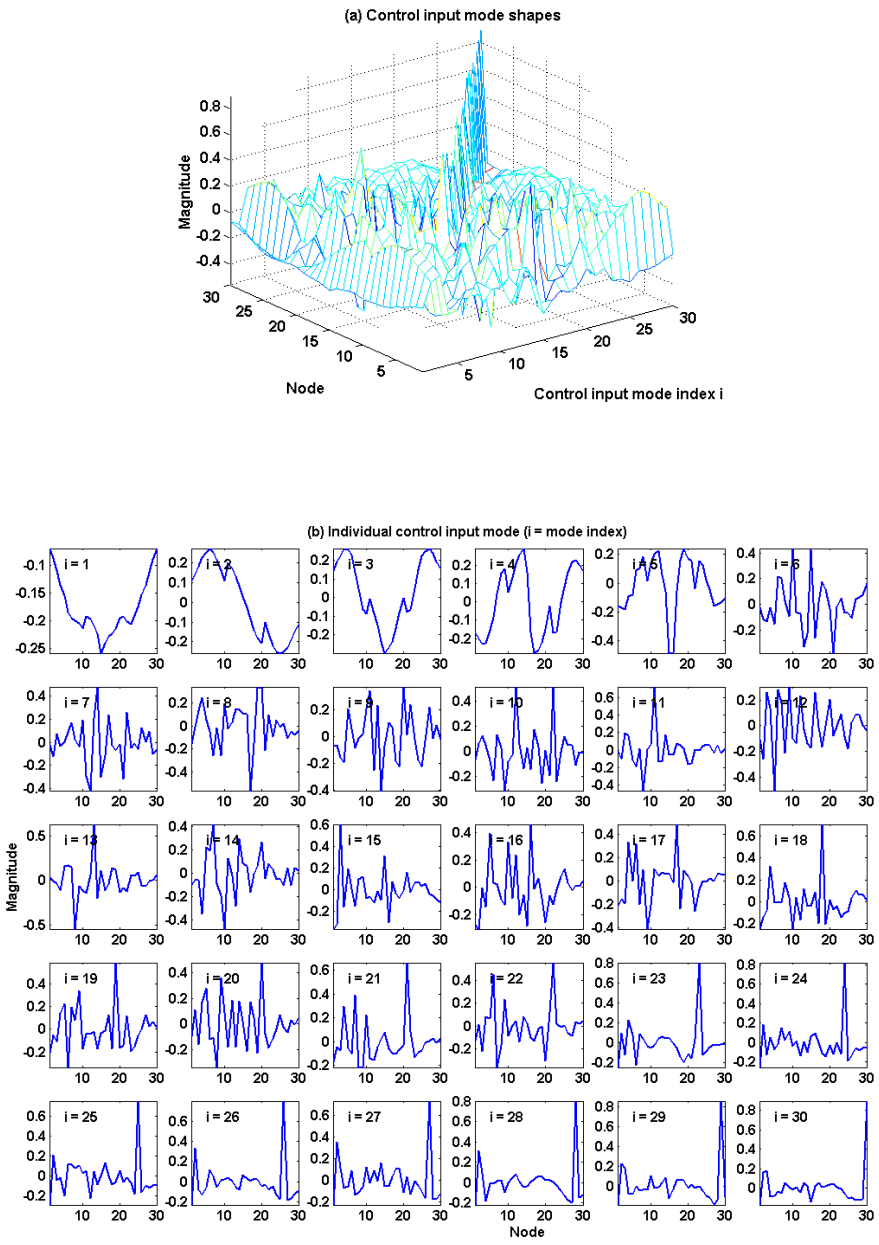

Figure 6.35 Input mode shape at 0.08sec when $\mathbf{v}_7$, $\mathbf{v}_8$, and $\mathbf{v}_9$ are truncated (a) control input mode shapes in 3-D plot (b) 30 individual control input mode shapes

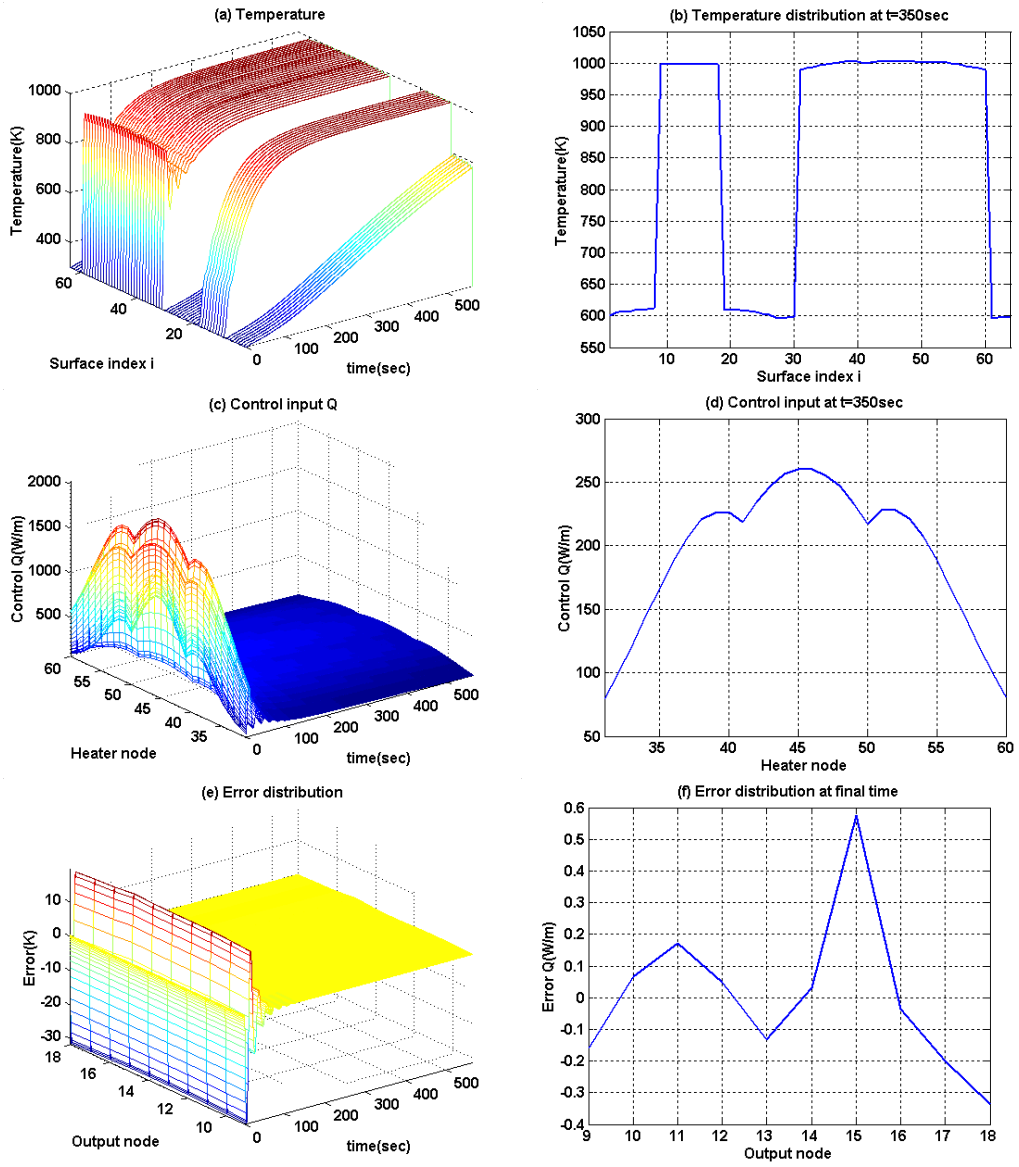

Figure 6.36 Responses when $\mathbf{v}_2, \cdots, \mathbf{v}_{10}$ are truncated (a) temperature distribution along the surfaces over the entire process and (b) at t=350sec, (c) control input distribution over the entire process and (d) at t=350sec, (e) error distribution over the entire process and (f) at final time.

Figure 6.36 shows the temperature responses and input distribution when the last nine modes, which contribute only 0.09% to the output, are truncated. Figure 6.36(a) shows excellent uniform tracking. The control input distribution in Fig. 6.36(b) is similar to the mirror image of $\mathbf{v}_1$ in Fig. 6.29(b) since the other nine modes are truncated and only $\mathbf{v}_1$ governs the shape of the control input distribution. All negative elements in $\mathbf{v}_1$ turn into positive ones due to the negative weight (actually, due to negative colinearity) and finally all the solutions satisfy the input constraints. Table 6.5 shows the performance measures for six cases.

Table 6.5. Performance measures for six cases of truncating input modes

Controller Input-Modes Truncated	Max. control input (W/m)	Total energy (J/m)	Max. error in design surface (K)	Max. steady- state error(K)
$\mathbf{v}_5, \cdots, \mathbf{v}_{10}$	2004	4.42e+6	-31.3	0.42
$\mathbf{v}_4, \cdots, \mathbf{v}_{10}$	1890	4.41e+6	-31.3	0.49
$\mathbf{v}_3, \cdots, \mathbf{v}_{10}$	2034	4.40e+6	-31.7	0.60
$\mathbf{v}_2, \cdots, \mathbf{v}_{10}$	2033	4.40e+6	-31.7	0.58
$\mathbf{v}_2, \cdots, \mathbf{v}_8, \ \mathbf{v}_{10}$	4496	2.06e+7	-31.9	1.95
None (FBL)	7517	2.64e+7	-31.1	0.00

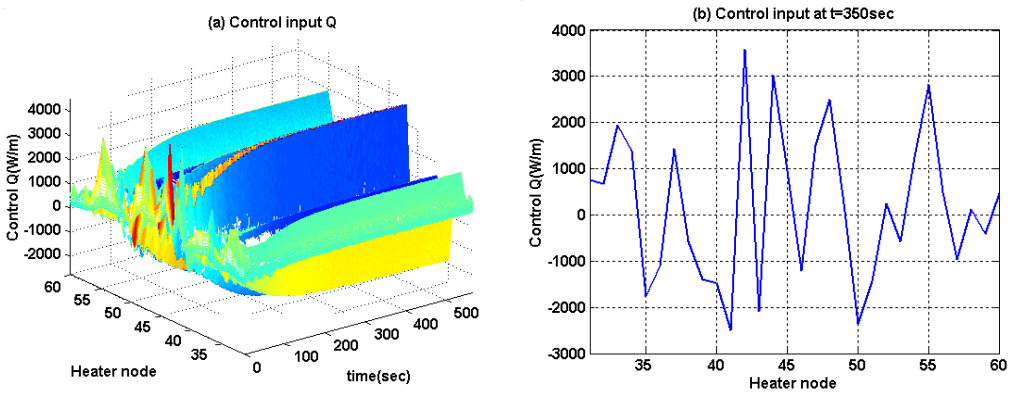

Figure 6.37 Control input distribution when $\mathbf{v}_2, \cdots, \mathbf{v}_8$, $\mathbf{v}_{10}$ are truncated

For this thermal problem, the more input modes that are truncated, the more effort savings is achieved. However, it should be noted from the Table 6.5 that even when eight modes other than $\mathbf{v}_1$ and $\mathbf{v}_9$ are truncated, the total effort used is larger than when five modes ($\mathbf{v}_5, \cdots, \mathbf{v}_{10}$) are truncated. This is because the contribution (weight) of $\mathbf{v}_9$ to the total control input is relatively larger than other modes as is shown in Fig. 6.30, thereby truncating other modes except $\mathbf{v}_9$ does not help much to save control effort. Also, truncating all modes except $\mathbf{v}_1$ and $\mathbf{v}_9$ makes the control input dependent largely on the shape of $\mathbf{v}_9$ which has mixed signs in its distribution and finally results in input-constraint-violating solution distributions as in Fig. 6.37. If nine modes ($\mathbf{v}_2, \cdots, \mathbf{v}_{10}$) including $\mathbf{v}_9$ are truncated, the savings in input effort is 83% compared to the effort required by the original FBL controller with almost the same performance, even though the comparison is not reasonable since the original controller would not be used since it violates the input constraints.

6.7.3. Structural analysis: control output mode shape and controller efficiency

So far, the focus of discussion has been on the input modes. Now, the focus is on the output mode shapes.

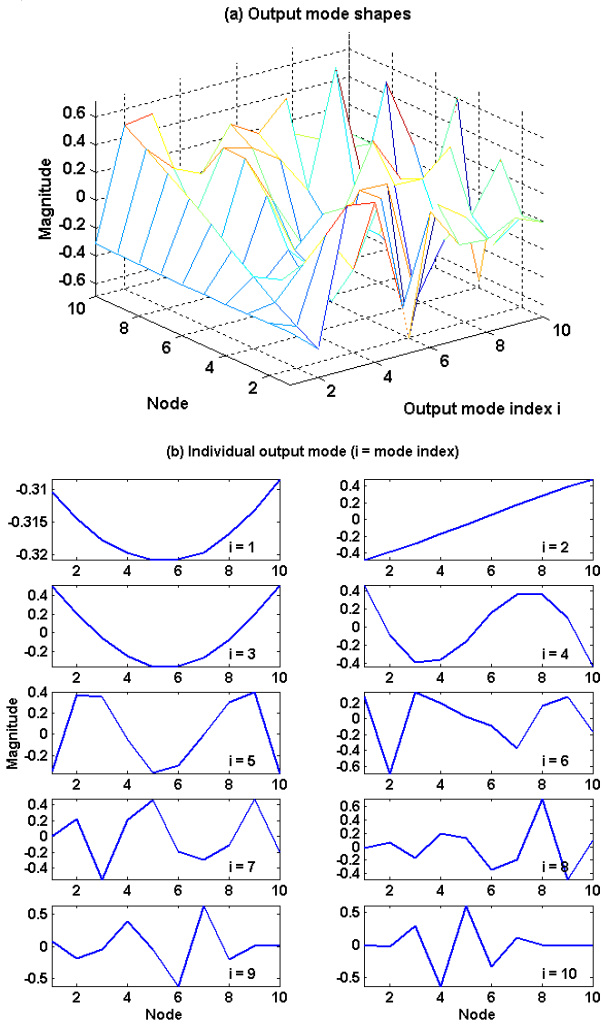

Figure 6.38 Output mode shapes at 0.08 sec with no truncation (a) in 3-D plot (b) 10 output mode shapes

From Fig. 6.32, it is known that target vector **b** is almost colinear with $\mathbf{u}_1$, meaning that the actual output will be similar to the shape of the first output mode shape. When nine modes are truncated, the only active output mode is $\mathbf{u}_1$ so the actual output will be exactly the same as the first mode shape, $\mathbf{u}_1$. As can be seen from the first mode shape in Fig. 6.38, all 10 elements have nearly the same magnitudes—i.e. the actual output temperature distribution should be almost uniform, which is verified in Fig. 6.36(a) and (b).

From the output mode shapes, the designer should surmise that the goal to maintain uniform temperature distribution in the design surfaces is easy to achieve since the first mode shape has a uniform distribution, and that this first mode is control-effort-efficient since it has large scaling singular values. So any target vector **b** set to be colinear with $\mathbf{u}_1$ will be achieved with small control effort. Alternatively if **b** set to be colinear with $\mathbf{u}_{10}$, i.e. the designer wants the temperature output to be non-uniform, this target will use more effort due to its small scaling factors. Hence, the control system designed in this research is a very efficient controller since the target vector is almost colinear with the most efficient mode, $\mathbf{u}_1$.

Summarizing, the proposed methods have been successfully applied to the temperature control of a thermal system. By truncating the input modes with mixed signs in their values, input-constraint-satisfying solutions are obtained with almost the same performance along with a reduction in control effort.

6.7.4. Summary

The structural analysis and optimization algorithm was applied to the temperature control of a thermal process. It was shown that the input-constraint-violating-control was due to oscillating input modes with different signs in their magnitudes. These oscillating modes caused constraint-violation and were shown to contribute only 0.09% of the total performance, but they required more control-effort than the single mode that contributed 99.91% of performance. Based on the analysis, truncating these oscillating modes gave input-constraint-satisfying-solutions with a reduction in control effort. Also, the control system designed for the thermal system was shown to be colinear with the most efficient single output mode, i.e. it proved to be a very efficient design.

Through this section, it is illustrated how one can interpret mode shapes under constraints, modify the controller (mode shapes) to satisfy the input constraints, optimize the controller and predict the input/outputs from the input/output mode shapes.

Chapter 7

Conclusions and Future Work

7.1. CONCLUSIONS

Structural analysis, design and optimization of nonlinear control systems are presented using the linear algebraic equivalence of nonlinear controllers (LAENC) to address the design issues of nonlinear control systems in a systematic way.

It is shown that FBL/SMC possess the very useful structural feature, the linear algebraic equivalence, on which many well-developed linear algebraic solution techniques can be applied directly. Based on this LAENC, it is shown that many problems such as minimization, optimization (tradeoff) and input-constraint handling, can be posed with respect to the nonlinear controller designs. As a result, input constrained nonlinear optimal control is proposed which is very robust in handling the input-constraints, able to find optimal (tradeoff) solutions, free of regularization parameters, and computationally efficient since it solves a linear least squares problem. It preserves the characteristics of FBL/SMC—desired error dynamics and sliding behavior are maintained which is not possible with LQ/MPC.

It is also shown that it is possible to apply singular value decomposition, a useful structural analysis tool but which is applicable to linear systems only, to the nonlinear control designs using LAENC. Structural analysis and optimization of

the nonlinear control designs show that control inputs/outputs are composed of a linear combination of finite numbers of mode shapes. The linear combination coefficient for the control input determines the final shape of the control inputs. Contribution of each output mode towards the target vector is determined by its colinearity, and it can be used as a criterion for mode truncation optimization.

The proposed algorithms are applied to the temperature control of an enclosed and radiation-dominant thermal system. The pure nonlinear controllers generate input-constraint-violating and large-oscillating solutions and it is shown by singular values of the controllers obtained by SVD that they are due to the ill-conditioned nonlinear controllers.

To treat these problems, first, using LAENC, new regularization embedded nonlinear control designs are presented. The new controllers produce physically meaningful, actuator-constraint-satisfying solutions. This approach is unique in that, it was the first attempt to overcome the input-constraint-violation of the nonlinear controller using regularization. Also, it was a unique attempt to diagnose the characteristics of the nonlinear controller using SVD on the LAENC. Design guidelines were provided for the selection of regularization parameter values. While the embedded controllers worked well on the given thermal process model, the designs can be extended to any ill-conditioned process model which could generate input-constraint-violating control solutions.

As another approach to the temperature control of an input-constrained thermal system, input-constrained nonlinear optimal controllers are applied. As shown, successful results are obtained. Linear least squares problem with

nonnegative constraints and constrained nonlinear optimal control problems are presented. Effect of optimization (balancing) parameter γ^2 is discussed.

Finally, the structural analysis and optimization of the nonlinear controllers were conducted. As a result, it was shown that the input-constraint-violating-control was due to oscillating input modes with different signs in their magnitudes. These oscillating modes caused constraint-violation and were shown to contribute only 0.09% of the total performance, but they required more control-effort than the single mode that contributed 99.91% of performance. Based on the analysis, truncating these oscillating modes gave input-constraint-satisfying-solutions with a reduction in control effort. Also, the control system designed for the thermal system was shown to be colinear with the most efficient single output mode, i.e. it proved to be a very efficient design.

Concluding, the structural analysis, design and optimization developed in this research provides a fundamental foundation for many design issues of nonlinear control systems by allowing the designer to investigate the structure of nonlinear controllers, to diagnose/identify the problem and to provide rudimentary cure for the problems.

The principal contributions of this research are summarized as follows.

1. Linear algebraic equivalences of nonlinear controllers are identified to which many well-developed linear algebraic solution techniques can be applied directly.
2. Based on the LAENC, an input-constrained nonlinear optimal controller is proposed

3. Based on the LAENC, structural analysis, design and optimization of nonlinear controllers are proposed
4. New regularization embedded nonlinear controllers are proposed for ill-conditioned thermal processes.
5. Successful results on the temperature control/optimization of an input-constrained thermal process are obtained using the proposed algorithms

7.2. PROPOSED FUTURE WORK

For the regularization embedded nonlinear controllers, CGM, the iterative method, was not used in this research since it was assumed not to be suitable for real-time applications. However it may well be appropriate to embed the CGM method to the nonlinear controller design because it is known that very few steps are needed for the computation of the solution.

In the thermal system problem, the proposed algorithm achieves structural optimization and input-constraint satisfaction by truncating control input modes that have different signs in their magnitudes. However, for this system those truncated modes contributed little towards the total target vector, hence truncating those modes result in little performance degradation. It is suggested to investigate the case where the control input modes with problematic behavior in its distribution contribute much toward the target vector. In such a case, simply eliminating such modes would cause serious performance degradation, so

different optimization approaches, e.g. modulation of linear combination coefficient q_i, would be necessary to attain satisfactory performance.

Appendix A

Mathematical Preliminaries

Lie derivatives of $\mathbf{h}(\mathbf{x})$ with respect to $\mathbf{f}(\mathbf{x})$, i.e., the directional derivative, is defined as

$$\mathbf{L_f h(x)} \equiv \langle \mathbf{dh, f} \rangle$$
$$= \frac{\partial \mathbf{h(x)}}{\partial x_1} f_1(\mathbf{x}) + \frac{\partial \mathbf{h(x)}}{\partial x_2} f_2(\mathbf{x}) + \cdots + \frac{\partial \mathbf{h(x)}}{\partial x_n} f_n(\mathbf{x}) = \frac{\partial \mathbf{h(x)}}{\partial \mathbf{x}} \mathbf{f(x)}$$

where $< \cdot , \cdot >$ is the inner product. Higher order Lie derivatives can be defined as

$$\mathbf{L_f^k h(x)} \equiv \mathbf{L_f}\left(\mathbf{L_f^{k-1} h(x)}\right) = < \mathbf{dL_f^{k-1} h(x)}, \mathbf{f} >$$

Appendix B

Controller Gain Selection

For the gain selection of error dynamics of FBL and SMC, consider the desired temperature trajectory defined in Eq. (A.1).

$$T_d(t) = T_{d,final} + (T_{d,initial} - T_{d,final}) \cdot \exp(-10 \cdot t/timetotal) \tag{A.1}$$

Since the dynamic part of the trajectory is

$$\exp(-10t / timetotal) \tag{A.2}$$

and, if we take the Laplace transform to the dynamic part of the T_d

$$L\left[e^{-at}u(t)\right] = \frac{1}{s+a}, \text{ where } \quad a = \frac{-10t}{timetotal} \tag{A.3}$$

From (A.3), it is noticed that the pole of the desired temperature trajectory is at –0.0177. To follow this profile, the error dynamic gains are selected such that the error dynamic poles are at least 3~4 times larger than the desired trajectory. Accordingly, for the FBL, λ_1=0.1, λ_2=0.1 are selected such that the error dynamic poles are located at -0.05 ± 0.3122i which satisfy the requirement. For SMC, in a same manner, λ_{SMC} = 0.2 is selected such that the error dynamics has a pole at –0.2. The strictly positive constant D which satisfies the reaching condition is adequately selected to be 0.5, not to make the magnitude of the chattering large, if any.

Appendix C

Simulation Results Verification

To validate the simulation results, the 1st law of Thermodynamics (Energy Conservation) was checked for all the runs.

$$\sum_{i}^{N} \rho_i c_{p,i} \delta_i \Delta l_i \Delta T_i = \sum_{j}^{N_j} \int_t Q_j dt \tag{B.1}$$

where, $\Delta T_i = T_{i,final} - T_{i,initial}$, N= number of total elements (=64), and N_j= number of heaters (=30).

Appendix D

Numerical Data of Matrix $\mathbf{A_c}$

Numerical data of matrix $\mathbf{A_c}$ of FBL with λ_1=0.1, λ_2=0.1 at t=350sec is presented for the reference.

$\mathbf{A_c}$ =

Columns 1 through 5

2.4206e-004	2.5180e-004	3.8233e-004	4.8786e-004	2.6731e-004
2.5899e-004	2.7350e-004	4.2697e-004	5.4312e-004	2.9833e-004
2.8409e-004	2.9910e-004	4.6035e-004	5.9821e-004	3.2701e-004
3.1498e-004	3.3002e-004	5.2114e-004	6.7241e-004	3.7202e-004
3.5240e-004	3.7404e-004	5.9915e-004	7.6655e-004	4.2339e-004
4.0041e-004	4.2829e-004	6.7709e-004	8.7647e-004	4.8749e-004
4.5191e-004	4.9462e-004	7.8372e-004	1.0179e-003	5.6915e-004
5.2172e-004	5.7753e-004	9.2046e-004	1.2043e-003	6.5338e-004
6.2600e-004	6.8564e-004	1.0859e-003	1.4022e-003	7.5530e-004
7.5191e-004	8.3182e-004	1.3026e-003	1.6501e-003	8.6970e-004

Columns 6 through 10

4.9170e-004	7.1621e-004	5.5433e-004	5.1539e-004	7.4001e-004
5.4331e-004	7.8989e-004	6.1323e-004	5.6508e-004	7.9594e-004

6.0882e-004	8.8539e-004	6.7562e-004	6.2015e-004	8.7073e-004
6.8556e-004	9.8644e-004	7.4454e-004	6.8230e-004	9.3500e-004
7.6894e-004	1.1154e-003	8.2567e-004	7.4181e-004	9.8355e-004
8.7833e-004	1.2574e-003	9.1870e-004	8.1230e-004	1.0180e-003
1.0035e-003	1.4063e-003	1.0122e-003	8.6314e-004	1.0573e-003
1.1479e-003	1.5606e-003	1.0929e-003	8.9022e-004	1.0922e-003
1.3050e-003	1.7295e-003	1.1612e-003	9.1571e-004	1.1037e-003
1.4379e-003	1.8341e-003	1.1931e-003	9.1440e-004	1.0754e-003

Columns 11 through 15

2.9188e-004	6.7392e-004	4.2802e-004	1.6628e-003	1.3070e-003
3.3057e-004	7.6093e-004	4.7694e-004	1.8197e-003	1.3386e-003
3.7465e-004	8.6137e-004	5.1084e-004	1.9180e-003	1.4756e-003
4.1199e-004	9.2437e-004	5.6260e-004	2.1023e-003	1.5734e-003
4.5299e-004	1.0226e-003	6.1147e-004	2.2590e-003	1.6483e-003
5.0483e-004	1.1244e-003	6.5072e-004	2.3547e-003	1.6731e-003
5.5659e-004	1.2079e-003	6.8928e-004	2.3927e-003	1.6383e-003
5.9104e-004	1.2643e-003	6.9404e-004	2.3624e-003	1.5802e-003
6.1894e-004	1.2765e-003	6.8691e-004	2.2636e-003	1.4723e-003
6.3301e-004	1.2641e-003	6.6361e-004	2.0996e-003	1.3850e-003

Columns 16 through 20

7.1525e-004	1.0672e-003	1.7696e-003	1.7910e-003	7.0598e-004
7.6301e-004	1.1448e-003	1.8409e-003	1.8150e-003	6.9228e-004
8.0971e-004	1.1969e-003	1.8784e-003	1.7875e-003	6.6052e-004
8.4994e-004	1.2068e-003	1.8296e-003	1.7070e-003	6.1777e-004
8.6483e-004	1.1950e-003	1.7500e-003	1.5840e-003	5.6290e-004
8.4955e-004	1.1401e-003	1.6384e-003	1.4541e-003	5.0358e-004
8.1517e-004	1.0695e-003	1.5076e-003	1.3225e-003	4.6030e-004
7.5599e-004	9.7340e-004	1.3845e-003	1.2195e-003	4.1292e-004
6.9922e-004	9.2179e-004	1.2706e-003	1.0842e-003	3.6390e-004
6.8056e-004	8.4314e-004	1.1373e-003	9.6688e-004	3.2564e-004

Columns 21 through 25

6.3506e-004	9.3922e-004	1.2887e-003	1.6478e-003	1.7848e-003
6.5013e-004	9.3710e-004	1.2470e-003	1.5332e-003	1.6055e-003
6.4334e-004	9.1503e-004	1.1825e-003	1.3919e-003	1.4210e-003
6.2229e-004	8.7994e-004	1.0935e-003	1.2480e-003	1.2433e-003
5.9637e-004	8.3901e-004	9.8866e-004	1.1089e-003	1.0890e-003
5.8144e-004	7.6189e-004	8.9480e-004	9.8856e-004	9.6167e-004
5.5527e-004	7.0542e-004	8.0344e-004	8.8121e-004	8.4784e-004
5.1074e-004	6.3655e-004	7.2293e-004	7.9119e-004	7.5722e-004
4.7129e-004	5.8070e-004	6.5709e-004	7.0582e-004	6.7520e-004

4.3353e-004 5.3156e-004 5.9275e-004 6.3342e-004 6.1621e-004

Columns 26 through 30

1.2992e-003 8.9343e-004 1.1209e-003 7.3398e-004 7.7319e-004
1.1414e-003 7.5867e-004 9.4138e-004 6.0875e-004 6.3665e-004
9.7970e-004 6.4757e-004 7.9013e-004 5.1674e-004 5.4457e-004
8.5011e-004 5.5600e-004 6.7838e-004 4.4007e-004 4.6542e-004
7.3541e-004 4.7729e-004 5.8077e-004 3.7761e-004 4.0161e-004
6.3981e-004 4.1573e-004 5.0950e-004 3.3613e-004 3.5903e-004
5.6388e-004 3.6724e-004 4.4748e-004 2.9889e-004 3.1838e-004
4.9664e-004 3.2039e-004 3.9896e-004 2.6633e-004 2.9341e-004
4.4135e-004 2.8786e-004 3.6015e-004 2.3902e-004 2.6754e-004
3.9938e-004 2.6308e-004 3.2915e-004 2.2036e-004 2.4655e-004

Bibliography

[1] Aguilar, J.L., Garcia, R.A., and D'attellis, C.E., "Exact Linearization of Nonlinear Systems: Trajectory Tracking with Bounded Controls and State Constraints", *Intl J. Control*, v65, n3, pp. 455-467, 1996.

[2] Aling, H., et al.,"Application of Feedback Linearization to Models of Rapid Thermal Processing (RTP) Reactors", 3rd Int'l Rapid Thermal Processing Conference-RTP'95, pp.356-366, 1995.

[3] Baker, J., and Christofides, P.D., "Output Feedback Control of Parabolic PDE System with Nonlinear Spatial Differential Operators", *Ind. Eng. Chem. Res*. v.38, pp.4372-4380, 1999.

[4] Balakrishinan, K.S., and Edgar, T.F., "Model-Based Control in Rapid Thermal Processing", *Thin Solid Films*, v.365, n2, pp.322-333, 2000.

[5] Balakrishnan, K.S., Cho, W.H., and Edgar, T.F., "Comparison of Controller Tuning Methods for Temperature Uniformity Control in a Rapid Thermal Processor", SPIE, v2336, pp.70-80, 1994.

[6] Beard, R.W., and McLain, T.W., "Successive Galerkin Approximation Algorithm for Nonlinear Optimal and Robust Control", *Int'l. J. Control*, v.71, n.5, pp. 717-743, 1998.

[7] Botto, M., Boom, T.V.D., A. Krijgsman and Costa, J.S.D., "Predictive Control Based on Neural Network Models with I/O Feedback Linearization", *Intl J. Control*, v72, n17, pp. 1538-1554, 1999.

[8] Braake, H.A.t., Botto, M.A., Can, H.J.v., Costa, J.S.d., and Verbruggen, H., "Linear Predictive Control Based on Approximate Input-Output Feedback Linearization", IEE Proc. Control Theory and Applications, v146, n4, pp. 295-300,1999.

[9] Breedijk, T., Edgar, T.F., and Trachtenberg, I., "Model-Based Control of Rapid Thermal Processes", Proc. of American Control Conference, pp. 887-891, 1994.

[10] Cho, Y.M., and Gyugyi, P., "Control of Rapid Thermal Processing: A System Theoretic Approach", *IEEE Transactions on Control Systems Technology*, v.5, n.6, pp.644-653, 1997.

[11] Choi, J.Y., and Do, H.Y., "A Learning Approach of Wafer Temperature Control in a Rapid Thermal Processing System", *IEEE Trans. On Semiconductor Manufacturing*, V.14, n1, pp. 1-10, Feb. 2001.

[12] Edwards, C., and Spurgeon, S.K., Sliding Mode Control: Theory and Applications, Taylor & Francis, 1998.

[13] Elia, C.F., "RTP Multivariable Temperature Controller Development", Proc. of American Control Conference, pp. 907-912, June, 1994.

[14] Ericsson-Jackson, J., Bainum, P.M., and Xing, G., "Application of Singular Value Decomposition Method to Digitally Controlled Large

Orbiting Platforms", *J. of Guidance, Control and Dynamics*, v21, n4, pp.551-557, 1998.

[15] Erturk, H., Ezekoye, O.A. and Howell, J.R., "Inverse Solution of Radiative Heat Transfer In Two-Dimensional Irregularly Shaped Enclosures", Proc. 2000 IMECE, ASME HTD, v.366-1, pp. 109-116, 2000.

[16] Erturk, H., Ezekoye, O.A. and Howell, J.R., "Inverse Transient Boundary Condition Estimation Problem in a Radiating Enclosure", Proc. 2001 ASME National Heat Transfer Congress, 2001.

[17] Erturk, H., Ezekoye, O.A. and Howell, J.R., "Inverse Design of a Three Dimensional Furnace with Moving Design Environment", Proc. 2001 IMECE, ASME HTD, 2001.

[18] Fernández, B., Class Notes for Nonlinear Control Systems, The University of Texas at Austin, 1998.

[19] Freeman, R.A., and Kokotovic, P.A., "Inverse Optimality in Robust Stabilization", *SIAM J. Control and Optimization*, v.34, n.4, pp. 1365-1391, 1996.

[20] Freeman, R.A., and Kokotovic, P.A., "Optimal Nonlinear Controllers for Feedback Linearizable Systems", Proc. American Control Conference, Seattle, pp. 2722-2726, 1995.

[21] Hansen, P.C., Rank-Deficient and Discrete Ill-Posed Problems : Numerical Aspects of Linear Inversion, Soc. Industrial and Applied Mathematics, Philadelphia, 1998.

[22] Hansen, P.C., "Numerical Tools for Analysis and Solution of Fredholm Integral Equations of the First Kind", *Inverse Problems*, Vol. 8, pp. 849-872, 1992.

[23] Henson, M., and Kurtz, M., "Input-Output Linearization of Constrained Nonlinear Processes", Proc. AIChE Annual Meeting, San Francisco, pp. 1-20, 1994

[24] Howell, J.R., Class Notes for Inverse Design of Thermal Systems with Dominant Radiative Transfer, The University of Texas at Austin, 2001.

[25] Huang, C.J., Yu, C.C., and Shen, S.H., "Selection of Measurement Locations for the Control of Rapid Thermal Processor", *Automatica*, v.36, pp. 705-715, 2000.

[26] Inman, D. J., Engineering Vibration, Prentice Hall, 1996.

[27] Isiori, A., Nonlinear Control Systems, 3rd edition, Springer-Verlag, London, 1994.

[28] Karlsmore, J., Koggersbol, A., Jensen, N., and Jorgensen, S.B., "A Two Stage Procedure for Control Structure Analysis and Design", *Computers Chem. Engng*, v18, pp.S465-S470, 1994.

[29] Kapoor, N., and Daoutidis, P., "An Observer-Based Anti-Windup Scheme for Non-Linear Systems with Input Constraints", *Intl J. Control*, v72, n1, pp. 18-29, 1999.

[30] Kendi, T.A., and Doyle, F.J., "Nonlinear Internal Model Control for Systems with Measured Disturbances and Input Constraints", *Industrial and Engineering Chemistry Research*, v37, pp. 489-505, 1998.

[31] Khalil, H.K., Nonlinear Systems, 2nd ed., Prentice Hall, Upper Saddle River, NJ, 1996.

[32] Kokotovic, P., and Arcak, M., "Constructive Nonlinear Control: A Historical Perspective", *Automatica*, v.37, pp.637-662, 2001.

[33] Kristic, M., Kanellakopoulos, I., and Kokotovic, P., Nonlinear and Adaptive Control Design, John Wiley & Sons, New York, NY, 1995.

[34] Kristic, M., and Tsiotras, P., "Inverse Optimal Stabilization of a Rigid Spacecraft", *IEEE Trans. Automatic Control*, v.44, n.5, pp. 1042-1049, 1999.

[35] Kurtz, M., Zhu, G.-Y., and Henson, M., "Constrained Output Feedback Control of a Multivariable Polymerization Reactor", *IEEE Trans. Control Systems Technology*, v8, n1, pp. 87-97, 2000.

[36] Kurtz, M., and Henson, M., "Input-Output Linearizing Control of Constrained Nonlinear Processes", *J. of Process Control*, v7, n1, pp. 3-17, 1997.

[37] Kurtz, M., and Henson, M., "Feedback Linearzing Control of Discrete-Time Nonlinear Systems with Input Constraints", *Intl J. Control*, v70, n4, pp. 603-616, 1998.

[38] Liu, G.P., and Patton, R.J., "Parametric State Feedback Design of Multivariable Control Systems Using Eigenstructure Assignment", Proc. IEEE Conf. on Decision and Control, pp.835-836, 1993

[39] Lu, Y.-S., and Chen, J.-S., "Design of a Global Sliding-Mode Controller for a Motor Drive with Bounded Control", *Intl J. Control*, v62, n5, pp.1001-1019, 1995.

[40] Lyshevshki, S.E., "Optimal Tracking Control of Nonlinear Dynamic Systems with Control Bounds", Proc. IEEE. Conf. on Decision and Control, Phoenix, AZ, pp. 4810-4815, 1999.

[41] Lyshevshki, S.E., "Robust Control of Nonlinear Continuous-time Systems with Parameter Uncertainties and Input Bounds", *Intl. J. Systems Science*, v.30, n.3, pp. 247-259, 1999.

[42] McLain, T.W., Bailey, C.A., and Beard, R.W., "Synthesis and Experimental Testing of Nonlinear Optimal Tracking Controller", Proc. American Control Conference, pp. 2847-2851, 1999.

[43] Morales, J.C., "Radiation Exchange Within Enclosure of Diffuse Gray Surfaces: The Inverse Problem", Ph.D. Dissertation, Dept. of Mechanical Engineering, The University of Texas at Austin, May, 1998.

[44] Nael, E.-F.H., and Christofides, P.D., "Integrating robustness, Optimality and Constraints in Control of Nonlinear Processes", *Chemical Engineering Science*, v. 56, pp.1841-1868, 2001.

[45] Nijmeijer, H., and Schaft, A. J. van der, Nonlinear Dynamical Control Systems, Springer-Verlag, New York, NY, 1990.

[46] Norman, S.A., and Boyd, S.P., ”Multivariable Feedback Control of Semiconductor Wafer Temperature”, Proc. of American Control Conference, pp. 811-816, 1992.

[47] Okabayashi, R., and Furuta, K., “Design of Sliding Mode Control Systems with Constrained Inputs”, Proc. 35th IEEE Conf. on Decision and Control, pp. 3492-3497, 1996.

[48] Pappas, G., Lygeros, J., and Godbole, D., “Stabilization and Tracking of Feedback Linearizable Systems under Input Constraints”, Proc. 34th IEEE Conf. on Decision and Control, pp. 596-601, 1995.

[49] Park, H.M., Yoon, T.Y., and Kim, O.Y., “Optimal Control of Rapid Thermal Processing Systems by Empirical Reduction of Modes”, *Ind. Eng. Chem. Res*. v.38, pp.3964-3975, 1999.

[50] Pil, A., and Asada, H., “Rapid Recursive Structure Redesign for Improved Dynamics of a Single Link Robot”, *ASME J. of Dynamic Systems, Measurements, and Control*, v117, pp.520-526, 1995.

[51] Pil, A., and Asada, H., “Integrated Structure/Control Design of Mechatronic Systems Using a Recursive Experimental Optimization Method”, *IEEE Trans. Mechatronics*, v1, n3, pp.191-203, 1996.

[52] Qin, S., and Badgwell, T., “A Survey of Industrial Model Predictive Control Technology”, Dept. of Chemical Eng., The University of Texas at Austin, 2001.

[53] Rai, S., and Asada, H., "Computer-Aided Structure Modification of Electromechanical Systems Using Singular Value Decomposition", *ASME J. of Mechanical Design*, v.116, pp. 1148-1156, 1994.

[54] Rai, S., and Asada, H., "Integrated Structure/Control Design of High Speed Flexible Robots Based on Time Optimal Control", *ASME J. of Dynamic Systems, Measurements, and Control*, v.117, pp. 503-512, 1995.

[55] Repperger, D.W., "Application of Singular Value Decomposition Methods for Optimization of Fixed Parameter Involving Resolved Rotational Motion Rate Control in a Motion Simulator", Proc. American Control Conference, v3, pp.2468-2472, 1992.

[56] Sagfors, M.F., and Waller, K.V., "Multivariable Control of Ill-Conditioned Distillation Columns Utilizing Process Knowledge", *J. of Process Control*, v8, n3, pp.197-208, 1998.

[57] Schaper, C.D., Kailath, T., and Lee, Y.J., "Decentralized Control of Wafer Temperature for Multizone Rapid Thermal Processing Systems", *IEEE Trans. Semiconductor Manufacturing*, v.12, n. 2, pp. 193-199, 1999.

[58] Shyu, K.-K., and Lin, H.-Y., "Adaptive Sliding Mode Control for Variable Structure Systems with Constraint Control Input", *Dynamics and Control*, v6, pp. 49-61, 1996.

[59] Skogestad, S., Morari, M., and Doyle, J.C., "Robust Control of Ill-Conditioned Plants: High-Purity Distillation", *IEEE Trans. Automatic Control*, v33, n12, 1988.

[60] Slotine, J.J.E., and Li, W., Applied Nonlinear Control, Prentice Hall, Englewood Cliffs, NJ, 1991.

[61] Tan, L., Cameron, D., and McCorkell, C., "Multivariable Decoupling Control System Design for the Plasma Etching Process", IECON Proc., v3, pp.1971-1976, 1994.

[62] Utkin, V., Guldner, J., and Shi, J., Sliding Mode Control in Electromechanical Systems, Taylor & Francis, 1999.

[63] Utkin, V., Sliding Modes in Control Optimization, Springer-Verlag, Berlin, 1992.

[64] Valluri, S. and Soroush, M., "Input Constraint Handling and Windup Compensation in Nonlinear Control", Proc. 1997 American Control Conf., v3, pp. 1734-1738, 1997.

[65] Yip, P. and Hedrick, J., "Controller Design for Nonlinear Systems under Input Constraints", Proc. ASME Dynamic Systems and Control Division, 1995 IMECE, pp. 359-363, 1995.

[66] Zhu, Z.–X. and Jutan, A., "Robust Multivariable Control Using an SVD-based Controller", *Chemical Engineering Science*, v53, n6, pp.1145-1151, 1998.

Vita

Kwan-Woong Gwak was born in Kwang-Ju, Korea on February 1, 1970, the son of Sa-Ho Gwak and Soo-Ja Han. After completing his work at Dongshin High School, Kwang-Ju, Korea, in 1988, he entered Korea University, Seoul, Korea, in 1988. He received the degree of Bachelor of Science in Mechanical Engineering from Korea University in 1993. He received the degree of Master of Science from the same school in 1995. His research focused on the development of vehicle traction control system via engine torque control approach. In July 1995, he joined Korea Institute of Science and Technology (KIST) as a research scientist. Until July 1996, he had been involved in two projects: development of die polishing robot system and tactile feedback device for teleoperation/human robot. During the Fall of 1996 and the Spring of 1997, he attended the University of Michigan. In January 1998 he entered The University of Texas at Austin to pursue his doctoral degree.

Permanent address: 154-8 DongMyoung-Dong,
Kwang-Ju, South Korea 501-071

This dissertation was typed by the author.